Modeling the ecology and evolution of biodiversity: Biogeographical cradles, museums, and graves

Article aar5452 - Title:

Modeling the ecology and evolution of biodiversity: Biogeographical cradles, museums, and graves

Authors:

Thiago F. Rangel[1*†], Neil R. Edwards[2], Philip B. Holden[2], José Alexandre F. Diniz-Filho[1], William D. Gosling[2,3], Marco Túlio P. Coelho[1], Fernanda A. S. Cassemiro[1,4], Carsten Rahbek[5,6], and Robert K. Colwell[1,5,7,8*†]

Affiliations:

[1]Departmento de Ecologia, Universidade Federal de Goiás, CP 131, 74.001-970 Goiânia, Goiás, Brazil.

[2]School of Environment, Earth, and Ecosystems, The Open University, Milton Keynes, UK

[3]Department of Ecosystem & Landscape Dynamics, Institute of Biodiversity & Ecosystem Dynamics, University of Amsterdam, Science Park 904, Amsterdam, Netherlands

[4]Núcleo de Pesquisa em Ictiologia, Limnologia e Aquicultura. Universidade Estadual de Maringá, Maringá, PR, Brazil.

[5]Center for Macroecology, Evolution and Climate, Natural History Museum of Denmark, University of Copenhagen, Universitetsparken 15, 2100 Copenhagen O, Denmark

[6]Department of Life Sciences, Imperial College London, Ascot SL5 7PY, United Kingdom

[7]Department of Ecology and Evolutionary Biology, University of Connecticut, Storrs, CT 06269, USA

[8]University of Colorado Museum of Natural History, Boulder, CO 80309, USA.

*Contributed equally

[†]Corresponding Author

Structured Abstract

INTRODUCTION: Individual processes that shape geographical patterns of biodiversity are increasingly understood, but their complex interactions on broad spatial and temporal scales remain beyond the reach of analytical models and traditional experiments. To meet this challenge, we built a spatially-explicit, mechanistic model that simulates the history of life on the South American continent, driven by modeled climates of the past 800,000 years. Operating at the level of geographical ranges of populations, our simulations implemented adaptation, geographical range shifts, range fragmentation, speciation, long-distance dispersal, competition between species, and extinction. Only four parameters were required to control these processes (dispersal distance, evolutionary rate, time for speciation, and intensity of competition). To assess the effects of topographic heterogeneity, we experimentally smoothed the climate maps in some treatments.

RATIONALE: The simulations had no target patterns. Instead, the study took a fundamental approach, relying on the realism of the modeled ecological and evolutionary processes, theoretical derivations of parameter values, and the climatic and topographic drivers to produce meaningful biogeographical patterns. The model encompassed only the Late Quaternary (last 800,000 years), with its repeated glacial-interglacial cycles, beginning at a time when South America was already populated with a rich biota, comprising many distinct lineages. Nonetheless, current consensus holds that the contemporary flora and vertebrate fauna of South America include numerous lineages that have undergone rapid diversification during the Quaternary, particularly in the Andes. In our model, over the course of each simulation, a complete phylogeny emerged from a single founding species. Based on the full historical records for each species range, at each 500-year interval, we recorded spatial and temporal patterns of speciation (*cradles*), persistence (*museums*), extinction (*graves*), and species richness.

RESULTS: Simulated historical patterns of species richness, as recorded by maps of the richness of persistent (museum) species, proved remarkably successful in capturing the broad features of maps of contemporary species richness for birds, mammals, and plants. Factorial experiments

varying parameter settings and initial conditions revealed the relative impact of the evolutionary and ecological processes we modeled, as expressed in spatial and temporal patterns of cradles, museums, graves, and species richness. These patterns were most sensitive to the geographical location of the founding species and to the rate of evolutionary adaptation. Experimental topographic smoothing confirmed a crucial role for climate heterogeneity in the diversification of clades, especially in the Andes. Analyses of temporal patterns of speciation (cradles) and extinction (graves) emerging from the simulations implicated Quaternary glacial-interglacial cycles as drivers of both diversification and extinction on a continental scale.

CONCLUSION: Our biogeographical simulations were constructed from the bottom up, by integrating mechanistic models of key ecological and evolutionary processes, following well supported, widely accepted explanations for how these processes work in nature. Despite being entirely undirected by any target pattern of real-world species richness and covering only a tiny slice of the past, strikingly realistic continental and regional patterns of species richness emerged from the model. Our simulations confirm a powerful role for adaptive niche evolution, in the context of diversification and extinction driven by topography and climate.

Figure Legend:

Figure 0. Observed species richness versus modeled richness. *Left map:* Contemporary South American bird richness (2,967 species). *Right map:* The simulated spatial pattern for museum richness.

Article aar5452 - Title:

Modeling the ecology and evolution of biodiversity: Biogeographical cradles, museums, and graves

[96 characters]

Authors:

Thiago F. Rangel[1*†], Neil R. Edwards[2], Philip B. Holden[2], José Alexandre F. Diniz-Filho[1], William D. Gosling[2,3], Marco Túlio P. Coelho[1], Fernanda A. S. Cassemiro[1,4], Carsten Rahbek[5,6], and Robert K. Colwell[1,5,7,8*†]

Affiliations:

[1]Departmento de Ecologia, Universidade Federal de Goiás, CP 131, 74.001-970 Goiânia, Goiás, Brazil.

[2]School of Environment, Earth, and Ecosystems, The Open University, Milton Keynes, UK

[3]Department of Ecosystem & Landscape Dynamics, Institute of Biodiversity & Ecosystem Dynamics, University of Amsterdam, Science Park 904, Amsterdam, Netherlands

[4]Núcleo de Pesquisa em Ictiologia, Limnologia e Aquicultura. Universidade Estadual de Maringá, Maringá, PR, Brazil.

[5]Center for Macroecology, Evolution and Climate, Natural History Museum of Denmark, University of Copenhagen, Universitetsparken 15, 2100 Copenhagen O, Denmark

[6]Department of Life Sciences, Imperial College London, Ascot SL5 7PY, United Kingdom

[7]Department of Ecology and Evolutionary Biology, University of Connecticut, Storrs, CT 06269, USA

[8]University of Colorado Museum of Natural History, Boulder, CO 80309, USA.

*Contributed equally

[†]Corresponding Author

Abstract:

Individual processes shaping geographical patterns of biodiversity are increasingly understood, but their complex interactions on broad spatial and temporal scales remain beyond the reach of analytical models and traditional experiments. To meet this challenge, we built a spatially-explicit, mechanistic simulation model implementing adaptation, range shifts, fragmentation, speciation, dispersal, competition, and extinction, driven by modeled climates of the past 800,000 years in South America. Experimental topographic smoothing confirmed the impact of climate heterogeneity on diversification. The simulations identified regions and episodes of speciation (cradles), persistence (museums), and extinction (graves). Although the simulations had no target pattern and were not parameterized with empirical data, emerging richness maps closely resembled contemporary maps for major taxa, confirming powerful roles for evolution and diversification driven by topography and climate.

[124 words]

One-sentence Summary:

Mechanistic simulations of climate dynamics, speciation, and adaptive evolution yield realistic geographical patterns of biodiversity.

Main Text:

Despite continually improving documentation of the global distribution of biodiversity and increasing awareness of its vulnerability, we remain confronted by our ignorance of the fundamental ecological and evolutionary processes that have shaped the diversity and complex biogeography of continental biotas (*1-3*). Narrative accounts (*4*) and correlative studies (*5-10*) suggest underlying causes, and theoretical models demonstrate possible mechanisms (*7, 11-17*), but spatially- and temporally-explicit, process-based models (*18, 19*), founded on a comprehensive suite of well-studied, widely-accepted mechanisms, have the greatest potential to assess the complex and sometimes indeterminate interactions among underlying processes (*20-25*). Here, we offer such a comprehensive model, for a simulated biota. We applied it to a fine-scale topographical representation of South America—the most climatically and biologically diverse continent on Earth—driven by a spatially-explicit paleoclimate model for the past 800 ka, for both temperature and precipitation.

In a changing climate, the geography of species distributions is governed by many interacting environmental and biological processes. These processes include the shifting spatial pattern of environmental variables (*16, 26*), range shifts (*27*), dispersal (*28*), the geographical effects of competition between species (*29*), niche evolution (*30*), range fragmentation and re-joining (*31, 32*), speciation (*33-35*), and extinction (*36*). Our biogeographical simulation model (Fig. 1) incorporated all these processes at the level of geographical ranges of populations, as realistically as feasible, given the inevitable computational limitations. Our principal objective was to evaluate, experimentally, the relative importance of these mechanisms in a multifactorial framework.

Current understanding of South American biogeography

The crucial role of the Andes

The rise of the Andes, beginning 25 Ma ago (*37*), launched a biogeographical experiment unique in Earth's history (*38, 39*)— the juxtaposition of a long, trans-tropical mountain chain and a tropical

rainforest (*40*). Throughout their history, the environmental heterogeneity of the Andes is thought to have driven species diversification by (1) providing novel, high-altitude mountain environments; (2) erecting dispersal barriers that promoted vicariant speciation, both between east and west slopes (*41, 42*) and between internal valleys and peaks along the mountain chain (*43, 44*); (3) offering a north-south, climatically driven, biogeographical corridor; (4) sheltering species threatened with extinction by reducing regional climate velocity (*45, 46*); and (5) offering refugia from climatic extremes (*4, 47-49*).

Our model (Fig. 1) encompasses all of these drivers of Andean diversification. Separately from our assessment of the relative importance of these processes, we investigated the role of Andean climate heterogeneity, itself, as a driver of diversification, within the experimental design. To do so, we simulated the biogeographical consequences of gradually smoothing the topography of South America, with the expectation that these diversification processes would be progressively eliminated.

Historical biome dynamics

Although biogeographers unequivocally view the Andes as a driver of species diversification (*38-41*), historical linkages among South American biomes are still under debate. The present-day northeast–southwest Caatinga-Cerrado-Chaco "hot-dry diagonal" poses a dispersal barrier between Amazonian and Atlantic rainforests for vertebrates and plants (*50-52*). However, multiple cases of disjunct distributions across this barrier (*53-56*) support Por's (*57*) proposal of an ephemeral connection between the Amazon and Atlantic Rainforest during late Quaternary climate cycles (*58-60*). Seasonally dry tropical forests have also been viewed as important drivers of plant diversity in South America, and they offer a potential explanation for disjunct distributions of woody plants between Atlantic Forest and the Amazon and Andes (*50, 61*).

Within the Amazon, recent empirical and model-based studies have suggested the existence of a large-scale dipole in hydroclimate dynamics between Western and Eastern Amazonia—a consequence of the regionally discordant effect of glacial cycles on patterns of precipitation (*62,*

63). Together with smaller-scale, patchy dynamics of forest canopy density (*64*), recent lineage diversification in the Amazon Basin may have occurred principally as a consequence of sporadic dispersal events and subsequent persistence in isolation (*32*). While not at the scale of local forest dynamics, our simulations allow us to assess the degree to which these regional patterns may have been driven by each of the processes we modeled (Fig. 1), in the context of Quaternary climate cycles.

Strategy and scope of the study

Predecessors of our simulation model (*22, 23*) targeted documented patterns of species richness and range size distributions to guide the exploration of parameter space and to assess the sensitivity of outcomes to individual parameters and their values. The present study takes a more fundamental approach, relying on the realism of the modeled climatic and topographic drivers and modeled ecological and evolutionary processes (Fig. 1) to produce meaningful biogeographical patterns. The simulations had no target pattern and were not parameterized with empirical data. Remarkably, as we will show, richness maps nonetheless emerged from the simulations that closely resemble contemporary richness maps for South American birds, mammals, and plants, including regional details that mirror conjectures in the biogeographical literature, as outlined above.

While our paleoclimate model extends further into the past than any three-dimensional atmosphere model previously applied at this temporal resolution, the model nonetheless encompasses only the Late Quaternary (800 ka to the present), with its repeated glacial-interglacial cycles, extending as far into the past as the high-precision CO_2 record from Antarctic ice core data (*65*). South America was, of course, already populated with a rich biota comprising many distinct lineages—some quite ancient—at the beginning of this period(*66*) (*66*).

Nonetheless, current consensus among biogeographers and paleoecologists is that the contemporary flora (*67, 68*) and vertebrate fauna (*4, 33, 34, 69, 70*) of South America include numerous lineages that have undergone rapid diversification during the Quaternary, particularly in the Andes. In contrast, the flora and fauna of the South American tropical lowlands, including the

Amazon, are generally considered to be more ancient (*33, 40, 70*). It is likely, however, that the geographical distributions of most species, whether belonging to an old lineage or a young one, have been shaped by Quaternary climate cycles (*71, 72*) (Movie 1 and Fig. S2).

Cradles, museums, and graves

Although conceptually simple (Fig. 1), the model yielded extraordinarily complex patterns of diversity in space and time. To make sense of the simulations, we examined the history of each simulated species and its contribution to these patterns. Over the course of each simulation, a complete phylogeny emerges from a single founding species. Based on this phylogeny and on full historical records of each range and range fragment at each 500-year interval of the modeled paleoclimate data (Movie 1), we analyzed and illustrated spatial and temporal patterns of speciation (*cradles*), persistence (*museums*), extinction (*graves*), and species richness within South America.

Stebbins (*73*) began a long tradition of referring to locations with unusually high rates of speciation as "cradles" of diversity, and to locations with unusually low rates of extinction as "museums." Although these terms have previously been applied almost exclusively to broad comparisons between tropical and boreal latitudes (*16, 74-78*), here we follow Fjeldså *et al.* (*4*) in downscaling these analogies to the regional level, within South America. In addition, the full evolutionary and biogeographical records that arise from our simulations allow us to define and map a third biogeographical category, "graves"—locations with unusually high extinction rates—and to document not only where, but also when cradles, museums, and graves were most and least active.

As we define them here, *cradles* are about speciation, *museums* about persistence, and *graves* about extinctions. Previously, cradles and museums have generally been viewed as fixed geographical places (*4*). Because our simulations take place in both space and time, we treat all three patterns as driven dynamically by the processes of speciation, persistence, and extinction. A cradle, museum, or grave has extension and intensity in both space and time, and may move though space and change shape, size, and intensity as time passes.

Lifetime trajectories

Every species in the simulation has a *lifetime trajectory*, in space and time (Fig. 2). Temporally, each species' lifetime trajectory extends from its time of origination (a range fragmentation event that leads subsequently to speciation) to one of three endpoints: the point in time when the species splits into two isolated populations (range fragments) that eventually become daughter species, the point in time of its extinction, or the present time—if the species is still alive at the end of the simulation. Each species' lifetime trajectory is subdivided into three consecutive, distinct, and fully inclusive segments: a *speciation trajectory*, a *persistence trajectory*, and, if the species goes extinct during the simulation, an *extinction trajectory* (Fig. 2). (Species that give rise to daughter species or persist into the present lack an extinction trajectory.) The speciation trajectory covers the period of population isolation between range fragmentation and full genetic isolation, T_{min} years later. The extinction trajectory begins when a species starts an inexorable decline (defined statistically) toward extinction. The persistence trajectory comprises the time interval between the consolidation of speciation at T_{min} and the beginning of the extinction trajectory.

Occupancy maps and time series

At the end of each simulation, we determined the lifetime trajectory of each species (Fig. 2) and its component segments (speciation, persistence, and extinction) by moving backwards in time through the records of the simulation. We recorded the number of time steps that each map cell was occupied by each species for each segment of its lifetime trajectory. We then summed these records for all species—separately for speciation, persistence, and extinction trajectories—to produce five *cumulative occupancy maps* for the entire simulation: a *cradles map*, a *museums map*, a *graves map*, a *net diversification map* (cradles minus graves), and a *total richness map* (Fig. S15). Each of these maps is a summation over time. The cumulative total richness map is simply the spatial overlay (summation) of the cradles, museums, and graves maps—a map of total occupancy by all descendants of the founding species, summed over the course of the simulation. Each species in the simulation, whether extinct, an ancestor of other species, or living at the end of the simulation,

contributes to these maps. To visualize the temporal pattern behind these cumulative maps, in relation to climate and to each other, we plotted *occupancy time series* for cradles, museums, graves, net diversification, and total richness, by summing occupancy over all cells for each time step, for each map (Fig. S13).

Cumulative occupancy maps provide a deep compilation of historical information on emerging patterns of richness and their dynamics, summed over the time course of a simulation. Occupancy time series, in contrast, represent cradles, museums, graves, or total richness, summed over the entire continent, for each time step of a simulation.

Results

We carried out 10,500 simulations, each spanning the entire 800 ka scope of the paleoclimate time series, to assess sensitivity of the model to its parameters and to a battery of initial conditions. As detailed below in Methods, we treated the four model parameters (Fig. 1) and two sets of initial conditions (founder location and climate smoothing) as factors in a fully realized factorial design, specified in Table S5. Movie 2 illustrates the structure and dynamics of these simulations for a small clade, together with a corresponding phylogeny. The temporal and spatial dynamics of species richness, cradles, graves, and net diversification for a larger clade are illustrated in Movie 3.

Impact of parameters and initial conditions

To assess the impact of parameters and initial conditions on emerging spatial and temporal patterns in biodiversity, we partitioned sources of variation (*79, 80*) among these patterns, based on matrices of quantitative Bray-Curtis dissimilarities computed between pairs of cumulative occupancy maps for cradles, museums, graves, and total richness generated by each simulation (Table S7, Figs. S16-S19). In these analyses, a parameter or initial condition was judged to be influential if it yielded consistent spatial patterns for any particular parameter setting or initial condition, and different patterns for different settings, regardless of the settings of other parameters or initial conditions. Factors that varied little in their influence on the mean behavior of the simulations, regardless of their settings, were judged less important.

Model parameters and initial conditions varied greatly in their impact on the simulations, but none was as influential, overall, as founder location (Figs. 3-5; Figs. S16-S19; Table S7), suggesting an underappreciated impact of historical contingencies in current patterns in species richness (*81*). The second-most-influential model parameter was the maximum sustainable evolutionary rate realizable by a population (H_{max}), which limits the adaptability of niche limits and evolutionary rescue (*82-85*) in the face of changing climates (Figs. S16-S19; Table S7). Low H_{max} values indicate that niche traits have low genetic variance, low population growth rates, or both—preventing species from tracking and adapting to changing climates. On evolutionary time scales, this limitation yields a pattern of niche conservatism. Although the balance varied among founders, intermediate levels of adaptive evolution promoted the greatest diversification. If H_{max} was too low (strong niche conservatism), species and lineages were subject to extinction. If too high (fast niche evolution), a few species became ubiquitous and little diversification occurred.

The effect of spatial and temporal heterogeneity in climate, as assessed by sequential levels of experimental climate-smoothing, ranked third in its capacity to drive variation among simulation outcomes (Fig. 6 and S14-S19; Table S7), as higher levels of heterogeneity promoted faster diversification.

Maximum dispersal distance (D_{max}) ranked somewhat lower in overall impact. Greater dispersal capacity increased speciation (cradle richness) by promoting occupation of disjunct, yet climatically suitable regions that initially lay within D_{max} but that later became isolated through climate change (Figs. S14-S19; Table S7). Extinction rates (grave richness), in contrast, decreased with greater D_{max}, as declining populations were rescued from extinction by dispersal to suitable climates. Thus, net diversification increased with larger D_{max}, by its combined effects in increasing speciation and decreasing extinction rates.

The remaining model parameters, minimum time in isolation for speciation (T_{min}) and maximum intensity of competition allowing coexistence (C_{max}), proved to have surprisingly little effect on the simulations, compared with the other parameters (Figs. S14-S19; Table S7).

Regardless of the rate of speciation, similar spatial patterns eventually emerged. We surmise that competitive exclusion at the map cell level, as we modeled it, tends to have only local and probably ephemeral effects, as climates change and species adapt to these changes, with little net impact on large-scale patterns of species richness.

Founder location, cradles, and graves

Figs. 3-5 show the results for Andean, Atlantic Forest, and Amazon founders (each figure summarizes 375 simulations—all those without experimental topographies), and Fig. 6 combines the results for all three founders. The maps in these figures display cumulative occupancy, summed over the course of the simulations, for cradles, graves, net diversification, and species richness. The corresponding occupancy time series plots in these figures capture the temporal dimension of speciation and extinction by summing occupancy over all cells in South America for each time step, based on the time-specific occupancy maps of cradles and graves.

In space, Figs. 3-5 illustrate the strong influence of founder location. The initial niche of the single founder, in each region, necessarily differed among regions for initial survival, and constraints on niche evolution limited continental-scale convergence in pattern, but these figures share many features of spatial pattern and temporal dynamics, independent of starting location.

With regard to time, the most striking feature shared by all simulations is the obvious quasi-periodicity of peaks and valleys of speciation (cradles) and extinction (graves), as shown in the occupancy time series plots in Figs. 3-6. Time-series analysis of log-transformed, de-trended data for cradles and graves, in relation to mean annual continental temperature, yielded many significant, time-lagged, cross-correlations (Table S6), confirming a subtle but certain role for glacial-interglacial temperature cycles (and thus, for orbital forcing (*86*)) in driving cycles of speciation and extinction for all founders. Both speciation and extinction tended to peak during glacial terminations, as warming climates returned. Peaks of extinction closely followed peaks of speciation for all three founders—by 18 ka for an Andean founder (Fig. 3), by 20 ka for an Atlantic

Forest founder (Fig. 4), and by 24.5 ka for an Amazon founder (Fig. 5). (Time-series analysis for precipitation variables yielded very low correlations, so was not pursued further.)

A striking feature of these simulations—for the Atlantic Forest and Amazonian founders (Figs. 3 and 4)—is the spatial coincidence of cradles and graves, best illustrated by the net-diversification maps, which plot net spatial differences in magnitude between speciation and extinction. In contrast, cradles for the Andean founder are concentrated along the Andean slopes, whereas graves tend to be at lower elevations in the upper Amazon Basin (Fig. 3). Population decline drives both speciation and extinction—speciation through range fragmentation and extinction by range contraction. We conjecture that environmental heterogeneity (driven by topographic complexity and elevational climate gradients) in the Andes promotes range fragmentation, while at the same time offering climatic refugia from extinction compared with lower elevations (*46, 49*), thereby focusing cradles at mid-elevations and graves at lower elevations.

Experimental topographies

Our experiments with climate-smoothing, as a proxy for decreased topographic heterogeneity, yielded clear-cut evidence for the role of spatial heterogeneity in the location and intensity of cradles of speciation and net diversification, with considerably less effect on graves of extinction (Figs. 7 and S21). Overall, non-smoothed (realistic) climates promoted three times more diversification than spatially smoothed climates, with the effect tapering off for smoothing kernels larger than 250km. The strongest effects were experienced by the Andean founder clade (Fig. 7), where even the smallest possible kernel radius reduced diversification by a factor of seven, whereas the reduction for Atlantic Rainforest founder was only by half.

Biogeographical interpretations

Emerging role of the Andes

By mapping the distribution of South American cradles of diversification, in time and space, our simulations offer strong support for the role of the Andes as an episodic "species pump" (*38, 69,*

87). This phenomenon has been documented not only for endemic Andean clades (*43*), but also for clades later centered in the Amazon and Atlantic Rainforest (*40, 52, 88*).

By experimentally smoothing South American topography, we gradually eliminated all of diversification processes driven by Andean topography. The extent and magnitude of Andean cradles declined drastically, while South American graves broadened and intensified (Figs. 7 and S21) and net diversification decreased (Figs. 7, S14, S20). With experimentally smoothed topography, the simulations ceased to produce realistic spatial patterns of species richness (Fig. S21). These experiments offer compelling evidence that topographic complexity—or more accurately, the fluctuating climatic complexity that constantly mirrors it—drives diversification and biogeographical patterns. This result shows unambiguously not only that climatic complexity promotes diversification, but also that diminished complexity drastically slows diversification.

Emerging regional patterns

Regional biogeographical dynamics in our simulations, on a broader scale, also conform to many expectations from empirical studies. Our simulations (Movie 3) directly support Por's (*57*) proposal of an ephemeral connection between the Amazon and Atlantic Rainforest during late Quaternary climate cycles (*58-60*), as well as recent suggestions that Atlantic Rainforest birds may have dispersed through the Cerrado during glacial maxima and through the Chaco during interglacial periods (*52, 59*).

Our simulations display a pattern of ephemeral, circum-Amazonia "arcs" of seasonally dry climates—sometimes patchy and sometimes continuous—connecting the tropical Andes and Atlantic Forest (*50, 61, 89*). In our simulations, these episodic biogeographical bridges acted for some species as dispersal corridors, for others as refugia from extinction, but for many others as graves. We did not find evidence, at the scale of our current analysis, for the Amazonian dipole hypothesis (63, 64), although a specific, local investigation might be fruitful.

Emerging patterns of speciation and extinction

Our analyses of temporal patterns of speciation (cradles) and extinction (graves) offer strong support for both generative and erosive effects on biodiversity arising from continental-scale climate change driven by Quaternary glacial-interglacial cycles (Figs. 3-6). As warming accelerated following glacial episodes, first speciation, then extinctions spiked. These results are in accord with accumulating evidence for episodes of heightened extinction during Quaternary deglaciations (*90-92*), and support concerns about extinction under rapid anthropogenic climate warming.

In space, cradles and graves closely coincided for Amazonian clades (Fig 5), suggesting that gradual warming promoted speciation, and more rapid or extensive warming in the same region drove extinctions. For an Andean clade (Fig. 3 and Movie 3), cradles were concentrated in the highlands, while graves accumulated the adjacent Amazonian lowlands, perhaps suggesting that high climate velocity (*93*) or climatic divergence (*94*) in the warming lowlands overwhelmed their capacity to escape to the Andean slopes. This process is also likely to have been a cause of Amazonian extinctions.

Comparison with contemporary patterns of richness

If the processes that we have modeled are realistic representations of the processes that have shaped contemporary biogeography, then a comparison between simulated, historical patterns and empirical, contemporary patterns of species richness should be instructive. Our simulations were not carried out with regard to the richness pattern of any particular real-world taxon, nor were model parameters fitted by targeting such patterns. Indeed, not only the model design, but also the ranges of parameter values were defined strictly on first principles of biogeography, ecology, and evolutionary biology, without regard to any empirical data. Thus, any resemblance between model output and real-world richness patterns must be attributed to (1) the underlying processes built into the model, (2) the topographic and modeled climatic *milieux* in which they operated, and (3) theoretically estimated parameter values that regulated the simulated ecological and evolutionary processes.

Each simulation began with a single founder, 800 ka ago, and unfolded over a geologically brief period of time until the present. Thus, in principle, the present time in each simulation might seem the most appropriate for comparison with the empirical maps of contemporary richness. However, preliminary tests showed that many simulated maps of contemporary richness, especially for Andean founders, were surprisingly species-poor, following massive extinctions in post-last-glacial-maximum warming. Fig. 3 shows that this Holocene extinction peak is just one of several, each associated with an interglacial warming period for the Andean simulation. In contrast, Amazon founders (Fig. 5) do not show this pattern. We conjecture that the model, as it stands, exaggerates episodes of clade extinction by failing to account for the survival of species under outlier climates in some regions, perhaps supporting a role for micro-refugia (*4, 49*) that lie under the radar of the spatial scale of the model. Moreover, our paleoclimate model exhibits LGM cooling at the high end the range of full-complexity climate models (see *Comparisons against other paleoclimate models* in in (*95*)), perhaps contributing to the high rates of extinction simulated during deglaciations. Finally, our model does not account for potentially important factors hypothesized to promote speciation, such as sub-canopy forest dynamics (*64*) and the historical origins of the hydrographic network, which are thought to have promoted isolation and vicariance effects in some clades (*96*).

In contrast with the simulated contemporary map of species richness, *cumulative* maps (Figs. 3-6) provide a richer compilation of historical information on emerging patterns of richness and their dynamics over the time course of the simulations. By aggregating patterns from every phase of the diverse (*97*) glacial-interglacial cycles and averaging over all parameter values, these maps represent the broader range of possible patterns arising from local and regional processes captured by the model. Thus, cumulative maps of species richness offer a much more representative historical account of model behavior than any single point in time in the simulation, including the present, which represents contemporary climatic conditions—an outlier within the distribution of Quaternary climates.

Cumulative cradle maps record the frequency and location of species origination, grave maps point to regions where species tend to collapse under climate change, and museum maps show

where species tend to persist over longer historical periods. Thus, if contemporary patterns of species richness for large clades are representative of deep and persistent historical patterns, we should find stronger correspondence with simulated patterns of museum species richness. For rapidly-speciating clades, in contrast, we would expect stronger correspondence with cradle richness, and for clades on the decline we might expect a better correspondence with grave richness.

Because continental-scale maps of contemporary species richness for South America are scarce and fraught with sampling and data quality problems (*98*), we used a lower resolution 1° latitude x 1° longitude grid of 1659 cells to develop maps for 2967 species of birds, 1342 species of mammals, and 61,724 species of plants. To compare our simulation outputs with these maps of contemporary richness, we re-scaled our hybrid-scale richness maps (Fig. S1 and S15-S19) to the same, uniform 1° x 1° resolution.

Simulated historical patterns of species richness, as recorded by maps of cumulative museum richness, proved remarkably successful in capturing, proportionally, the broad outlines of the empirical richness maps (Fig. 8 and Movie 4) for birds ($r^2 = 0.6337$ for an Atlantic Forest founder, Fig. S22), mammals ($r^2 = 0.6548$ for an Atlantic Forest founder, Fig. S23), and plants ($r^2 = 0.4146$ for an Andean founder; Fig. S24 and S25). Tables S12-S14 provide more detail, and make clear that the maps in Figs. 8 and S22-S25 represent the best of strong patterns, not one-off accidents.

This high level of correspondence between modeled and empirical richness raises an obvious question about time scales. Although several lineages are known to have diversified actively during the timespan of our Quaternary simulations, particularly in the Andes (*67, 68*), most living species in South America are much older than any species in our simulations (*33, 40, 70*). We do not suggest that our simulations over the geologically brief period of 800 ka might reproduce the actual ranges, evolutionary dynamics, or phylogeny of any living species in the South American biota. Our simulated "species," however, may just as well be viewed as independent evolutionary units below the level of taxonomic species, nonetheless subject to the same ecological and

evolutionary processes. As phylogeographical studies (*88*) and tools for studying ancient DNA reach farther into the past (*91*), models such as ours can be expected to take on even greater realism.

A second question is why richness patterns of living species, from the present (outlier) interglacial climate—a single point in time, should correspond so well with *cumulative* richness patterns from the simulations. Our cumulative richness maps pool both glacial and interglacial distributions, and we know from paleoecological studies that Quaternary temperature cycles (including Holocene warming) shuffled many extant species over elevational (*71*) and latitudinal (*72*) gradients, just as in our simulations (Movies 3 and 4). We conjecture, first, that the geographical core of richness patterns may have been more persistent over geological time than generally thought, and, second, that the maps of residuals between simulated and empirical richness (right column in Figs. 8 and S22-S24) may correspond, at least in part, to regions where past richness differed from present empirical patterns—a topic that merits further research.

What does it all mean?

Our simulations have three strengths. First, they take place in a topographically realistic continental landscape, driven by a paleoclimate model built on well-established principles. Second, the biogeographical simulations were constructed from the bottom up, by integrating mechanistic models of key ecological and evolutionary processes, following well supported, widely accepted explanations for how these processes work in nature (Fig. 1). Third, despite being entirely undirected by any target pattern of species richness, covering only a tiny slice of the past, and being controlled by only four parameters (two of which turned out not to be very important), remarkably realistic biogeographical patterns nonetheless emerged from the simulations, not only on continental scale (Fig. 8), but also on regional scales.

Adaptive niche evolution as a biogeographical force

Phylogenetic niche conservatism (*30*) is the universal tendency of descendant species to retain the fundamental niche of their ancestors (*99-101*). It may be strong or weak. By modeling adaptation to climate in the trailing edge of a shifting range, our simulation model explicitly regulates the

capacity of a species' climatic niche to respond to climate change by adaptive evolution (evolutionary rescue) (*102, 103*). When the potential for adaptive evolution is weak (low H_{max}, Fig. 1), a pattern of strong niche conservatism emerges. Descendant species accumulate in regions that are climatically similar and geographically close to the original range of the ancestor, with a gradual decline in richness of descendant species with increasing distance and decreasing climatic similarity (*104*). The distribution of descendant species is constrained by higher extinction rates, as species fail to adapt to changes in trailing-edge conditions. In contrast, when the potential for adaptive evolution is strong (high H_{max},,weak niche conservatism) a pattern of niche evolution emerges, with adaptive shifts to novel climates and a broader geographical spread of descendant species, but little diversification, because ranges rarely fragment, as niches adapt to all challenges. Our simulations provide unequivocal support for intermediate levels of adaptive niche evolution as a key factor driving realistic patterns of species richness (Fig. S16, Table S7, S12-S14), confirming the findings of previous simulations (*22, 23*).

Emerging patterns on a continental scale

In the simulations, the facilitating influence of adaptive niche evolution, acting within the constraints of topography and climate, yielded cumulative patterns of species persistence (museum richness) that correspond well with contemporary richness patterns of birds, mammals, and plants (Figs. 8 and S22-S24; Movie 4). The inference that contemporary empirical patterns of richness have their origins in the same underlying processes, driven by climatic changes in the same landscapes, seems nearly inescapable.

By revealing the regions and periods of speciation, persistence, and extinction that underlie richness patterns, our results illuminate the role of history in shaping contemporary patterns of species richness on broad spatial scales—an emerging theme in the recent macroecological literature (*104-106*). Observed statistical correlations between contemporary richness patterns and current climate variables (*9*) should be viewed not as a direct causal link, but rather as a

consequence of accumulated historical events driven by geographically-structured climate dynamics (*86, 107*).

Methods

Geographical domain

The simulations took place on a gridded map of contemporary South America. The computational demands of spatially and temporally explicit simulations impose a limit on the complexity of simulation models at very high spatial resolutions. Nonetheless, at the large spatial and temporal scales at which we model ecological and evolutionary systems here, topographic heterogeneity, expressed as habitat diversity, is thought to be a key driver of species distributions and evolutionary niche dynamics. Thus, to capture as much of the climate heterogeneity of South America as feasible, while accounting for computational limits imposed by the spatial resolution of the geographic domain, we developed a map grid of "hybrid" spatial scale, in which the 4820 square map cells vary in size in inverse relation to topographical complexity. Cell sizes ranged from 625 km^2 in rugged areas of the Andean slopes, where environmental conditions vary greatly within short distances, to 10,000 km^2 in flatter regions, such as the Amazon Basin and Patagonia, where large areas have relatively similar environmental conditions (Fig. S1). Given the ecological and evolutionary mechanisms implemented in our simulation model (see below), the spatial resolution of our hybrid grid constitutes a balanced tradeoff between (1) the computational demand imposed by the number of map cells; (2) the inherent uncertainty in reconstructing terrestrial paleoclimate dynamics at high spatial resolution; (3) the organizational level of the mechanisms that drive the evolutionary dynamics of geographical ranges and climatic niches; and (4) the low resolution of current data on the distribution of real-world species (which we used to evaluate the predictions of the simulation model), and the consequent uncertainty of mapping empirical spatial patterns of biodiversity at higher resolutions.

Paleoclimate simulations

A paleoclimate emulator was developed to overcome the computational challenge of simulating 800,000 years of climate. The emulator was built around the PLASIM intermediate-complexity atmospheric general circulation model, coupled to the ENTS dynamic land surface model and to flux-corrected ocean and sea-ice models, at a 5° latitude-longitude resolution (*108*). Orbitally-forced climates at 500-year intervals were estimated using principal component emulation (*109*). A transient 800 ka simulation (*110*) with the faster GENIE-1 model was applied to scale these emulated climates for CO_2 and ice sheet climate forcing. Spatial resolution matching the hybrid-scale map was achieved by treating modeled climate variables as anomalies from contemporary climate data, spatially referenced to each map cell.

For each 500-year time interval, from 800 ka to the present (1600 time steps through the Late Quaternary glacial-interglacial cycles), the paleoclimate model assigned to each of the 4280 map cells an estimate of the mean temperature of the warmest and coolest quarters (henceforth *minimum* and *maximum annual temperature*) and the mean daily precipitation of the wettest and driest quarters (henceforth *minimum* and *maximum annual precipitation*) (Movie 1 and Fig. S2).

The temporal resolution of the 500-year interval between time steps is compatible with the macroecological framework used in this study. Assuming a species with a generation time of 5 years, one time step would encompass 100 generations, a reasonable resolution for the population-level biogeographical processes that we are modeling, such as dispersal, competition, range dynamics, and niche evolution. Thus, the full temporal scope of the simulation would encompass ~160,000 generations, well beyond a reasonable time for the emergence of medium-sized lineages (*4, 33, 34, 69, 70*). Indeed, a finer temporal resolution would probably convert the current model from the population/species level closer to the individual level of organization, requiring a full redesign of the implemented mechanisms (e.g. individual movement, birth-death processes).

Our 500-year resolution is also compatible with currently available knowledge of paleoclimate dynamics and the complexity of our paleoclimate emulator. In fact, our climate model

479 does not capture shorter-timescale variability in climate dynamics, because the emulator is built
480 from quasi-equilibrium snapshots, forced by only orbit, CO2, and ice-sheets and therefore does not
481 capture variability due to relatively short-term phenomena such as glacial meltwater-driven ocean
482 circulation changes, ENSO, or volcanic eruptions.

483 To evaluate the reliability of our paleoclimate emulator we compared spatial patterns of
484 temperature and precipitation variables, at specific time steps, against multi-model predictions
485 carried out by the Paleoclimate Model Inter-comparison Project, phases two and three
486 (PMIP2/PMIP3) (see *Comparisons against other paleoclimate models* in (*95*)). We focused the
487 validation of our emulator at three specific moments of the Quaternary: the Last Interglacial (LIG)
488 at ~126.5 ka (*111, 112*), the Last Glacial Maximum (LGM) at 21 ka (*112, 113*), and the mid-
489 Holocene (MH) climate optimum at 6 ka (*112, 113*). The LIG and MH interglacial states, with CO_2
490 and ice sheets similar to present day, provide an opportunity to validate our emulated response to
491 orbital forcing, while our estimates of paleoclimate at the LGM test the emulated response to very
492 different CO_2 and ice-sheet forcings. The climate patterns predicted by our model correspond
493 closely with existing predictions from complex, multi-model paleoclimate reconstructions,
494 suggesting that our emulator can be reliably used in biogeographical simulations, given currently
495 available parallel evidence from independent models.

496 *Biogeographical simulations*

497 In the simulations, geographical space was represented by the gridded map of South America (as
498 detailed above), with each grid cell characterized by its area and geographical position. Each
499 simulation began 800,000 years ago, advancing at 500-year time steps. At each time step, each map
500 cell was characterized by four climatic conditions (minimum and maximum temperature and
501 precipitation), as reconstructed by the paleoclimate simulations (Fig. 1, Movie 1)

502 *Populations and species*

503 The smallest biological unit explicitly modeled was regarded as a population, characterized as a
504 geographically isolated and continuous species range or range fragment. Thus, the complete range

of a species might consist of a single population or of multiple, isolated populations. At each time step, the niche of each population was defined as a two-dimensional region within temperature and precipitation axes, in the same space as the modeled paleoclimate of South America,.

Climatic niche and geographic distribution

We model the evolution of the *fundamental climatic niche* (*114*) of populations, which defines the extremes of temperature and precipitation that a population can tolerate at any given time step (Movie 2 and Fig. S7). Thus, cells occupied by a population must have climatic conditions within the limits of its fundamental niche. The *realized climatic niche* is an emergent property of the population, defined by the climatic conditions that it actually experiences across the whole set of *occupied* cells (e.g. population's range). However, not every cell with suitable climatic conditions is necessarily occupied by the population (Movie 1). Indeed, the bounds of the population's evolving fundamental climatic niche may at times extend beyond the limits of its realized niche (*115*), owing either to dispersal limitation (additional, climatically suitable regions currently exist, but cannot be reached), niche conservatism (the fundamental niche has not yet responded to the disappearance of previously suitable climates) (*26*), or exclusion by competing species (see below).

Founders

In each realization of the biogeographical simulation, an evolutionary lineage develops on the grid from a single founding species—initially a single population. The initial geographical range of the founder is determined by its assigned geographical location (a single map cell—an initial condition of the model, Table S2), and by a preset environmental niche (see section "*Initial conditions*" below).

Dispersal

Within each time step, each existing population expands its range to occupy not only adjacent cells, but also disjoint cells with suitable climates, as long as these cells are not separated by cells with unsuitable climate spanning a distance greater than D_{max} (a model parameter; Fig. 1 and Table S1).

All subsequent events are autonomous and deterministic (repeatable), driven by the interaction between climate, topography, and modeled processes.

Evolutionary niche dynamics and evolutionary rescue

The four paleoclimatic conditions in each cell change asynchronously over time and space. Climate dynamics may open opportunities for range expansion by turning an unsuitable cell into a suitable one (a *leading edge* cell of a shifting range). In this case, the population simply expands its range to occupy any newly suitable cell, whether contiguous or not, as long as the cell lies within D_{max} of the existing range. Climate change, however, may also render a suitable cell unsuitable (a *trailing edge* cell of a shifting range), imposing selection pressure on the population in the grid cell. The outcome of trailing-edge selection may be (1) local population extirpation in the trailing edge cell, if the population cannot adapt, or (2) niche evolution (partial or full adaptation to the new environmental conditions), allowing continued occupation of the trailing edge cell. In nature, selection pressure from climate change, especially in the trailing edge, may cause a gradual adaptive niche shift, bringing niche limits closer to new climatic limits within the current geographic range of the local population (*30, 116*). This process has been called "evolutionary rescue" (*82-85*), as it promotes species persistence by means of evolutionary changes in niche limits in response to selection pressure imposed by climate change.

We implemented niche evolution as a response to climate change in a simple, quantitative evolutionary genetics framework (*117, 118*). The evolutionary rate (H) required for sufficient niche adaptation to allow the population to persist in the trailing edge cell c may be estimated by comparing the magnitude of climate change between two consecutive time steps (t and $t + 1$) in cell c,

$$H_c = [(E_{c,t+1} - \bar{E}_t) / \sigma_t)] / \Delta t \ ,$$

where H_c is the adaptive rate necessary for evolutionary rescue (measured in units of Haldanes, (*119, 120*)), $E_{c,t+1}$ is the value of an environmental variable (e.g., maximum annual temperature) in cell c after climate change (time t+1), and $\bar{E}_t$ and σ_t are the average and standard deviation of the

same environmental variable, before climate change (time t), in all cells occupied by the local population within the *genetic neighborhood* of c (modeled as a circle centered at c, with radius D_{max}). Thus, in our model, genetic variation within a species' range is geographically structured, so that the evolutionary potential of each trailing-edge cell is set, at each time step, by the genetic variation for climate (standard deviation) within the genetic neighborhood of the cell.

In the simulation model, a maximum (critical) evolutionary rate in response to climate change (model parameter H_{max}, Table S1) is defined for all species, in all trailing-edge cells, uniformly throughout the entire time span of the simulation. Thus, for a trailing-edge cell c, if $H_c < H_{max}$ the population is rescued at c by adapting to the new climate, expanding its niche. Conversely, if $H_c > H_{max}$ the evolution required for persistence is beyond the maximum evolutionary potential of the population in cell c, and the population is extirpated from the cell.

Competition

In classical ecology, species with excessively similar resource requirements cannot coexist in sympatry (*121*). However, models on broad spatial scales must somehow account for the resources for which species compete, without modeling individual consumers and a myriad of resources and their respective depletion rates. We modeled interspecific competition, without explicitly modeling resources, by implementing the classic assumption that competition is an inverse function of phylogenetic relatedness (*122*), as measured by the explicit phylogeny generated by our model (*123*). Assuming that the use of resources by species (e.g. food items, foraging time/strategy) evolves at a constant average rate with variance proportional to time (i.e. a Brownian motion model of trait evolution), the expected intensity of competition between two species declines with phylogenetic distance (*PD*) between species. Once a pair of sister species achieves a threshold phylogenetic age of P_{min} (a model parameter, Fig. 1 and Table S1) since divergence, they may coexist in sympatry without competing.

Among the species in each map cell, each species competes against all others from which its phylogenetic distance is less than P_{min}. We quantified the *intensity of competition* between a pair of

582 species as 1 – (PD / P_{min}). Thus, the *total diffuse competition* affecting a particular species in a cell
583 is the summation of the pairwise intensities of competition between that species and all other
584 species present in the cell.

585 *Climatic stress*

586 Assuming that the environmental niche of a population is analogous to a fitness function,
587 individuals occurring in cells with extreme environmental conditions (with respect to the
588 environmental tolerances of the population) have lower fitness than conspecific individuals in
589 climatically more-suitable cells, leading to a lower population density. Conversely, because grid
590 cells with environmental conditions near the center of a population's environmental niche are more
591 suitable for the population, individuals in these cells are assumed to have higher fitness, leading to
592 higher population density. Thus, the cells mapping to the niche center for a species can be
593 considered to offer the most suitable (least stressful) environmental conditions, whereas cells
594 mapping near the niche limits can be considered as the most stressful environmental conditions that
595 nonetheless permit persistence.

596 We calculated an environmental stress index for each population, in each grid cell, at each
597 time step, as the ratio between (1) the environmental distances between maximum and minimum
598 environmental conditions within the cell and the niche center, and (2) the maximum environmental
599 scope tolerated by the population. (See *Environmental niche and ecological stress* in (*95*).) Thus, in
600 a cell with little seasonality and with average climatic conditions similar to the niche center of the
601 population, the population has a small environmental stress index. Conversely, a population has a
602 large environmental stress index if the scope of conditions in the cell spans the full range of the
603 climatic tolerance of the population (its niche breadth).

604 *Competitive exclusion*

605 If two coexisting species compete intensely in a particular cell, one of them may be extirpated from
606 the cell. The excluded species is likely to be the competitor under stronger environmental stress, as
607 its population density is likely to be lower. Thus, if the intensity of competition and/or

608 environmental stress is high, the population under greater environmental stress will be excluded
609 from the cell (see *Competitive exclusion* in (*95*)).

610 For our simulation model, the index of environmental stress and the index of the intensity of
611 competition were calculated for each population, in cell c, at each time step. These two indexes
612 were then added, for each population, resulting in a single *index of competition,* C_c, for each
613 population in each cell. All populations occupying a particular cell were then sorted according to
614 the magnitude of this combined index C_c. If the population with the highest competition index C_c
615 had a value greater than the maximum intensity of competition allowing coexistence, parameter
616 C_{max}, then that population was eliminated from the cell. The competition index was then re-
617 calculated for all remaining populations in the cell c, assuming the absence of the eliminated
618 population, and remaining populations were sorted again. If the population with the highest
619 competition index C_c again had an index greater than C_{max}, then that population is also removed.
620 The algorithm iterated until the population with highest competition index in the cell had an index
621 C_c that fell below the threshold C_{max}.

622 *Extinction*

623 The potential geographic distribution of species in our model at any given time step was constrained
624 by available climate, niche limits, dispersal limits, and competitive exclusion. A species became
625 extinct if, at any time step, its entire range was extirpated from all map cells, because of either
626 climate change or competition.

627 *Range fragmentation and coalescing populations*

628 Climate dynamics and competition may cause range fragmentation by imposing barriers of
629 unsuitable climate (Movie 2). When the geographic distribution (range) of an ancestor population
630 became fragmented into independent populations, all smaller populations inherited the
631 environmental niche of the ancestor population (Movie 2). However, due to founder effects and the
632 spatial structure of genetic variability, smaller populations did not inherit exactly the same niche
633 properties as larger populations. Thus, in our model, in the event of range fragmentation of an

ancestor population, the niche limits of the newly isolated, descendant populations were determined by the ancestral population's niche limits, local environmental conditions, and population size. (See *Environmental niche dynamics of fragmenting and coalescing populations* in (*95*).) Each population (range fragment) subsequently followed its own evolutionary course.

When the ranges of two populations of the same species were separated by a distance less than D_{max}, it was assumed that gene flow was reestablished, therefore coalescing the two populations. Although the niches of the two populations each contributed to the definition of the environmental niche of the newly coalesced population, smaller populations contributed less to the coalescent niche than larger populations. To account for this asymmetry, the contribution of each population was weighted by its range size (total area of occupied cells). Thus, the maximum and minimum tolerance limits of the newly coalesced population, for each niche dimension, were the average of the maximum and minimum tolerance limits of all coalescencing populations, weighted proportionally by their respective range sizes. See *Environmental niche dynamics of fragmenting and coalescing population* in (*95*).

Speciation

Populations that persisted in isolation beyond a threshold age for speciation T_{min} (a model parameter, Fig. 1 and Table S1) were assumed to be reproductively isolated and were thus subsequently treated as distinct species (Movie 2). As time passed in the simulation, surviving descendant lineages generated an explicit phylogeny and populated the gridded map, developing patterns of species richness, as species ranges came to overlap following evolutionary divergence (*secondary sympatry*).

Initial conditions

Certain initial conditions for the model were specified before launching each simulation (Table S2). A *center of origin* (one map cell) was defined for the original founder species, as well as its *initial niche* (minimum and maximum annual precipitation and temperature tolerated). The historical influence of founder species is believed to have great impact across all scales of spatial and

temporal biodiversity patterns (*124-126*). However, because our simulations did not aim to reconstruct any specific real-world lineage, we evaluated spatial patterns in South American biodiversity that emerged from four hypothetical founder lineages, covering the major climatic and geographic zones in South America: high-elevation tropical Andes, lowland Amazonia, lowland Atlantic rainforest, and lowland temperate Patagonia. (See *Experimental design and parameter exploration* in (*95*).)

Spatial and temporal environmental heterogeneity, particularly in the context of climate change, is widely believed to drive both the extinction and diversification of lineages (*81, 127-129*). In South America, the most extreme climatic heterogeneity is driven by the steep and rugged topography of the Andean mountain chain. Our simulations offer a unique opportunity to assess and quantify the role of topography-driven climatic heterogeneity in ecological and evolutionary modeled mechanisms, as manifested in patterns of cradles, museums, and graves. Thus, we applied a spatial smoothing function to the paleoclimate series, effectively simulating alternative *experimental topographies* in South America. The *climate smoothing factor* (an initial condition of each simulation), a specifies a smoothing level for all minimum and maximum annual precipitation and temperature maps in the paleoclimate series, thereby generating levels of experimental climatic heterogeneity that defined alternative South American topographies.

Experimental design and model evaluation

To understand the role of the mechanisms implemented in the model (Fig. 1) on emergent patterns of biodiversity, we ran 10,500 distinct simulations, with varying combinations of parameter settings and initial conditions. The factorial design of our simulation experiment consisted in running the model with all possible combinations of parameter values, as listed in *Summary of explored parameter levels and initial conditions* in (*95*). In our experimental design we integrated two strategies to define the range of values to be explored for each parameter: (1) a biologically informed definition of the minimum, maximum, and intermediate levels for each parameter, based on the biological interpretation and realism of the implemented process; and (2) a preliminary

686 experimental evaluation of the feasibility of the simulation, carried out by testing the proposed
687 extreme levels of each parameter. Here, we provide a summary of parameter exploration, but the
688 full conceptual justification may be found in (*95*).

689 *Parameter exploration*

690 (1) Maximum dispersal distance (D_{max}) is a parameter that sets the maximum geographic map
691 distance that a population can disperse across unsuitable climate, over one simulation step of 500
692 years, to occupy a climatically suitable cell. We specified three intermediate steps between the
693 minimum possible D_{max}, given our spatial resolution (150km), and the maximum D_{max} that we
694 considered biologically reasonable, given our temporal resolution (750km): 200km, 350km and
695 500km. (2) Maximum niche evolutionary rate (H_{max}) is a parameter that sets the upper limit of
696 potential climatic adaptation of the population in a trailing edge cell. After a preliminary
697 exploration for a meaningful range of H_{max} values, we set five levels, ranging between 0.005 and
698 0.02 Haldanes, which is, respectively, half and twice the theoretical expectation under natural
699 conditions (*117, 118*). (3) Minimum time for speciation (T_{min}) is a parameter that regulates the time
700 that a population must remain in genetic isolation before being declared a new species. Although
701 there are no theoretical bounds to T_{min} values (except zero), we set three levels for this parameter
702 (17.5, 20, and 22.5 kyr—or 3,500, 4,000, and 5,500 generations, assuming a generation time of 5
703 years), which we considered sufficient for an experimental exploration of meaningful variation in
704 simulated diversification rates. (4) Maximum intensity of competition allowing coexistence (C_{max})
705 is a parameter that sets the maximum intensity of competition that nonetheless permits coexistence
706 among competing species. We set the minimum experimental value of C_{max} to 1.5 units, which in
707 practice specifies that a species under maximum tolerable environmental stress can nonetheless
708 coexist with just one competing species that is phylogenetically close. We gradually explored larger
709 values of C_{max}, up to 5 units, a level at which a species under maximum tolerable environmental
710 stress would nonetheless be capable of coexisting with up to four very closely related species. (5)
711 Minimum phylogenetic divergence for coexistence without competition (P_{min}) is a parameter that

712 regulates the phylogenetic distance (PD) beyond which a pair of sister species could no longer
713 compete. Because of the mechanistic association between P_{min} and C_{max}, we held P_{min} at the fixed
714 value of 30,000 generations (150,000 years), to optimize the use of computational resources.

715 *Quantifying the importance of modeled mechanisms*

716 Our experimental design for parameter exploration allowed us to estimate the relative importance of
717 the ecological and evolutionary processes implemented in the simulation model, as they were
718 regulated by parameters and initial conditions. The relative importance of these processes was
719 assessed by quantifying the relative magnitude of divergence among the species richness patterns
720 produced by the model as a consequence of experimental variation of model parameters, each of
721 which regulates one or more of the processes implemented. To quantify the relative influence of
722 initial conditions and parameters we employed a series of Analyses of Molecular Variance
723 (AMOVA) analyses of the simulated spatial patterns in species richness.

724 *Evaluating model performance*

725 The exploration of parameter space was not designed to replicate the real-world diversity pattern of
726 any extant or extinct group of species or lineages. Nonetheless, we evaluated the correspondence
727 between the predictions of our model and contemporary, empirical patterns of species richness of
728 birds, mammals, and plants of South America. To compare our results with published
729 macroecological data at similar spatial resolution, and because of uncertainty in the geographic
730 distribution of real-world species, we created a regular grid of 1659 square cells, each measuring 1
731 degree of latitude-longitude. We re-projected the maps of simulated species, from the higher
732 resolution grid used for simulation, into this lower-resolution grid, and re-calculated spatial patterns
733 in total, cradle, museum, and grave species richness. Because we aimed to compare predictions of
734 our model against empirical richness patterns, we included in this analysis only the patterns in
735 species richness emerging from the 1500 simulations that used real-world South American
736 topography, excluding from the analysis all simulations that assumed alternative, experimental
737 South American topographies. We used simple OLS regression to estimate the coefficient of

738 determination (r^2) of the relationship between empirical maps of species richness (response
739 variable) and simulated maps of species richness variables (predictor variable) See *Contrasting*
740 *empirical and simulated spatial patterns in species richness* in (*95*).

741 **References and Notes**

742 1. C. Körner, E. M. Spehn, *Mountain Biodiversity: A Global Assessment* (Parthenon New
743 York, 2002).
744 2. W. Barthlott *et al.*, Geographic patterns of vascular plant diversity at continental to global
745 scales (Geographische Muster der Gefäßpflanzenvielfalt im kontinentalen und globalen
746 Maßstab). *Erdkunde*, 305-315 (2007).
747 3. B. R. Riddle, Comparative phylogeography clarifies the complexity and problems of
748 continental distribution that drove AR Wallace to favor islands. *Proc. Natl. Acad. Sci.*
749 *U.S.A.* **113**, 7970-7977 (2016).
750 4. J. Fjeldså, R. C. Bowie, C. Rahbek, The role of mountain ranges in the diversification of
751 birds. *Annu. Rev. Ecol. Evol. Syst.* **43**, 249-265 (2012).
752 5. M. Kessler, L. Salazar, J. Homeier, J. Kluge, Species richness–productivity relationships of
753 tropical terrestrial ferns at regional and local scales. *J. Ecol.* **102**, 1623-1633 (2014).
754 6. R. G. Davies *et al.*, Topography, energy and the global distribution of bird species richness.
755 *Proc. R. Soc. London Ser. B* **274**, 1189-1197 (2007).
756 7. D. Storch *et al.*, Energy, range dynamics and global species richness patterns: reconciling
757 mid-domain effects and environmental determinants of avian diversity. *Ecol. Lett.* **9**, 1308-
758 1320 (2006).
759 8. W. Jetz, C. Rahbek, Geometric constraints explain much of the species richness pattern in
760 African birds. *Proc. Natl. Acad. Sci. USA* **98**, 5661-5666 (2001).
761 9. B. A. Hawkins *et al.*, Energy, water, and broad-scale geographic patterns of species
762 richness. *Ecology* **84**, 3105–3117 (2003).
763 10. C. Rahbek, G. R. Graves, Multiscale assessment of patterns of avian species richness. *Proc.*
764 *Natl. Acad. Sci. USA* **98**, 4534–4539 (2001).

11. M. A. M. de Aguiar, M. Baranger, E. M. Baptestini, L. Kaufman, Y. Bar-Yam, Global patterns of speciation and diversity. *Nature* **460**, 384-387 (2009).

12. G. G. Mittelbach *et al.*, Evolution and the latitudinal diversity gradient: speciation, extinction and biogeography. *Ecol. Lett.* **10**, 315-331 (2007).

13. J. J. Wiens, Speciation and ecology revisited: phylogenetic niche conservatism and the origin of species. *Evolution* **58**, 193-197 (2004).

14. C. Graham, S. Ron, J. Santos, C. Schneider, C. Moritz, Integrating phylogenetics and environmental niche models to explore speciation mechanisms in dendrobatid frogs. *Evolution* **58**, 1781-1793 (2004).

15. M. Doebeli, U. Dieckmann, Speciation along environmental gradients. *Nature* **421**, 259-264 (2003).

16. K. Roy, E. E. Goldberg, Origination, extinction, and dispersal: integrative models for understanding present-day diversity gradients. *Am. Nat.* **170**, S71-S85 (2007).

17. J. Rosindell, L. J. Harmon, R. S. Etienne, Unifying ecology and macroevolution with individual-based theory. *Ecol. Lett.* **18**, 472-482 (2015).

18. S. R. Connolly, S. A. Keith, R. K. Colwell, C. Rahbek, Process, mechanism, and modeling in macroecology. *Trends Ecol. Evol.* **32**, 835-844 (2017).

19. N. Gotelli *et al.*, Patterns and causes of species richness: a general simulation model for macroecology. *Ecol. Lett.* **12**, 873-886 (2009).

20. J. S. Cabral, L. Valente, F. Hartig, Mechanistic simulation models in macroecology and biogeography: state-of-art and prospects. *Ecography* **40**, 267–280 (2017).

21. R. Barnes, A. T. Clark, Sixty-five million years of change in temperature and topography explain evolutionary history in Eastern North American plethodontid salamanders. *Am. Nat.* **190**, E000-E000 (2017).

22. R. K. Colwell, T. F. Rangel, A stochastic, evolutionary model for range shifts and richness on tropical elevational gradients under Quaternary glacial cycles. *Phil. Trans. R. Soc. London Ser. B* **365** 3695–3707 (2010).

792 23. T. F. L. V. B. Rangel, J. A. F. Diniz-Filho, R. K. Colwell, Species richness and evolutionary
793 niche dynamics: a spatial pattern-oriented simulation experiment. *Am. Nat.* **170**, 602-616
794 (2007).
795 24. C. Rahbek *et al.*, Predicting continental-scale patterns of bird species richness with spatially
796 explicit models. *Proc. R. Soc. London Ser. B* **274**, 165-174 (2007).
797 25. H. Qiao, E. E. Saupe, J. Soberón, A. T. Peterson, C. E. Myers, Impacts of niche breadth and
798 dispersal ability on macroevolutionary patterns. *Am. Nat.* **188**, 149-162 (2016).
799 26. J. W. Williams, S. T. Jackson, J. E. Kutzbach, Projected distributions of novel and
800 disappearing climates by 2100 AD. *Proc. Natl. Acad. Sci. U.S.A.* **104**, 5738 (2007).
801 27. F. A. La Sorte, W. Jetz, Projected range contractions of montane biodiversity under global
802 warming. *Proc. R. Soc. London Ser. B*, rspb20100612 (2010).
803 28. K. A. Jønsson *et al.*, Tracking animal dispersal: from individual movement to community
804 assembly and global range dynamics. *Trends Ecol. Evol.* **31**, 204-214 (2016).
805 29. J. M. Alexander, J. M. Diez, S. P. Hart, J. M. Levine, When climate reshuffles competitors:
806 a call for experimental macroecology. *Trends in Ecology and Evolution* **31**, 831-841 (2016).
807 30. D. D. Ackerly, Community assembly, niche conservatism, and adaptive evolution in
808 changing environments. *Int. J. Plant Sci.* **164**, S165-S184 (2003).
809 31. J. T. Weir, E. Bermingham, M. J. Miller, J. Klicka, M. A. González, Phylogeography of a
810 morphologically diverse Neotropical montane species, the Common Bush-Tanager
811 (Chlorospingusophthalmicus). *Mol. Phylogen. Evol.* **47**, 650-664 (2008).
812 32. B. T. Smith *et al.*, The drivers of tropical speciation. *Nature* **515**, 406 (2014).
813 33. J. T. Weir, Divergent timing and patterns of species accumulation in lowland and highland
814 neotropical birds. *Evolution* **60**, 842-855 (2006).
815 34. J. T. Weir, Implications of genetic differentiation in Neotropical montane forest birds. *Ann.*
816 *Mo. Bot. Gard.* **96**, 410-433 (2009).

817 35. E. F. Toussaint, K. Sagata, S. Surbakti, L. Hendrich, M. Balke, Australasian sky islands act
818 as a diversity pump facilitating peripheral speciation and complex reversal from narrow
819 endemic to widespread ecological supertramp. *Ecol. Evol.* **3**, 1031-1049 (2013).
820 36. J. T. Weir, D. Schluter, The latitudinal gradient in recent speciation and extinction rates of
821 birds and mammals. *Science* **315**, 1574-1576 (2007).
822 37. K. Gregory-Wodzicki, Uplift history of the Central and Northern Andes: a review. *Geol.*
823 *Soc. Am. Bull.* **112**, 1091 (2000).
824 38. A. Antonelli, I. Sanmartín, Why are there so many plant species in the Neotropics? *Taxon*
825 **60**, 403-414 (2011).
826 39. F. Luebert, M. Weigend, Phylogenetic insights into Andean plant diversification. *Front.*
827 *Ecol. Evol.* **2**, 27 (2014).
828 40. C. Hoorn *et al.*, Amazonia through time: Andean uplift, climate change, landscape
829 evolution, and biodiversity. *Science* **330**, 927-931 (2010).
830 41. F. M. Chapman *et al.*, The distribution of bird-life in Ecuador: a contribution to a study of
831 the origin of Andean bird-life. *Bull. Am. Mus. Nat. Hist. N. Y.* **55**, (1926).
832 42. M. J. Miller *et al.*, Out of Amazonia again and again: episodic crossing of the Andes
833 promotes diversification in a lowland forest flycatcher. *Proc. R. Soc. B* **275**, 1133-1142
834 (2008).
835 43. L. Struwe, S. Haag, E. Heiberg, J. R. Grant, Andean speciation and vicariance in
836 Neotropical *Macrocarpaea* (Gentianaceae–Helieae). *Ann. Mo. Bot. Gard.* **96**, 450-469
837 (2009).
838 44. G. R. Graves, Elevational correlates of speciation and intraspecific geographic variation in
839 plumage in Andean forest birds. *Auk* **102**, 556-579 (1985).
840 45. M. T. Burrows *et al.*, Geographical limits to species-range shifts are suggested by climate
841 velocity. *Nature* **507**, 492 (2014).

842 46. J. Fjeldså, Geographical patterns for relict and young species of birds in Africa and South
843 America and implications for conservation priorities. *Biodivers. Conserv.* **3**, 207-226
844 (1994).
845 47. B. Sandel *et al.*, The influence of Late Quaternary climate-change velocity on species
846 endemism. *Science* **334**, 660-664 (2011).
847 48. A. Hampe, A. S. Jump, Climate relicts: past, present, future. *Annu. Rev. Ecol. Evol. Syst.* **42**,
848 313-333 (2011).
849 49. B. G. Valencia *et al.*, Andean microrefugia: testing the Holocene to predict the
850 Anthropocene. *New Phytol.* **212**, 510-522 (2016).
851 50. R. T. Pennington, M. Lavin, A. Oliveira-Filho, Woody plant diversity, evolution, and
852 ecology in the tropics: perspectives from seasonally dry tropical forests. *Annu. Rev. Ecol.*
853 *Evol. Syst.* **40**, 437-457 (2009).
854 51. H. Batalha-Filho, J. Fjeldså, P.-H. Fabre, C. Y. Miyaki, Connections between the Atlantic
855 and the Amazonian forest avifaunas represent distinct historical events. *J. Ornithol.* **154**, 41-
856 50 (2013).
857 52. R. M. D. Ledo, G. R. Colli, The historical connections between the Amazon and the Atlantic
858 Forest revisited. *J. Biogeogr.* **44**, 2551-2563 (2017).
859 53. J. M. C. da Silva, Biogeographic analysis of the South American Cerrado avifauna.
860 *Steenstrupia* **21**, 49-67 (1995).
861 54. A. R. Percequillo, M. Weksler, L. P. Costa, A new genus and species of rodent from the
862 Brazilian Atlantic Forest (Rodentia: Cricetidae: Sigmodontinae: Oryzomyini), with
863 comments on oryzomyine biogeography. *Zool. J. Linn. Soc.* **161**, 357-390 (2011).
864 55. S. R. Gradstein, M. E. Reiner-Drehwald, The status of *Neopotamolejeunea* (Lejeuneaceae)
865 and description of a new species from Ecuador and Southern Brazil. *Syst. Bot.* **32**, 487-492
866 (2007).

867 56. M. Gehara *et al.*, High levels of diversity uncovered in a widespread nominal taxon:
868 continental phylogeography of the Neotropical tree frog *Dendropsophus minutus*. *PLoS One*
869 **9**, e103958 (2014).
870 57. F. D. Por, *Sooretama, the Atlantic Rain Forest of Brazil* (SPB Academic Publishing, 1992).
871 58. I. Prates, D. Rivera, M. T. Rodrigues, A. C. Carnaval, A mid-Pleistocene rainforest corridor
872 enabled synchronous invasions of the Atlantic Forest by Amazonian anole lizards. *Mol.*
873 *Ecol.* **25**, 5174-5186 (2016).
874 59. N. Trujillo-Arias *et al.*, The niche and phylogeography of a passerine reveal the history of
875 biological diversification between the Andean and the Atlantic forests. *Mol. Phylogen. Evol.*
876 **112**, 107-121 (2017).
877 60. J. W. Lynch Alfaro *et al.*, Explosive Pleistocene range expansion leads to widespread
878 Amazonian sympatry between robust and gracile capuchin monkeys. *J. Biogeogr.* **39**, 272-
879 288 (2012).
880 61. D. E. Prado, P. E. Gibbs, Patterns of species distributions in the dry seasonal forests of
881 South America. *Ann. Mo. Bot. Gard.* **80**, 902-927 (1993).
882 62. H. Cheng *et al.*, Climate change patterns in Amazonia and biodiversity. *Nature Comms.* **4**,
883 1411 (2013).
884 63. X. Wang *et al.*, Hydroclimate changes across the Amazon lowlands over the past 45,000
885 years. *Nature* **541**, 204 (2017).
886 64. S. A. Cowling, M. A. Maslin, M. T. Sykes, Paleovegetation simulations of lowland
887 Amazonia and implications for neotropical allopatry and speciation. *Quatern. Res.* **55**, 140-
888 149 (2001).
889 65. D. Lüthi *et al.*, High-resolution carbon dioxide concentration record 650,000-800,000 years
890 before present. *Nature* **453**, 379 (2008).
891 66. R. Morley, "Cretaceous and Tertiary climate change and the past distribution of
892 megathermal rainforests" in *Tropical Rainforest Responses to Climatic Change,* M. Bush, J.
893 Flenley, W. Gosling, Eds. (Springer, 2011), pp. 1-34.

894 67. H. Hooghiemstra, T. Van der Hammen, Quaternary Ice-Age dynamics in the Colombian
895 Andes: developing an understanding of our legacy. *Phil. Trans. R. Soc. London Ser. B* **359**,
896 173-181 (2004).
897 68. K. M. Kay, P. A. Reeves, R. G. Olmstead, D. W. Schemske, Rapid speciation and the
898 evolution of hummingbird pollination in neotropical *Costus* subgenus *Costus* (Costaceae):
899 evidence from nrDNA ITS and ETS sequences. *Am. J. Bot.* **92**, 1899 (2005).
900 69. J. Fjeldså, C. Rahbek, Diversification of Tanagers, a species rich bird group, from lowlands
901 to montane regions in South America. *Integr. Comp. Biol.* **46**, 72-78 (2006).
902 70. C. Moritz, J. Patton, C. Schneider, T. Smith, Diversification of rainforest faunas: an
903 integrated molecular approach. *Annu. Rev. Ecol. Syst.*, 533-563 (2000).
904 71. M. B. Bush, M. R. Silman, D. H. Urrego, 48,000 years of climate and forest change in a
905 biodiversity hot spot. *Science* **303**, 827-829 (2004).
906 72. F. E. Mayle, R. Burbridge, T. J. Killeen, Millennial-scale dynamics of southern Amazonian
907 rain forests. *Science* **290**, 2291-2294 (2000).
908 73. G. L. Stebbins, *Flowering Plants: Evolution Above the Species Level* (Harvard University
909 Press, 1974).
910 74. S. L. Chown, K. J. Gaston, Areas, cradles and museums: the latitudinal gradient in species
911 richness. *Trends Ecol. Evol.* **15**, 311-315 (2000).
912 75. D. Jablonski, K. Roy, J. W. Valentine, Out of the tropics: evolutionary dynamics of the
913 latitudinal diversity gradient. *Science* **314**, 102-106 (2006).
914 76. H. Arita, E. Vazquez-Dominguez, The tropics: cradle, museum or casino? A dynamic null
915 model for latitudinal gradients of species diversity. *Ecol. Lett.* **11**, 653–663 (2008).
916 77. N. C. Stenseth, The tropics: cradle or museum? *Oikos* **43**, 417-420 (1984).
917 78. D. D. McKenna, B. D. Farrell, Tropical forests are both evolutionary cradles and museums
918 of leaf beetle diversity. *Proc. Natl. Acad. Sci. U.S.A.* **103**, 10947-10951 (2006).

79. L. Excoffier, P. E. Smouse, J. M. Quattro, Analysis of molecular variance inferred from metric distances among DNA haplotypes: application to human mitochondrial DNA restriction data. *Genetics* **131**, 479-491 (1992).

80. M. J. Anderson, A new method for non-parametric multivariate analysis of variance. *Austral Ecol.* **26**, 32-46 (2001).

81. T. J. Killeen, M. Douglas, T. Consiglio, P. M. Jørgensen, J. Mejia, Dry spots and wet spots in the Andean hotspot. *J. Biogeogr.* **34**, 1357-1373 (2007).

82. R. Gomulkiewicz, R. D. Holt, When does evolution by natural selection prevent extinction? *Evolution* **49**, 201-207 (1995).

83. G. Bell, Evolutionary Rescue. *Annu. Rev. Ecol. Evol. Syst.* **48**, 605-627 (2017).

84. A. Gonzalez, O. Ronce, R. Ferriere, M. E. Hochberg, Evolutionary rescue: an emerging focus at the intersection between ecology and evolution. *Phil. Trans. R. Soc. B* **368**, 1610 (2013).

85. S. M. Carlson, C. J. Cunningham, P. A. Westley, Evolutionary rescue in a changing world. *Trends Ecol. Evol.* **29**, 521-530 (2014).

86. R. Jansson, M. Dynesius, The fate of clades in a world of recurrent climate change: Milankovitch oscillations and evolution. *Annu. Rev. Ecol. Syst.* **33**, 741-777 (2002).

87. C. R. Hutter, J. M. Guayasamin, J. J. Wiens, Explaining Andean megadiversity: the evolutionary and ecological causes of glassfrog elevational richness patterns. *Ecol. Lett.* **16**, 1135-1144 (2013).

88. L. P. Costa, The historical bridge between the Amazon and the Atlantic Forest of Brazil: a study of molecular phylogeography with small mammals. *J. Biogeogr.* **30**, 71-86 (2003).

89. R. Linares-Palomino, A. T. Oliveira-Filho, R. T. Pennington, "Neotropical seasonally dry forests: diversity, endemism, and biogeography of woody plants" in *Seasonally Dry Tropical Forests*. (Springer, 2011), pp. 3-21.

90. A. Rozas-Davila, B. G. Valencia, M. B. Bush, The functional extinction of Andean megafauna. *Ecology* **97**, 2533-2539 (2016).

946 91. A. Cooper *et al.*, Abrupt warming events drove Late Pleistocene Holarctic megafaunal
947 turnover. *Science* **349**, 602-606 (2015).
948 92. A. D. Barnosky, E. L. Lindsey, Timing of Quaternary megafaunal extinction in South
949 America in relation to human arrival and climate change. *Quatern. Intl.* **217**, 10-29 (2010).
950 93. S. R. Loarie *et al.*, The velocity of climate change. *Nature* **462**, 1052-1055 (2009).
951 94. A. Ordonez, J. W. Williams, J.-C. Svenning, Mapping climatic mechanisms likely to favour
952 the emergence of novel communities. *Nat. Clim. Change* **6**, 1104-1109 (2016).
953 95. p. Supplementary materials.
954 96. F. E. Hayes, J. A. N. Sewlal, The Amazon River as a dispersal barrier to passerine birds:
955 effects of river width, habitat and taxonomy. *J. Biogeogr.* **31**, 1809-1818 (2004).
956 97. P. Tzedakis *et al.*, Interglacial diversity. *Nat. Geosci.* **2**, 751-755 (2009).
957 98. B. W. Nelson, C. A. Ferreira, M. F. da Silva, M. L. Kawasaki, Endemism centres, refugia
958 and botanical collection density in Brazilian Amazonia. *Nature* **345**, 714-716 (1990).
959 99. J. J. Wiens, C. H. Graham, Niche conservatism: integrating evolution, ecology, and
960 conservation biology. *Annu. Rev. Ecol. Evol. Syst.* **36**, 519-539 (2005).
961 100. J. Losos, Phylogenetic niche conservatism, phylogenetic signal and the relationship between
962 phylogenetic relatedness and ecological similarity among species. *Ecol. Lett.* **11**, 995-1003
963 (2008).
964 101. J. J. Wiens *et al.*, Niche conservatism as an emerging principle in ecology and conservation
965 biology. *Ecol. Lett.* **13**, 1310-1324 (2010).
966 102. A. Duputié, F. Massol, I. Chuine, M. Kirkpatrick, O. Ronce, How do genetic correlations
967 affect species range shifts in a changing environment? *Ecol. Lett.* **15**, 251-259 (2012).
968 103. A. A. Hoffmann, C. M. Sgrò, Climate change and evolutionary adaptation. *Nature* **470**, 479
969 (2011).
970 104. J. Wiens, M. Donoghue, Historical biogeography, ecology and species richness. *Trends*
971 *Ecol. Evol.* **19**, 639-644 (2004).

105. G. Mittelbach *et al.*, Evolution and the latitudinal diversity gradient: speciation, extinction and biogeography. *Ecol. Lett.* **10**, 315-331 (2007).

106. D. Schluter, M. W. Pennell, Speciation gradients and the distribution of biodiversity. *Nature* **546**, 48-55 (2017).

107. T. S. Romdal, M. B. Araújo, C. Rahbek, Life on a tropical planet: niche conservatism and the global diversity gradient. *Global Ecol. Biogeogr.* **22**, 344-350 (2013).

108. P. Holden *et al.*, PLASIM-ENTSem v1. 0: a spatio-temporal emulator of future climate change for impacts assessment. *Geosci. Model Dev.* **7**, 433-451 (2014).

109. P. B. Holden, N. R. Edwards, P. H. Garthwaite, R. D. Wilkinson, Emulation and interpretation of high-dimensional climate model outputs. *J. Appl. Stat.* **42**, 2038-2055 (2015).

110. P. B. Holden, N. Edwards, K. I. C. Oliver, T. Lenton, R. Wilkinson, A probabilistic calibration of climate sensitivity and terrestrial carbon change in GENIE-1. *Clim. Dyn.* **35**, 785-806 (2010).

111. D. Lunt *et al.*, A multi-model assessment of last interglacial temperatures. *Clim. Past* **9**, 699-717 (2013).

112. V. Masson-Delmotte *et al.*, Information from paleoclimate archives. *Climate change* **383464**, 2013 (2013).

113. P. Braconnot *et al.*, Results of PMIP2 coupled simulations of the Mid-Holocene and Last Glacial Maximum–Part 1: experiments and large-scale features. *Clim. Past* **3**, 261-277 (2007).

114. J. Soberon, Grinnellian and Eltonian niches and geographic distributions of species. *Ecol. Lett.* **10**, 1115-1123 (2007).

115. R. K. Colwell, T. F. Rangel, Hutchinson's duality: the once and future niche. *Proc. Natl. Acad. Sci. USA* **106**, 19651-19658 (2009).

116. R. D. Holt, On the evolutionary ecology of species' ranges. *Evol. Ecol. Res.* **5**, 159-178 (2003).

117. R. Burger, M. Lynch, Evolution and extinction in a changing environment: a quantitative-genetic analysis. *Evolution* **49**, 151-163 (1995).

118. M. Kopp, S. Matuszewski, Rapid evolution of quantitative traits: theoretical perspectives. *Evol. Appl.* **7**, 169-191 (2014).

119. P. D. Gingerich, Quantification and comparison of evolutionary rates. *Am. J. Sci.* **293**, 453 (1993).

120. P. D. Gingerich, "Rates of evolution on the time scale of the evolutionary process" in *Microevolution Rate, Pattern, Process,* A. P. Hendry, M. T. Kinnison, Eds. (Springer, 2001), pp. 127-144.

121. R. H. MacArthur, *Geographical Ecology: Patterns in the Distribution of Species* (Harper and Row, New York, 1972), pp. 269.

122. C. Darwin, *The Origin of Species by Means of Natural Selection* (Murray, London, 1859), pp. 812.

123. J. Cavender-Bares, K. H. Kozak, P. V. Fine, S. W. Kembel, The merging of community ecology and phylogenetic biology. *Ecol. Lett.* **12**, 693-715 (2009).

124. R. G. Moyle, C. E. Filardi, C. E. Smith, J. Diamond, Explosive Pleistocene diversification and hemispheric expansion of a “great speciator”. *Proc. Natl. Acad. Sci. U.S.A.* **106**, 1863-1868 (2009).

125. R. Ricklefs, "Speciation, extinction and diversity" in *Speciation and Patterns of Diversity,* R. Butlin, J. Bridle, D. Schluter, Eds. (2009), chap. 257-277.

126. J. M. Waters, C. I. Fraser, G. M. Hewitt, Founder takes all: density-dependent processes structure biodiversity. *Trends Ecol. Evol.* **28**, 78-85 (2013).

127. J. Terborgh, Bird species diversity on an Andean elevational gradient. *Ecology* **58**, 1007-1019 (1977).

128. G. Vivian-Smith, Microtopographic heterogeneity and floristic diversity in experimental wetland communities. *J. Ecol.* **85**, 71-82 (1997).

129. A. Stein, K. Gerstner, H. Kreft, Environmental heterogeneity as a universal driver of species richness across taxa, biomes and spatial scales. *Ecol. Lett.* **17**, 866-880 (2014).

130. R. J. Hijmans, S. E. Cameron, J. L. Parra, P. G. Jones, A. Jarvis, Very high resolution interpolated climate surfaces for global land areas. *Int. J. Climatol.* **25**, 1965-1978 (2005).

131. K. Fraedrich, A suite of user-friendly global climate models: hysteresis experiments. *The European Physical Journal Plus* **127**, 53 (2012).

132. K. Fraedrich, E. Kirk, U. Luksch, F. Lunkeit, The portable university model of the atmosphere (PUMA): Storm track dynamics and low-frequency variability. *Meteorologische Zeitschrift* **14**, 735-745 (2005).

133. M. Williamson, T. Lenton, J. Shepherd, N. Edwards, An efficient numerical terrestrial scheme (ENTS) for Earth system modelling. *Ecol. Model.* **198**, 362-374 (2006).

134. P. Holden, N. Edwards, Dimensionally reduced emulation of an AOGCM for application to integrated assessment modelling. *Geophys. Res. Lett.* **37**, (2010).

135. A. Berger, Long-term variations of caloric insolation resulting from the Earth's orbital elements. *Quatern. Res.* **9**, 139-167 (1978).

136. N. R. Edwards, R. Marsh, Uncertainties due to transport-parameter sensitivity in an efficient 3-D ocean-climate model. *Clim. Dyn.* **24**, 415-433 (2005).

137. P. Holden *et al.*, Interhemispheric coupling, the West Antarctic Ice Sheet and warm Antarctic interglacials. *Clim. Past* **6**, 431-443 (2010).

138. D. Lüthi *et al.*, High-resolution carbon dioxide concentration record 650,000–800,000 years before present. *Nature* **453**, 379-382 (2008).

139. W. R. Peltier, Ice age paleotopography. *Science* **265**, 195-201 (1994).

140. L. E. Lisiecki, M. E. Raymo, A Pliocene-Pleistocene stack of 57 globally distributed benthic δ18O records. *Paleoceanography* **20**, (2005).

141. T. J. Osborn, C. J. Wallace, I. C. Harris, T. M. Melvin, Pattern scaling using ClimGen: monthly-resolution future climate scenarios including changes in the variability of precipitation. *Clim. Change* **134**, 353-369 (2016).

142. C. S. Turney, R. T. Jones, Does the Agulhas Current amplify global temperatures during super-interglacials? *J. Quatern. Sci.* **25**, 839-843 (2010).

143. B. L. Otto-Bliesner *et al.*, How warm was the last interglacial? New model–data comparisons. *Phil. Trans. R. Soc. A* **371**, 20130097 (2013).

144. G. Bell, Evolutionary rescue and the limits of adaptation. *Phil. Trans. R. Soc. B* **368**, 20120080 (2013).

145. B. F. J. Manley, *The Statistics of Natural Selection* (Chapman & Hall, London, 1985).

146. M. Lynch, B. Walsh, *Genetics and Analysis of Quantitative Traits* (Sinauer Sunderland, MA, 1998), vol. 1.

147. M. J. Angilletta, *Thermal Adaptation: A Theoretical and Empirical Synthesis* (Oxford University Press, USA, 2009).

148. S. Matsumura, R. Arlinghaus, U. Dieckmann, Standardizing selection strengths to study selection in the wild: a critical comparison and suggestions for the future. *Bioscience* **62**, 1039-1054 (2012).

149. G. Martin, R. Aguilée, J. Ramsayer, O. Kaltz, O. Ronce, The probability of evolutionary rescue: towards a quantitative comparison between theory and evolution experiments. *Phil. Trans. R. Soc. B* **368**, 20120088 (2013).

150. M. Kirkpatrick, N. H. Barton, Evolution of a species' range. *Am. Nat.* **150**, 1-23 (1997).

151. J. Grinnell, The origin and distribution of the chest-nut-backed chickadee. *The Auk* **21**, 364-382 (1904).

152. F. Gause, *The Struggle for Existence* (Williams and Wilkins, Baltimore, 1934).

153. G. E. Hutchinson, The paradox of the plankton. *Am. Nat.* **95**, 137-145 (1961).

154. G. Hardin, The competitive exclusion principle. *Science* **131**, 1292-1297 (1960).

155. R. H. MacArthur, Population ecology of some warblers of northeastern coniferous forests. *Ecology* **39**, 599-619 (1958).

156. R. Levins, *Evolution in Changing Environments* (Princeton University Press, Princeton, N. J., 1968).

1079 157. E. R. Pianka, Niche overlap and diffuse competition. *Proc. Natl. Acad. Sci. U.S.A.* **71**, 2141-
1080 2145 (1974).
1081 158. L. L. Knowles, Tests of Pleistocene speciation in montane grasshoppers (genus *Melanoplus*)
1082 from the sky islands of western North America. *Evolution* **54**, 1337-1348 (2000).
1083 159. R. T. Pennington *et al.*, Contrasting plant diversification histories within the Andean
1084 biodiversity hotspot. *Proc. Natl. Acad. Sci. U.S.A.* **107**, 13783-13787 (2010).
1085 160. C. Hughes, R. Eastwood, Island radiation on a continental scale: Exceptional rates of plant
1086 diversification after uplift of the Andes. *Proc. Natl. Acad. Sci. USA* **103**, 10334-10339
1087 (2006).
1088 161. L. B. Buckley *et al.*, Phylogeny, niche conservatism and the latitudinal diversity gradient in
1089 mammals. *Proc. R. Soc. London Ser. B*, rspb20100179 (2010).
1090 162. J. A. Coyne, H. A. Orr, *Speciation* (Sinauer Associates, Inc, Sunderland, MA, 2004).
1091 163. A. P. Hendry, J. K. Wenburg, P. Bentzen, E. C. Volk, T. P. Quinn, Rapid evolution of
1092 reproductive isolation in the wild: evidence from introduced salmon. *Science* **290**, 516-518
1093 (2000).
1094 164. A. M. Latimer, J. A. Silander, R. M. Cowling, Neutral ecological theory reveals isolation
1095 and rapid speciation in a biodiversity hot spot. *Science* **309**, 1722-1725 (2005).
1096 165. S. R. Palumbi, Genetic divergence, reproductive isolation, and marine speciation. *Annu.*
1097 *Rev. Ecol. Syst.* **25**, 547-572 (1994).
1098 166. C. O. Webb, D. D. Ackerly, M. A. McPeek, M. J. Donoghue, Phylogenies and community
1099 ecology. *Annu. Rev. Ecol. Syst.*, 475-505 (2002).
1100 167. C. O. Webb, Exploring the phylogenetic structure of ecological communities: an example
1101 for rain forest trees. *Am. Nat.* **156**, 145-155 (2000).
1102 168. B. B. Simpson, Pleistocene changes in the flora of the high tropical Andes. *Paleobiology* **1**,
1103 273-294 (1975).
1104 169. B. B. Simpson, An historical phytogeography of the high Andean flora. *Rev. Chil. Hist. Nat.*
1105 **56**, (1983).

170. C. Rahbek, L. Hansen, J. Fjeldså, One degree resolution database of the global distribution of birds. *Natural History Museum of Denmark, University of Copenhagen, Denmark*, (2012).

171. B. G. Holt *et al.*, An update of Wallace's zoogeographic regions of the world. *Science* **339**, 74-78 (2013).

172. C. Rahbek, G. R. Graves, Detection of macro-ecological patterns in South American hummingbirds is affected by spatial scale. *Proc. R. Soc. London Ser. B* **267**, 2259-2265 (2000).

173. IUCN, Digital distribution maps of the IUCN red list of threatened species. Version 5.2. Downloaded August 2017. http://www.iucnredlist.org. (2017).

174. B. J. Enquist, R. Condit, R. K. Peet, M. Schildhauer, B. M. Thiers, "Cyberinfrastructure for an integrated botanical information network to investigate the ecological impacts of global climate change on plant biodiversity," (PeerJ Preprints, 2016).

175. C. Merow, BIEN range methods description. *Website: bien.nceas.ucsb.edu.*, (2017).

176. W. Barthlott, D. Rafiqpoor, G. Kier, H. Kreft, Global centers of vascular plant diversity. *Nova Acta Leopoldina NF* **92**, 61-83 (2005).

Acknowedgments

We thank M. B. Bush, K. J. Feeley, R. Jansson, C.N.H. McMichael, A.S. Melo, and members of the Rangel laboratory for discussions and C. Merrow for help with BIEN plant distributions. **Funding:** T.F.R. and J.A.F.D-F. have been continuously supported by Conselho Nacional de Desenvolvimento Científico e Tecnológico (CNPq) (grants PQ309550/2015-7, PQ301799/2016-4, and FAPEG/INCT465610/2014-5). T.F.R. and R.K.C. were supported by Coordenação de Aperfeiçoamento de Pessoal de Nível Superior (CAPES) (grant SWB134/2012). F.S.C. was supported by CNPq (grant DTI380.376/2017-2) and M.T.P.C. by a CAPES graduate fellowship. C.R. thanks the Danish National Research Foundation for its support of the Center for Macroecology, Evolution, and Climate (grant DNRF96). **Author contributions:** T.F.R. and

R.K.C. jointly conceived and led this study, designed the biogeographical simulation model, created the figures, and led the writing, with input from all authors. T.F.R. programmed the biogeographical model and ran the simulations. N.R.E. and P.B.H. designed, programmed, and ran the paleoclimate model. T.F.R., J.A.F.D-F, and M.T.P.C. performed statistical analyses. All authors contributed conceptually to the design of the study and interpretation of results. **Competing interests:** No author has a conflict of interest. **Data materials availability:** Paleoclimate data and source code for the biogeographcial simulation model and statistical analysis are available at www.ecoevol.ufg.br/rangel/SASQuat.

Supplementary Materials

Model description and justification

Supplementary desciption of analyses

Figures S1–S25

Tables S1–S10

Caption for Database S1

Database S1 as zipped archives: www.ecoevol.ufg.br/rangel/SASQuat

References (130–176) are called out only in the Supplementary Materials.

Figure Legends:

Figure 1. Simulation model structure. The processes and parameters implemented in the model, all illustrated here, link climate dynamics and topography to emerging biodiversity patterns. Key entities and patterns (Tables S3 and S4) appear in *rectangles* at the population, species, and assemblage levels. Processes are shown in *ovals*. *Control knobs* (Table S1) represent the four model parameters: D_{max}, maximum dispersal distance; H_{max}, maximum niche evolutionary rate; T_{min}, minimum time for speciation; and C_{max}, maximum intensity of competition allowing coexistence, estimated as a function of phylogenetic distance. Climate change, on a realistic topographical template, drives ecological and evolutionary processes, interacting with each population's environmental niche to determine range dynamics. Dispersal promotes range shift and range expansion. Interactions between climate change, niche, and geographic distribution may result in adaptive niche evolution, range fragmentation, or extinction. Fragments that remain isolated long enough become new species. Closely related species, in sympatry, may coexist or undergo competitive exclusion. Starting from a single, founding species (and its initial climatic niche), the simulation produces temporal and spatial patterns of biodiversity, including times and places of speciation (*cradles*), extinction (*graves*), and persistence (*museums*). See the Methods section, below, and the section *Model specification: process sequence* in (*95*).

Figure 2. Lifetime trajectory of species. Initially, the species on the left (labeled *ancestral population*) is in a *persistence trajectory* (*thick black line*), as a single, viable population. Driven by climate change, the population experiences *range fragmentation*, yielding two, isolated descendant populations (*blue* and *red dashed lines*). These two daughter populations enter *speciation trajectories*. Once they have remained isolated for at least T_{min} years, they are considered independent species (*speciation event*). Each descendant species then enters its own *persistence trajectory* (*blue* and *red solid lines*). In this example, after a short period of persistence, the red species enters an *extinction trajectory* (*thin dashed red line*), as its geographic range continuously contracts in a changing climate, ending in full range collapse (*species extinction*). The blue species

will eventually give rise to two daughter species, undergo extinction, or survive to the end of the simulation.

Figure 3. Simulation results for an Andean founder. *Upper panel*: Occupancy time series for speciation (cradle richness, *green*), extinction (grave richness, *red*), and mean continental temperature (*blue*) over the course of the simulation (time moves from left to right). The highest 5 to 7 peaks of speciation (*green dashed lines*) and extinction (*red dashed lines*) were marked manually, but time series cross-correlations were analyzed rigorously (Table S6). Precipitation time series appear in Fig. S2. *Lower panel:* Cumulative richness maps for cradles, graves, net diversification (cradles minus graves), and total richness. Each map is a summation over the course of the simulation. The figure shows the average of all parameter values for an Andean founder, excluding the climate-smoothing experimental treatments.

Figure 4. Simulation results for an Atlantic Rainforest founder. See the caption for Fig. 3.

Figure 5. Simulation results for an Amazon founder. See the caption for Fig. 3.

Figure 6. Pooled simulation results for the Andean, Atlantic Rainforest, and Amazon founders of Figs. 3–5. See the caption for Fig. 3.

Figure 7. The effect of topographic smoothing on rates and cumulative spatial patterns of speciation (cradles), extinction (graves), net diversification (cradles minus graves), and total richness, for Andes, Atlantic Forest, and Amazon founders, pooled. *Upper panel*: Occupancy time series for speciation (cradle richness, *green*), extinction (grave richness, *red*), and mean continental temperature (*blue*) over the course of the simulation (time moves from left to right). *Black* time series are for smoothed topographies. *Red* and *green* time series are the same as in Fig. S13. Rates of speciation (cradles) and extinction (graveyards) were both suppressed by smoothing.

Figure 8. Observed species richness versus modeled richness. *Left column of maps:* Contemporary spatial patterns for South American bird richness (2,967 species, *upper map*) and mammal richness (1,342 species, *lower map*). *Middle column map:* The simulated spatial pattern for cumulative museum richness, arising from the model (Fig. 1), averaged over all parameter

values for an Atlantic Rainforest founder. *Right column of maps:* The differences between observed (*left maps*) and simulated (*middle map*) richness for birds (*upper map*) and mammals (*lower map*). *Red* indicates that the model underestimates richness, and *blue* indicates overestimation. Simulated species richness is highly correlated with observed species richness for birds ($r^2 = 0.6337$) and for mammals ($r^2 = 0.6548$). Observed species richness was not targeted in any way by the simulations. A qualitative comparison of modeled richness with South American plants appears in *Contrasting empirical and simulated spatial patterns in species richness* in (*95*).

Supplementary Materials for

Modeling the ecology and evolution of biodiversity: Biogeographical cradles, museums, and graves

Rangel, T.F., Edwards, N.R., Holden, P. B., Diniz-Filho, J.A.F., Gosling, W.D., Coelho, M.T.P., Cassemiro, F.A.S., Rahbek, C., and Colwell, R.K.

Correspondence to: thiago.rangel@ufg.br and robert.colwell@uconn.edu

This PDF file includes:

Other Supplementary Materials for this manuscript includes the following:

Databases S1 as zipped archives: model source code available at www.ecoevol.ufg.br/rangel/SASQuat

Contents

Model overview and justification

In a changing climate, the geography of species distributions is governed by many interacting processes. These include the shifting spatial pattern of environmental variables, dispersal, niche evolution, interspecific competition, range fragmentation and rejoining, speciation, and extinction. We aim to model all these processes in the most realistic way we can, given computational limitations. The sections below outline the rationale for each component of the model, followed by a step-by-step specification of the procedural sequence. In addition, we summarize the model algorithm, parameters, initial conditions and emergent properties. We also describe the parameter exploration and experimental design. Finally, we provide a full account of the simulation results and analyses.

Geographical domain

In our spatially explicit simulation model, the geographical domain, South America, is described by a spatial grid composed of discrete regular areas (grid cells). However, the grid definition imposes a tradeoff between computational effort (fine scale spatial resolution increases the number of cells, increasing the computational burden) and representation of environmental heterogeneity (coarse scale spatial resolution is unable to capture the dramatic topography of the Andes).

To balance this tradeoff, we used a recursively defined, hybrid-scale spatial grid that captures the environmental heterogeneity of mountainous regions, while reducing the computational burden of unnecessary cells in more-homogeneous, flatter areas such as the Amazon and Patagonia. We started with an equal-area grid composed of 1868 cells, each one comprising 10,000 km^2. We then used a high-resolution digital elevation model (*130*) to estimate topographic heterogeneity within each cell, measured as the standard deviation of elevation at a 1km^2 resolution (pixel size). We identified 423 cells with very high topographic heterogeneity, defined by a standard deviation of elevation exceeding 250m. Each one of these 423 highly heterogeneous cells was then split into four equal-area grid cells, yielding 1692 smaller cells, each 2500 km^2. We iterated the procedure by re-calculating topographic heterogeneity in the 1692 cells of 2,500km^2, identifying 561 cells with very high topographic heterogeneity (standard deviation in elevation exceeding 500m). Each of these 561 cells was then split into four cells, each 625km^2 in area. Thus, the final grid was composed of 4820 cells of different areas: 1445 cells of 10,000 km^2, 1131 cells of 2,500km^2, and 2244 cells of 625km^2 (Fig. S1A). As expected, larger cells are distributed in topographically flatter areas (whether in the highlands or lowlands), whereas smaller cells were located in regions of steep slopes, particularly the mountainous terrain of the Andean region (Fig. S1B).

It is widely recognized in the ecological literature that spatial and temporal scales of analysis influence the perception of patterns and processes (*10*). As explained below, climate heterogeneity in space and time is a driver of many processes and patterns emerging from our model. The hybrid grid was an attempt to capture as much climate heterogeneity in South America as possible, given the current understanding of paleoclimatic dynamics and the computational limits imposed by the number of grid cells and the processes that take place in them. Given the ecological and evolutionary dynamics implemented in our model, if a large cell is split into four sub-cells, but all the four sub-cells share the same average climate as the large cell would have had at any given time step, the patterns emerging from the model would not be changed. However, the purpose of splitting large cells into smaller cells is to capture smaller-scale climatic heterogeneity, which is universally agreed to be driven in large part by topographic heterogeneity. Thus, large cells were split hierarchically in regions of higher topographic heterogeneity.

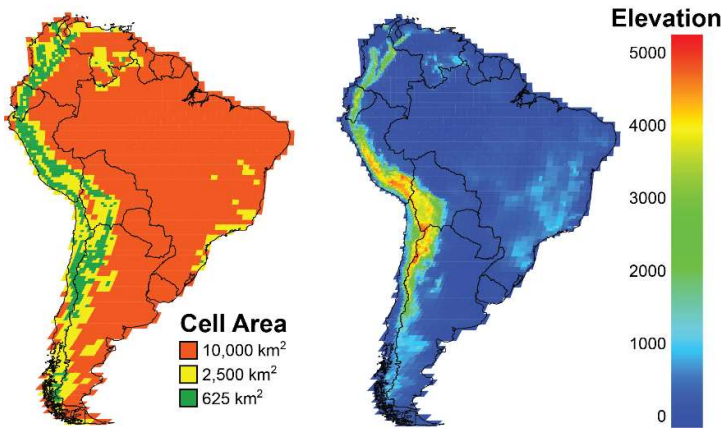

Figure S1. Hybrid-scale geographic grid used in the simulation model. *Left* (A): topographically homogeneous regions are gridded with larger cell areas, whereas topographically heterogeneous regions are gridded with smaller cell areas. *Right* (B): average elevation of each grid cell.

Because cells have geographic positions (they are spatially referenced), it is possible to calculate the geographic distance between pairs of cells. We used the geographic coordinate of the centroid of cell as a reference to calculate geodesic distances between cells.

Temporal dynamics of environmental (climatic) factors

For each 500-year time interval from 800 Ka (years ago) to the present (1600 time steps), the paleoclimate model (described below) assigns to each of the 4820 map cells an estimate of the mean temperature of the warmest and coolest quarters (henceforth *minimum and maximum annual temperature*) and the mean daily precipitation of the wettest and driest quarters (henceforth *minimum and maximum annual precipitation*). These four factors, on two environmental axes (*annual temperatur*e and *annual precipitation*) characterize the changing climate in each grid cell over the time-course of the simulation.

Palaeo-climate reconstruction

Atmospheric general circulation model

PLASIM-ENTS (*108*) is an intermediate complexity atmospheric general circulation model coupled to a dynamic land surface model and to flux-corrected slab ocean and sea-ice models. The atmosphere is PLASIM (*131*), itself built around the 3D primitive equation model PUMA (*132*). PLASIM's radiation scheme considers two wavelength bands in the short wave spectrum and uses the broad-band emissivity method for long wave. Other parameterized processes include large-scale precipitation, cumulus and shallow convection, dry convection and boundary layer heat fluxes. Fractional cloud cover is diagnosed. The land surface model is ENTS (*133*), which models vegetative and soil carbon densities, assuming a single plant functional type. Photosynthesis depends upon temperature (with a double-peaked response representing boreal and tropical forest), atmospheric CO_2 concentration, and soil moisture availability. Self-shading is also parameterized. Land surface albedo, moisture bucket capacity, and surface roughness are parameterized in terms of the simulated carbon pool densities. We ran PLASIM-ENTS at T21 resolution (~5°) and with 9 vertical layers in the atmosphere.

An ensemble of 50 PLASIM-ENTS 100-year, quasi-equilibrium simulations was performed (*109*). Orbital forcing inputs of eccentricity, obliquity, and precession were fixed in each simulation but varied randomly between simulations over their ranges in the Quaternary. Emulators were built for four bioclimatic outputs of this ensemble: the mean temperature of the warmest and coolest quarters and the mean daily precipitation of the wettest and driest quarters. These emulators were built using the dimensionally reduced approach of Holden and Edwards (*134*), following the "one-step emulator" algorithm described by Holden *et al.* (*109*). In summary, we performed a singular vector decomposition of the ensemble of output fields and then regressed the Principal Component scores against the orbital input parameters. This approach enabled the climate from any specified, arbitrary orbital configuration to be approximated. We applied the temporally-evolving orbital parameters of Berger (*135*) at 500-year intervals to generate a spatio-temporal description of orbitally-driven climate over the last 800,000 years. Emulator error occasionally produced negative dry-season precipitation in arid regions; these were set to zero. In regions with low seasonality, emulator error can lead to a warm-season temperature that is lower than the cool-season temperature; to correct for this occasional problem (~0.5 % of the calculations), we applied the constraint $max = max(min, max)$ to both temperature and precipitation.

Scaling for global climate

The intermediate complexity model GENIE-1 (*136*) provides the computational efficiency required to perform long transient simulations. The physical model comprises a 3-D frictional geostrophic ocean with eddy-induced and isopycnal mixing, coupled to a 2-D fixed wind-field energy-moisture balance model atmosphere, a dynamic thermodynamic sea-ice component, and the land surface model ENTS.

An 800,000-year transient GENIE-1 simulation was performed (*137*), varying orbital parameters (*135*), atmospheric CO_2 from Antarctic ice-core records (*138*), and Northern hemisphere ice sheets, with self-consistent freshwater exchange with the ocean. Ice sheets were derived by interpolating the spatio-temporal distribution of the Ice-4G deglaciation reconstruction (*139*) onto the benthic $\delta^{18}O$ record (*140*), and assuming that this relationship holds throughout the Quaternary (*137*).

We used this transient simulation to approximate large-scale climate response to the non-orbital forcings that are neglected in the PLASIM-ENTS emulator. At each time step of the model we calculated mean surface air temperature and precipitation over all GENIE-1 land cells in the latitude band 30°S to 30°N. This latitudinal range was chosen to be symmetric about the equator, so that orbitally-induced inter-hemispheric effects were largely cancelled, and to ensure adequate isolation from regions directly affected by North American ice-sheets. We calculated the temperature anomalies relative to the preindustrial and added these to the emulated values of maximum and minimum temperature, thereby approximating the effect of non-orbital forcing as spatially and seasonally uniform (but temporally evolving through the glacial cycles). For precipitation, we applied a multiplicative anomaly approach, thereby assuming that non-orbital forcing does not change the distribution of precipitation, only the strength of the hydrological cycle.

Contemporary climate variables, for each grid cell, were derived from *WorldClim* (*130*), which provides temperature and precipitation estimates at 1 km^2 resolution, interpolated from temporally averaged measurements (1950 to 2000) from ~15,000-50,000 weather stations globally (depending upon the variable).

The emulated bioclimatic variables were linearly interpolated onto the spatial grid and converted into anomalies with respect to the present day. Interpolation of climate model anomalies onto finer-resolution climatological data is a widely-used approach in future-impact assessment (e.g. (*141*)). We applied temperature anomalies additively to the *WorldClim* present-day climatology. Precipitation anomalies, in contrast, were applied multiplicatively to the climatology. While

multiplicative and additive anomaly methods would be equivalent, in theory, if the present-day modeled climate were identical to the observed (*WorldClim*) climatology, in practice precipitation fields are subject to a high degree of small-scale, topographically induced variability that is better represented by a multiplicative term. For instance, the extreme topographic discontinuity that leads to hyper-aridity of the Atacama Desert is automatically preserved under multiplicative transformation of the climatology. Most notably in our application, PLASIM-ENTS does not have the spatial resolution to simulate the hyper-aridity of the narrow Atacama Desert, so that applying an additive anomaly would inevitably lead to an unrealistic climate. Fig. S2 shows the average maximum and minimum annual temperature and precipitation across South America. Movie 1 shows the space-time dynamics of minimum and maximum annual temperature and precipitation.

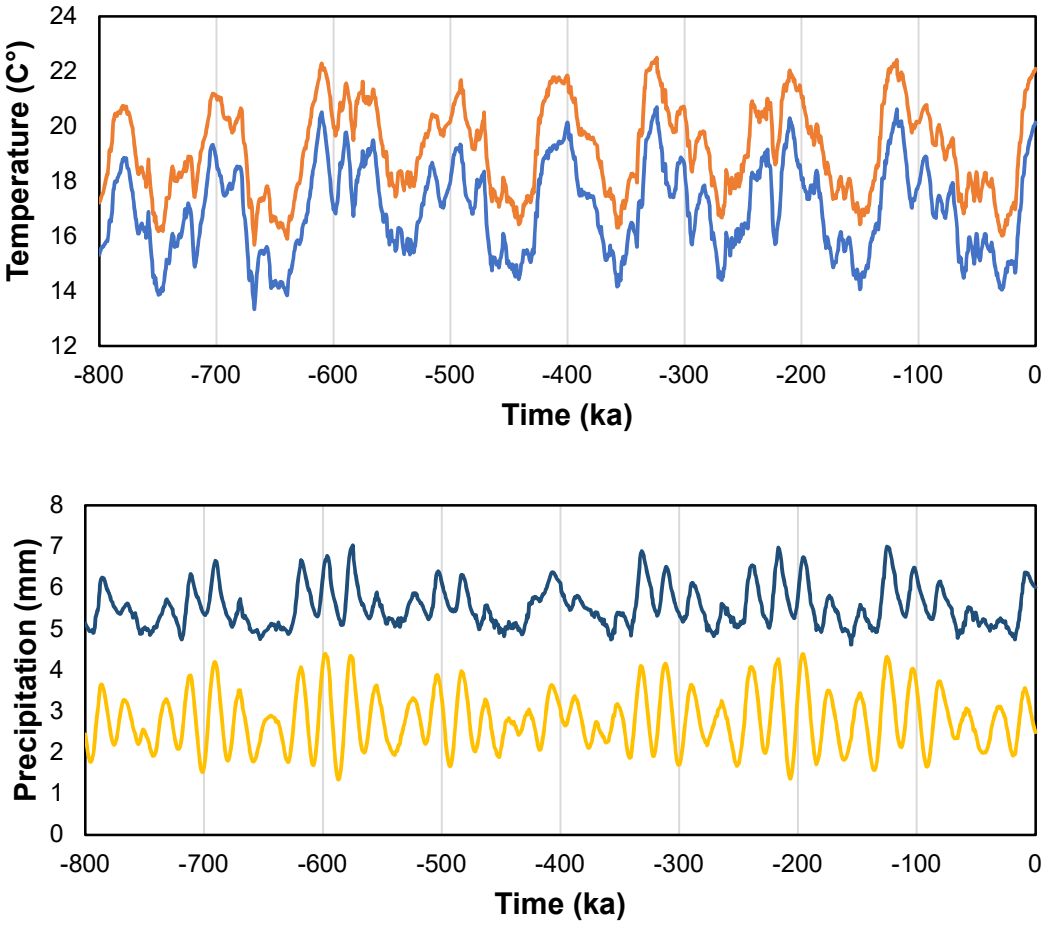

Figure S2. Time-series of average minimum and maximum temperature (top) and precipitation (bottom) for South America. See Movie 1.

Comparisons against other paleoclimate models

To evaluate the reliability of our emulator we contrasted spatial patterns of temperature and precipitation variables, at specific time steps, against multi-model predictions carried out through the paleoclimate model inter-comparison project, phases two and three (PMIP2/PMIP3). We

focused the validation of our emulator at three specific moments of the Quaternary: the Last Interglacial (LIG), at ~126.5 ka (*111, 112*), the Last Glacial Maximum (LGM) at 21 ka (*112, 113*) and the mid-Holocene (MH) climate optimum at 6 ka (*112, 113*). The LIG and MH interglacial states, with CO_2 and ice sheets similar to present day, provide an opportunity to validate our emulated response to orbital forcing, while our estimates of paleoclimate at the LGM test the emulated response to very different CO_2 and ice-sheet forcing.

During the LIG (peaking at ~126.5 ka), high eccentricity and the phasing of precession and obliquity resulted in positive annual insolation anomalies at high latitudes and negative anomalies at low latitudes. PMIP3 inter-comparison simulations predict a global change in temperature ranging from -0.5 to +0.5 K (*111*). In addition, a data synthesis suggests global temperatures were up to ~2 K warmer during the LIG than today (*142, 143*). Our paleoclimate emulator predicts 0.3 K warming during the LIG (Fig. S3).

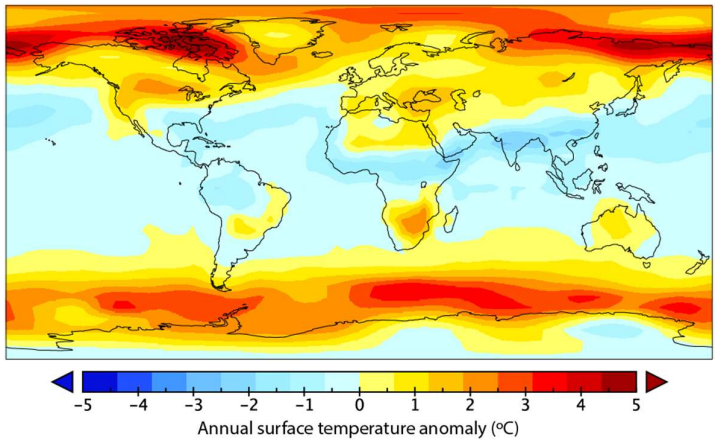

Figure S3: Emulated Last Interglacial (LIG) mean annual surface air temperature at 126.5 ka (approximated as the mean of maximum and minimum seasonal temperatures). For comparison, see IPCC AR5 Figure 5.6b(*112*).

During the Quaternary, global temperature change was characterised by oscillations between glacial and interglacial states. Based on a range of sources of evidence, IPCC AR5, concluded it is very likely (>90% probability) that global temperature at the LGM (21 ka) was between 3 K and 8 K colder than today, while PMIP3 and PMIP2 models estimate 3.1 to 5.9 K colder (*112*). Our paleoclimate emulator estimates global temperature ~5.5 K colder than today (Fig. S4). The precipitation estimates of our emulator are also consistent with PMIP2 (Fig. S4), suggesting reduced maximum (wet-season) precipitation across the whole of South America, but with an increase in minimum precipitation in southern Amazon.

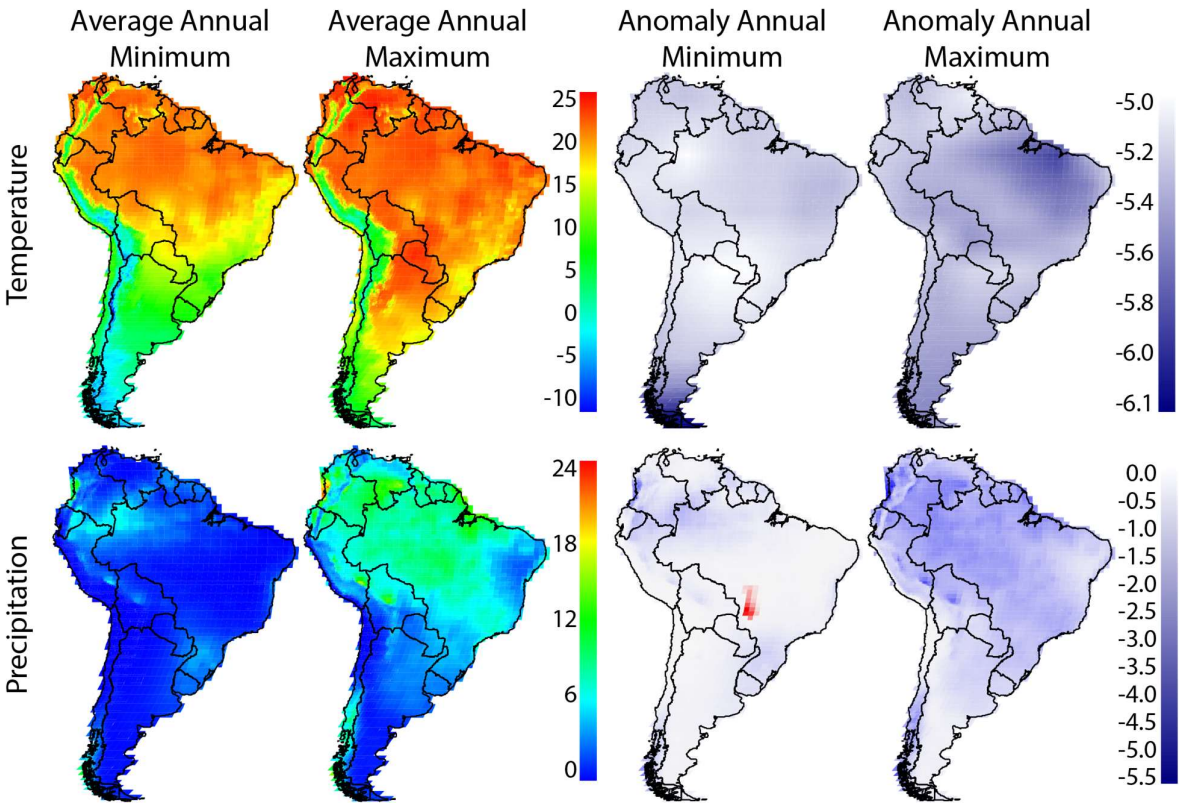

Figure S4: Emulated Last Glacial Maximum (21 ka) climate. Plotted data are the paleoclimate estimates used in this study, derived by interpolating emulated climate anomalies onto present day climatology. For comparison, see PMIP2 synthesis maps (https://pmip2.lsce.ipsl.fr)

There is general agreement between the estimated temperature patterns of our paleoclimate emulator and PMIP ensembles during the MH (6 ka) (Fig. S5). Although our emulator estimates a maximum temperature (warm-season) cooling over the Amazon, which disagrees with the average prediction by PMIP2, our estimates are still within the spread (uncertainty) of the ensemble of models. There is also an agreement between patterns of precipitation predicted by our emulator and PMIP2 during the MH. According to these models, maximum (wet-season) precipitation is reduced in southern Amazon, while it is increased in the north, reflecting an increase in the southerly expansion of dry-season monsoon (Fig. S6).

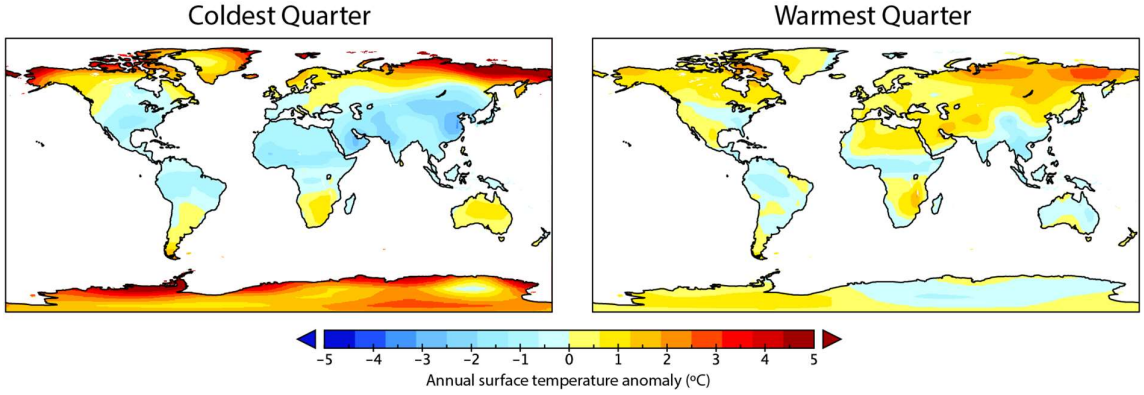

Figure S5: Emulated Mid Holocene (6 ka) surface air temperature anomalies of the warmest and coolest quarters. For comparison, see IPCC AR5 Figure 5.11 (*112*).

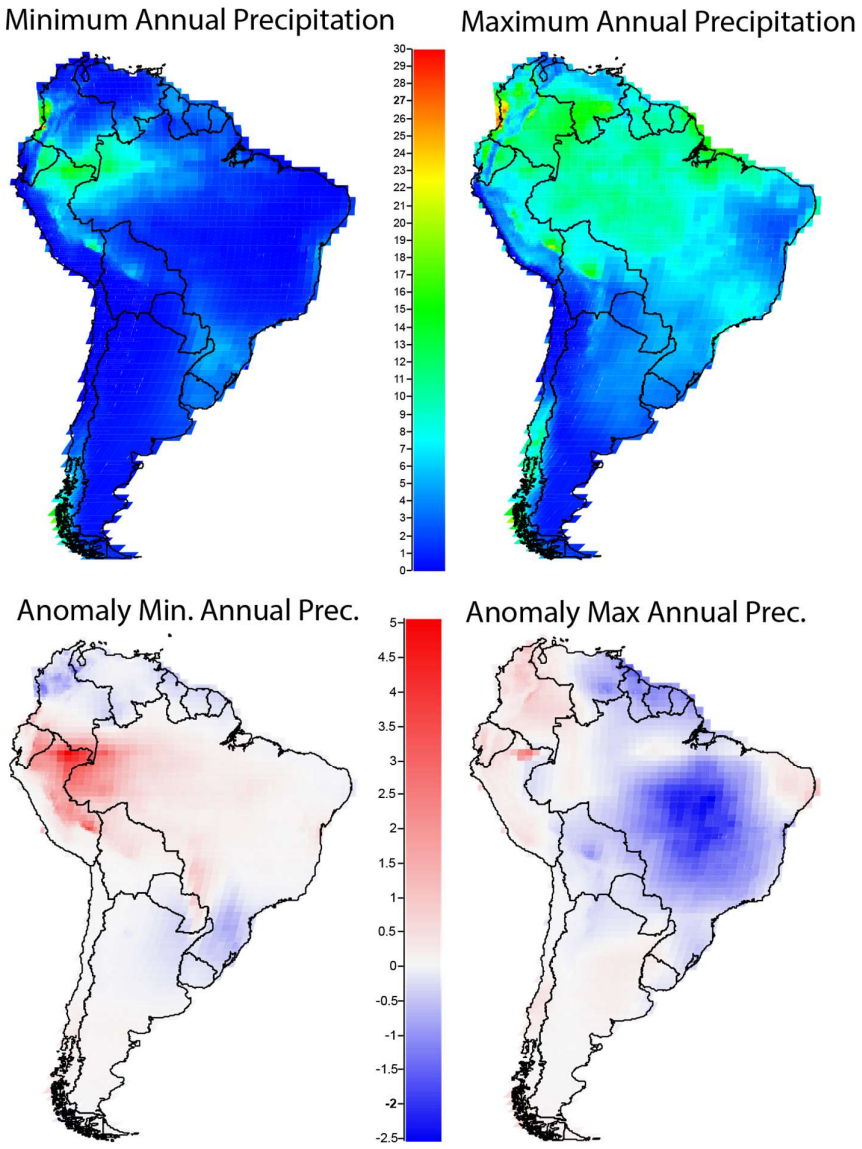

Figure S6: Emulated Mid Holocene (6 ka) climate. Plotted data are the paleoclimate estimates used in this study, derived by interpolating emulated climate anomalies onto present day climatology. For comparison, see PMIP2 synthesis maps (https://pmip2.lsce.ipsl.fr).

Simulated biogeography

The smallest biological unit explicitly modeled is regarded as a population, characterized as a geographically isolated and continuous fragment of a species range. The complete range of a species may be represented by a single population or by multiple populations (see below).

At each time step, each population of each species is characterized by an environmental tolerance limit for each of the four environmental variables (minimum and maximum annual temperature and precipitation). This population-specific set of four environmental tolerances defines the *fundamental environmental niche* of the population. Thus, at any given time, a population occupying a given cell must have the appropriate environmental tolerances to all four

environmental conditions of the cell (i.e. similar to a climate envelope niche model). In other words, the fundamental niche of the population must be as broad or broader than environmental conditions of the cell. Cells with environmental conditions that lie within the population's environmental niche are, hereafter, called *suitable*. Conversely, if one or more of the four environmental conditions lies outside the niche of a population for a cell, the cell is declared *unsuitable* for that population.

The figure below (Fig. S7) represents the two environmental axes used in our model (annual temperature and annual precipitation). The dashed square represents the environmental niche of a hypothetical population. The left and right sides of the square represent the minimum and maximum annual temperature tolerated by the population, whereas the lower and upper sides of the square represent the minimum and maximum precipitation tolerated by the species.

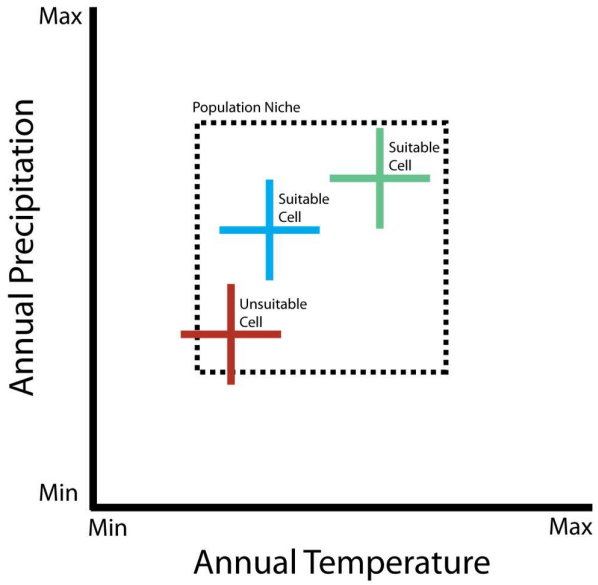

Figure S7. Graphical representation of the climatic niche of a hypothetical population (dashed square in the center), indicating minimum and maximum tolerance of temperature and precipitation, in relation to the climate in three grid cells (crosses) at a given time step of the simulation. Each cross represents a grid cell in the map, in which the horizontal length indicates the seasonality in temperature and the vertical length indicates the seasonality in precipitation. The green and blue grid cells are climatically suitable for the population, as they are enclosed within the population niche. The red grid cell is climatically unsuitable, because it is colder and drier than the limits tolerated by the population.

Analogously, the four environmental variables that characterize the environment of any cell can be depicted as a cross, defining the limits of a rectangular climate space. In Fig. S3, we represent two cells with suitable environmental conditions for the population (green and blue), each with environmental variables lying completely within the niche of the population. In contrast, the red cell is unsuitable because the minimum (coldest) temperature of the cell over an annual cycle is too extreme for the environmental tolerance of the population, and the minimum seasonal precipitation is too dry for the population to persist.

Climate change and geographic distributions

The four environmental conditions in each map cell are asynchronously dynamic over time. A change in environmental conditions may open opportunities for range expansion by turning an

unsuitable cell into a suitable one (a *leading edge* cell of a shifting range). Conversely, climate change may render a suitable cell unsuitable (a *trailing edge* cell of a shifting range).

Leading edge: range expansion

When climate dynamics change the condition of a cell from unsuitable to suitable, allowing the species to expand its range and occupy the newly suitable cell, then the cell is part of the leading edge of the population's range. In our model, the population simply expands its range to occupy any newly suitable cell, whether contiguous or not, that lies within the maximum dispersal distance of the population (see below, Movie 2).

Trailing edge: niche evolution or extirpation

When climate dynamics change the condition of an occupied cell from suitable to unsuitable, the cell is part of the trailing edge of the population's range, and the population in the cell is under selection pressure. The outcome of selection may be (1) niche evolution (adaptation to the new environmental conditions), allowing continued occupation of the trailing edge cell; or (2) local population extirpation in the trailing edge cell, if the population cannot adapt.

In the figure below (Fig. S8), climate change has increased minimum and maximum annual temperature and precipitation in all three cells, as indicated by the arrows. Because the red cell is now newly suitable (it now lies within the niche limits of the population), it is considered a leading edge cell. Conversely, because the green cell has become newly unsuitable (it now lies beyond the niche limits of the population), the green cell is part of the population's trailing edge. Although climate change has altered environmental conditions in the blue cell, it remains occupied by the population, because it continues to lie within the niche of the population.

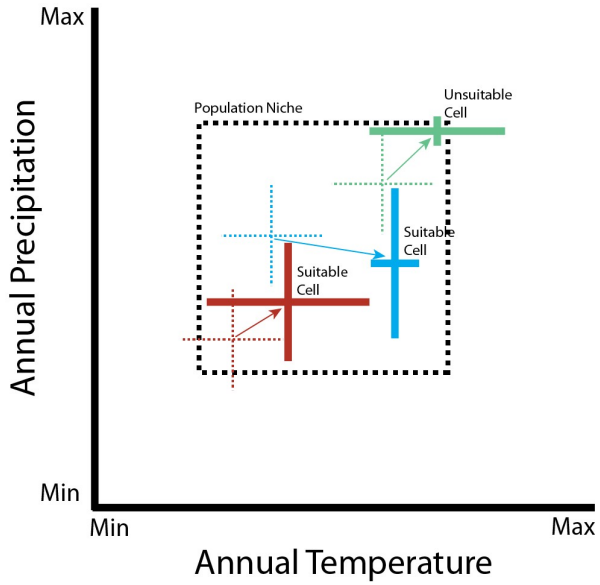

Figure S8. Graphical representation of the climatic niche of hypothetical population (dashed square in the center), indicating minimum and maximum tolerance of temperature and precipitation, in relation to the climate in three grid cells (crosses), after climate change (compare to Fig. S3). Dashed crosses indicate the climate in the cells in the previous time step, and solid lines indicate the climate in the same cells after climate change. The red cell has become warmer and wetter, with increases in both temperature and precipitation seasonality. The blue cell has become drier and warmer, from an increase in precipitation seasonality and a decrease in temperature seasonality. The green cell has become warmer and wetter, with an increase in temperature seasonality and a reduction in precipitation seasonality. Notice that, after climate

change, the red cell has become climatically suitable (inside the population niche), whereas blue cell has become climatically unsuitable (warmer and wetter than suitable for the species).

Climate change and niche evolution

Most studies dealing with effects of climate change simply assume perfect niche conservatism. Under this assumption, each species simply tracks climatic conditions by reconfiguring its geographic range (Movie 2). Of course, changes in climate may eventually promote species extinction (range collapse) or the rise of a widespread species. However, in nature, it may be possible that selective pressure from climate change, especially at the trailing edge, may cause a gradual adaptive niche shift, bringing niche limits closer to new climatic limits within the current geographic range of the local population (*30, 116*). This evolutionary process may promote persistence of species even under climate changes so severe that they would otherwise lead to extinction. Because the evolutionary changes in niche limits under selection pressure may prevent species extinction, this process has been called "evolutionary rescue," particularly in the context of recent anthropogenic climate changes (*82, 84, 85, 144*).

Like all adaptive evolution, the evolutionary potential of the climatic niche depends fundamentally on two factors: the strength of selection and the level of heritable variation in the selected trait that would allow adaptation to the new environment. As suggested by (*30*) and others, individuals at the trailing edge of a shifting population's range are under stronger selective pressure arising from climate change than those at the leading edge, which instead simply disperse into newly suitable habitat. In our simulations, we incorporate niche shifts by applying a simple quantitative evolutionary genetics framework (*145, 146*) to evaluate the potential for adaptation in each cell of the trailing edge of a shifting range at each time step.

Evolutionary rates and climate change

For each trailing-edge cell *c,* we estimated the evolutionary rate (H_c, in units of Haldanes, (*119, 120*)) that would be required to allow niche adaptation sufficient for the population in that cell to persist in the new climate. This evolutionary rate can be estimated by comparing the environment in a trailing-edge cell *before* (time *t*) and *after* (time $t + 1$) climate change, for each climatic variable. Thus, we assumed that individuals of each local population, in each cell, are at their environmental optimum at time *t*, given by the climatic conditions at time *t*. When the climate changes, the individuals in the trailing-edge cell may (or may not) be able to adapt genetically to new climatic condition that they face at time $t + 1$. The evolutionary rate in a focal trailing-edge cell (*c*) to allow persistence in that cell between two successive time steps is then given by:

$$H_c = [(E_{c,t+1} - \bar{E}_t) / \sigma_t)] / \Delta t$$

where $E_{c,t+1}$ is the value of an environmental variable (e.g., maximum annual temperature) in a focal trailing-edge cell *c* after climate change (time $t+1$), and $\bar{E}_t$ and σ_t are the average and standard deviation of the same environmental variable in all cells occupied by the local population within the *genetic neighborhood* of the cell. We define the genetic neighborhood of each trailing-edge *c* cell as all occupied cells within the maximum dispersal distance (D_{max}) from the cell. Thus, in our model, genetic variation within a species' range is geographically structured, so that the evolutionary potential of each trailing-edge cell is set, at each time step, by the genetic variation for climate (standard deviation) within the genetic neighborhood of the cell.

Traditionally, evolutionary rate *H* is calculated for a single generation of an organism. However, each time step in our simulation model comprises 500 years, which is far beyond the generation time of most organisms. To allow a direct and more plausible comparison against theoretical and empirical measures of evolutionary rates (*118*), we assumed that the generation time of the

simulated species is 5 years. Thus, we divided all H_c by 100.

Evolutionary rescue

In the simulation model, a maximum (critical) evolutionary rate in response to climate change (model parameter H_{max}, Table S1) is defined for all species, in all trailing-edge cells, constant throughout the entire time span of the simulation. For each trailing-edge cell c, from time t to $t + 1$, and for each environmental variable, the local population may continue to occupy a trailing edge-cell if and only if $H_c < H_{max}$. Thus, although the environment of the trailing-edge cell c at $t + 1$ lies outside the climatic niche of the population at time t, the amount of climate change lies within the maximum evolutionary potential (H_{max}) of the population of cell c if this condition is met. Thus, if $H_c < H_{max}$, the population of the trailing-edge cell persists because its climatic niche is expanded to encompass the new climate at time $t + 1$. Once the test is performed for all trailing-edge cells, the entire climatic envelope of the species is recalculated to reflect the maximum expansion of niche limits in the trailing edge, with these new limits applied to the entire population.

Conversely, if $H_c > H_{max}$ for any of the environmental variables in cell c, the required evolution for persistence is beyond the maximum evolutionary adaptability of the population in that cell, and the population is therefore extirpated from that trailing-edge cell. Thus, if H_{max} is infinitely large, the local population has an infinite evolutionary potential and will respond to any rate of climate change, however extreme, by expanding its climatic niche. In this case, climate change would never promote any local extirpation, as the geographic range would never contract. Conversely, if H_{max} is zero, the local population has no evolutionary potential, and will always be extirpated from all trailing-edge cells. In our simulations, we applied several values of H_{max} to study how evolutionary rescue may affect the patterns of biodiversity that emerge from the simulated ecological and evolutionary processes.

Niche heritability and selective pressure

Because H_c is a local measure of the environmental distance between two consecutive time steps in the trailing-edge cell c under climate change, under the assumption that the average environmental conditions $\bar{E}_t$ may be considered as a phenotypic trait, it is possible to interpret H_c in units of Haldanes (*119, 120*), and show how H_c may be used to describe evolutionary niche shifts (*147*). Because we scale H_c to represent evolutionary rate between two generations, and because H_c is standardized by variation in the genetic neighborhood σ_t, then

$$H_c = h^2 \beta ,$$

where h^2 is the heritability of the trait, given by the proportion of additive genetic variance in relation to total phenotypic variance, and β is the selection gradient standardized by standard deviation σ_t (i.e., the slope of the relationship between fitness and environmental variable E (*118*). Thus, under very high heritability, say $h^2 \sim 1$, (i.e., most of the variation is inherited between consecutive generations), a Haldane may approach 0.1, indicating that a shift of one standard deviation in the tolerance for variable E would shift relative fitness by 10% (*148*). Unfortunately, there are few empirical analyses of these genetic parameters calculated from experimental data of wild populations, and it is still challenging to directly predict responses to climatic adaptations based on genetic models (*149*). Thus, the threshold value H_{max} may be interpreted as the combination of selection strength (β) and heritability (h^2). In fact, a critical H_{max} value simulates the limits of evolutionary rescue (niche adaptation) imposed by the balance between (*i*) maximum tolerable intensity of selection pressure imposed by climate change and (*ii*) available additive variance in the population, as measured by the variation of realized climate niche in the genetic neighborhood of the focal cell c. Finally, assuming that the average intensity of selection pressured imposed by climate change is moderate for most populations (*147*), a critical H_{max} value of 0.01

would capture an evolutionary rate that is close to the maximum expected in most natural situations (*117, 118*).

Geographic structure of implicit genetic variation

Given that σ_t is the standard deviation of E within the genetic neighborhood of the trailing-edge cell c, as defined by maximum dispersal distance D_{max}, the model assumes the existence of a geographic structure in the genetic variation of the local population, which increases the potential of adaptation at a regional level and minimizes long-distance central-peripheral dynamics that can constrain adaptive potential (*150*). Thus, climate change in trailing-edge cell c (i.e. $E_{c,t+1} - \bar{E}_t$) is relative to the geographic variation in E realized by the local population at time t within the reach of its dispersal distance from the trailing-edge cell c. Although more complex theoretical models have been proposed for evolutionary rescue and adaptation to shifting environments (e.g., (*102, 118*), these models have a much higher number of parameters and are difficult to apply in spatially and temporally explicit scenarios, especially at macroecological and macroevolutionary levels. We believe that our simplified approach for H_{max} is the most parsimonious model for evaluating how variation in relative evolutionary potential may affect patterns of biodiversity under complex and stochastic climate fluctuations.

Dispersal, range fragmentation/coalescence, and environmental niche dynamics

As in Kirkpatrick and Barton's (*150*) model, we assume that geographic structure of implicit genetic variation and gene flow within the range of a population normally prevents unlimited genetic divergence in response to environmental heterogeneity, while simultaneously allowing a certain degree of local adaptation. Climate change can create barriers of unsuitable environment that fragment the population's range. If such a barrier is wider than the maximum dispersal distance of the population, D_{max}, the fragment becomes demographically and genetically isolated. The resulting lack of gene flow allows independent niche evolution within each range fragment. If populations come into secondary contact before speciation occurs, however, they coalesce, and their respective niches are blended, proportionally, to become one again (Movie 2). All coalescing populations contribute to redefining the niche of the newly reconstituted population, as explained below.

Dispersal and geographical range dynamics

In our model, at time step $t + 1$, each population initially colonizes all suitable cells that lie within a maximum distance D_{max} (maximum dispersal distance, a population-specific character; Table S1) from any cell that the population occupied in time step t. After trailing-edge selection for adaptation to changed climate (see the previous section), evolutionary rescue (still within time step t +1) allows re-colonization of any cells within distance D_{max} of a trailing-edge cell that were made newly suitable by adaptive evolution. (No second round of dispersal is allowed for leading-edge cells, thus ensuring that, within a single time step, only cells within D_{max} of previously-occupied cells become newly occupied.) In nature, of course, dispersal and trailing-edge selection take place continuously, but we are forced by the limitation of discrete time steps to take this two-step approach. The first dispersal episode is required before selection, because the genetic neighborhood of trailing-edge cells may include newly-suitable cells reached by dispersal (Movie 2).

Consider two map cells occupied by a population at time t, located a geographic distance apart greater than the dispersal limit of the population (D_{max}), but separated by a contiguous sequence of colonized cells (i.e. no barriers between the two cells). If climate change at time $t + 1$ allows the two cells to continue to be occupied, but removes all suitable habitat between the two occupied cells, then the range of the population is declared *fragmented*. In addition, the two newly-isolated cells (those located at a distance greater than D_{max}) become part of the range of evolutionarily

independent populations.

Conversely, consider two populations of the same species at time *t*, which, by definition of an independent population, are separated geographically by a distance at least as large as the maximum dispersal distance (D_{max}) of the population. If climate change creates environmentally suitable habitat in a cell that is at least as close to both populations as the dispersal limit (D_{max}), then the populations coalesce. Coalescing populations lose their distinct identity and become a single population.

Environmental niche dynamics of fragmenting and coalescing populations

When the geographic distribution (range) of an ancestor population becomes fragmented into independent populations, all smaller populations inherit the environmental niche of the ancestor population (Movie 2). However, due to founder effects and spatial structure of genetic variability, smaller populations do not inherit exactly the same niche properties as larger populations. Under either a center-to-periphery model of gene flow or an isolation-by-distance model, it is not expected that populations located in regions of different environmental conditions would inherit the same environmental niche, without any specialization to the local climate. In addition, if the fragmentation of the ancestor population yields sub-populations of varying sizes, it is unlikely that each sub-population would harbor the same amount of genetic variation.

Thus, in our model, in the event of range fragmentation of an ancestor population, the niche limits of the newly isolated, descendant populations are determined by the ancestral population's niche limits, local environmental conditions, and population size, according to the following formulas (applied to each niche dimension independently):

$$PopNicheMax = AncestorNicheMax - [(AncestorNicheMax - PopRangeEnvMax) \times (1 - FracAreaAncestorPop)]$$

$$PopNicheMin = AncestorNicheMin + [(AncestorNicheMin - PopRangeEnvMin) \times (1 - FracAreaAncestorPop)]$$

where (1) *PopNicheMax* and *PopNicheMin* are the new maximum and minimum tolerance limits of the new population to a given environmental factor, (2) *AncestorNicheMax* and *AncestorNicheMin* are the maximum and minimum tolerance limits of the ancestor population to the same environmental factor, (3) *PopRangeEnvMax* and *PopRangeEnvMin* are the maximum and minimum environmental conditions within the geographic range of the new population, and (4) *FracAreaAncestorPop* is the ratio between range size of the descendant sub-population (each new fragment, after fragmentation) and the ancestor population (the whole population, before fragmentation).

This model assumes that, after fragmentation, a newly isolated population of large area (similar to the range size of the ancestral population) inherits an environmental niche similar to its ancestor, because most of the genetic variation of the ancestral population is transmitted to this large descendant population. Conversely, a newly isolated population that represents only a small fraction of the original area of the ancestral population should hold a proportionally smaller fraction of the ancestral genetic variation. Thus, if genetic variation is spatially structured, the small sub-population is more prone to niche specialization, both in terms of niche optimum and niche breadth.

Conversely, when fragments rejoin and the populations coalesce, their respective niches contribute to the definition of the environmental niche of the newly coalesced population. However, smaller populations contribute less than larger populations. To account for this asymmetry, the contribution of each population is weighted by its range size (sum of area of occupied cells). Thus, the maximum and minimum tolerance limits of the newly coalesced population, for each niche dimension, are the average of maximum and minimum tolerance limits of all coalescencing populations, weighted proportionally by the respective range size of each coalescencing population.

Allopatric speciation

If a population remains isolated long enough from all other populations of its species, independent evolution will likely create reproductive barriers, consolidating allopatric speciation. Because the minimum time in isolation required for speciation is unknown, we model it as a free parameter (T_{min}). Thus, if a population (or lineage of populations) has been continuously geographically isolated from all other populations of the same species for a length of time equal to T_{min}, the population is declared a new and independent species (Movie 2). Because the new species has no further chance of future coalescense with other populations of its ancestral species, it has the potential for secondary sympatry with its sister species.

Interspecific competition and competitive exclusion

In classical ecology, two species with the very same resource use/requirements (i.e. same niche) cannot coexist (*151-155*). Until now, however, models on broad spatial, temporal, and taxonomic scales have failed to incorporate the effects of interspecific competition on biodiversity patterns through simulation of competitive mechanisms. The principal challenge has always been modeling the resources for which species compete, without modeling individual consumers and the myriad of resources and their respective depletion rates. Here we incorporate resource competition, without explicitly modeling resources. In our model, the potential geographic distribution of a population is a function of climate, but realized geographical distributions can be modified by interspecific competition and dispersal.

In the sections that follow, we describe the construction of a multi-part measure of population vulnerability to interspecific competition, which we call the *index of competition*, *C*. At each time step in the model, the fate of each population, in each cell, is determined by its index of competition in relation to C_{max}, a model parameter that sets the maximum intensity of competition in a given cell that nonetheless permits coexistence. Thus, if *C* for one or more species in a cell exceeds C_{max}, competition prevents one or more species from occupying that cell.

Intensity of competition and phylogenetic distance

Assuming that the use of resources by species (e.g. food items, foraging time/strategy) evolves at a constant average rate with variance proportional to time (i.e. a Brownian motion model of trait evolution), the expected intensity of competition ($0 < Comp < 1$) between two species declines with phylogenetic distance (*PD*) between the two species, which increases steadily with time. With that assumption, the actual resources for which the species compete for do not need to be explicitly modeled, for our purposes, because the overall effect of competition between species will consistently decrease with phylogenetic distance. This simplification assumes that competition is approximately symmetric between a pair of species (the intensity of competition of species A on species B is the same as intensity of competition of species B on species A), because phylogenetic distance between two species is also symmetric.

As the intensity of competition decreases with increasing phylogenetic distance (linearly in the case of a Brownian motion model of evolution, or non-linearly for a more complex evolutionary model), it is reasonable to assume a threshold in time after which resource competition between two species would become negligible and sympatry may occur, unimpeded by competition. Thus, we assume that a pair of species that are phylogenetically more distant than a minimum threshold P_{min} would have no resource overlap and therefore no resource competition between the two species. In this case, their environmental niches may continue to overlap without restriction; indeed, they must overlap, for sympatry.

Thus, the intensity of competition (*Comp*) suffered by a particular species can be calculated as:

$$Comp = 1 - \frac{PD}{P_{min}}$$

For example, if species A and B are 10 phylogenetic units apart, and the phylogenetic threshold for no competition P_{min} is 30 phylogenetic units, we calculate the intensity of competition imposed by species A on species B (or species B on A, since competition between any pair of species is symmetric) as:

$$Comp_{AB} = Comp_{BA} = 1 - \frac{PD_{|A-B|}}{P_{min}} = 1 - \frac{10}{30} = 0.666$$

In the simplest traditional approaches (e.g. Volterra-Gause models), competition and its effects on equilibrium population size are usually modeled between two species. However, all co-occurring species that share resources should be considered competitors (*121, 156*). Assuming that the presence of each additional competitor in a particular map cell causes an additive effect on the overall intensity of competition. To take account of all competing species, we calculate *diffuse competition* (*157*) as:

$$Comp_A = \sum_{i=1}^{p} \left(1 - \frac{PD_{A-i}}{P_{min}}\right), \; for\; A \neq i, for\; PD_{A-i} < P_{min}$$

where i is one of the p species present in a given cell.

For example, given the phylogeny below, one can calculate the following expressions to arrive at the total diffuse competition on each of four species, A-D, with a threshold of P_{min} = 30 phylogenetic units for escape from competition:

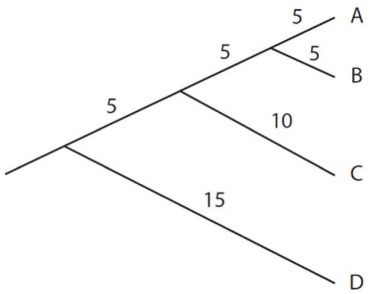

$$Comp_A = \left(1 - \frac{5+5}{30}\right) + \left(1 - \frac{5+5+10}{30}\right) + \left(1 - \frac{5+5+5+15}{30}\right) = 0.666 + 0.333 + 0 = 1$$

$$Comp_B = \left(1 - \frac{10}{30}\right) + \left(1 - \frac{20}{30}\right) + \left(1 - \frac{30}{30}\right) = 1$$

$$Comp_C = \left(1 - \frac{20}{30}\right) + \left(1 - \frac{20}{30}\right) + \left(1 - \frac{30}{30}\right) = 0.666$$

$$Comp_D = \left(1 - \frac{30}{30}\right) + \left(1 - \frac{30}{30}\right) + \left(1 - \frac{30}{30}\right) = 0$$

Environmental niche and ecological stress

Assuming that the environmental niche of a population is analogous to a fitness function, individuals occurring in cells with extreme environmental conditions (with respect to the environmental tolerances of the population) have lower fitness, leading to a lower population

density. Conversely, grid cells with environmental conditions near the center of a population's environmental niche are more "suitable" for the population, therefore individuals in these cells would have higher fitness, leading to higher population density. Thus, the niche center can be considered as the most suitable environmental conditions (e.g. less stressful), whereas niche limits can be considered as the most stressful environmental conditions still permitting persistence.

On one hand, if the maximum and minimum annual environmental conditions in a cell (*CellEnvMax* and *CellEnvMin*) are very different from the niche center of the population (*PopNicheMid*), then the cell is subject to extreme environmental conditions over the course of a year. On the other hand, if the maximum and minimum environment conditions in a cell are similar to the optimal environment of the population's niche center, then the environmental conditions in the cell are less stressful to the population. However, to judge the degree of similarity of the cell's environment to a population's niche, we must also take into account the overall size of the population's niche, based on niche limits *PopNicheMax* and *PopNicheMin*. Thus, we compute an *environmental stress index* of the following form:

$$EnvStress = \frac{\left((|CellEnvMax - PopNicheMid|) + (|CellEnvMin - PopNicheMid|)\right)}{\left((|PopNicheMax - PopNicheMid|) + (|PopNicheMin - PopNicheMid|)\right)}$$

This equation calculates the ratio between (1) the environmental distances between maximum and minimum environmental conditions of the cell and the niche center, and (2) the maximum environmental scope tolerated by the population, defined as the distance between niche limits and the niche center. The same calculations can be extended to a multi-dimensional environmental space by averaging the *environmental stress index* of multiple environmental factors (e.g. temperature and precipitation):

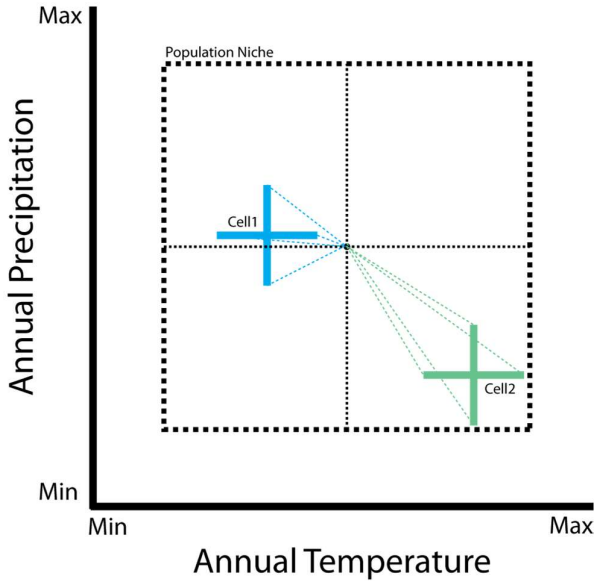

Figure S9. Graphical representation of the *environmental stress index*. The dashed box represents the population niche, in which the center of the box represents the niche center (optimum). The crosses represent two grid cells occupied by the population, in which the vertical line in each cross is precipitation seasonality (minimum and maximum), and the horizontal line is the temperature seasonality. The sum of the lengths of dashed colored lines, measuring the environmental distance between the climatic extremes of a grid cell to the niche center of the population, is divided by half the perimeter of the niche box. In this hypothetical example, the population is under more intense environmental stress in the

green cell.

In the example illustrated above (Fig. S9), the niche of the population is depicted as the outer square (dashed black line). The niche optimum is depicted as the blue dot at the center of the square, and the niche amplitude is illustrated as the narrow-dashed lines connecting the optimum of the niche (center of the square) to the niche limits (sides of the square). The environments of two cells are represented by the blue and green crosses. The magnitude of stress imposed on the population by occupying each cell is represented by the dashed lines connecting each of the environmental extremes for the cells (the tips of the crosses) to the niche center. In this example, the average length of the blue dashed lines indicates the average stress of the population occupying the blue cell. It is clear from this figure that the population is under more intense stress in the blue cell than in the green cell, because the average length of the dashed green lines is greater than the average of the dashed blue lines. Finally, the environmental stress in any cell (the average length of the dashed blue and green lines) is standardized by the niche amplitude (half the perimeter of the niche box).

Competitive exclusion

Two species may coexist if the resources that they utilize are sufficiently distinct. In our model, two recently diverged species are assumed to utilize the same resources and therefore compete maximally. However, in the model, the degree of resource use overlap between the two species decreases linearly with time since divergence (i.e. with phylogenetic distance). However, if the two coexisting species compete (i.e. they are phylogenetically closer than P_{min}), one of them may be extirpated from the cell. The excluded species is likely to be the competitor that is under stronger environmental stress in the cell where the two species overlap. Thus, if the intensity of competition and/or environmental stress is high, the more environmentally stressed population will be removed from the cell. Assuming that the effects of intensity of competition and environmental stress are additive, their interaction is illustrated below.

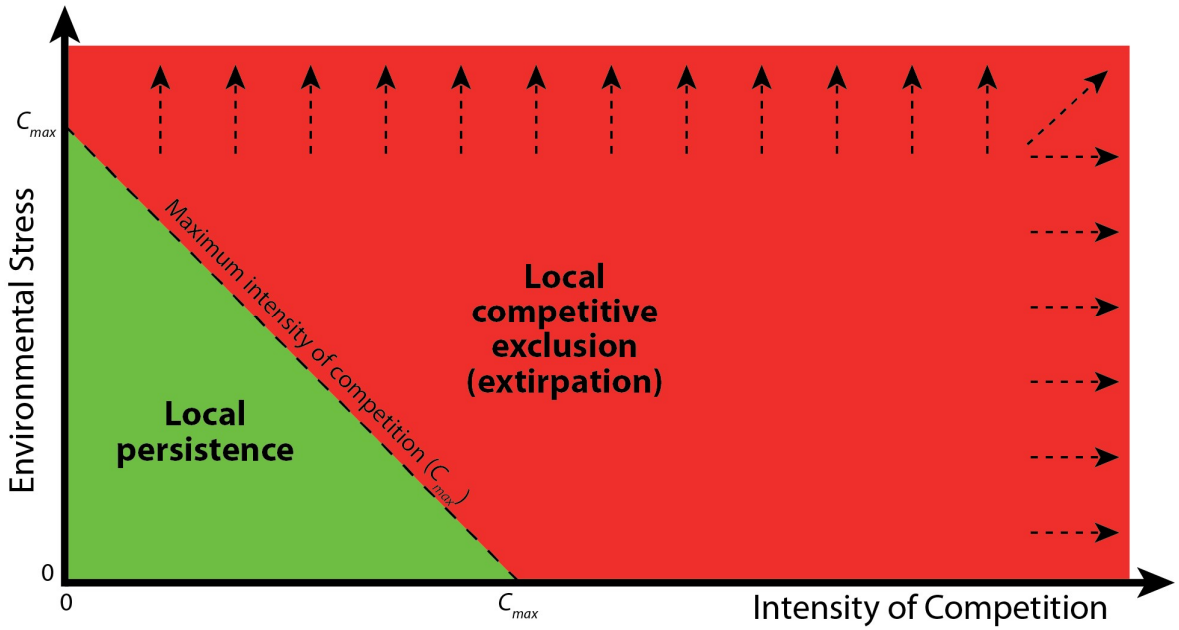

Figure S10. A population occupying a given grid cell, at a given time step, will be under some degree of environmental stress (given its niche and the current climate in the cell, as measured by the *environmental stress index*) and the local intensity of competition (given the co-occurring species in the

same cell, as measured by the *competition index*). If the population in the cell falls in the green zone of low environmental stress and/or weak competition, it persists in the cell. If the population in the cell falls in the red zone of high environmental stress and/or strong competition, it is eliminated from the cell (extirpated) as a consequence of competitive exclusion.

In the diagram above (Fig. S10), each cell occupied by a given species can be plotted according to the intensity of competition with all co-occurring populations of other species (X axis) and environmental stress (Y axis). Thus, a population, in a given cell, will be located in the green zone if it is under low environmental stress (the environmental condition of the cell is close to the niche center of the population) and/or if the intensity of competition is low (all other populations coexisting in the cell are phylogenetically distant). Conversely, populations under high intensity of competition and/or high environmental stress (red zone) become locally extirpated (removed from the cell).

For our simulation model, the index of environmental stress and the index of the intensity of competition are calculated for each population, in each cell c, at each time step. These two indexes are then added, for each population, resulting in a single *index of competition,* C_c, for that population, in that cell c. All populations occupying a single cell are then sorted according to the magnitude of this combined index C_c. If the population with highest competition index C_c has a value greater than the maximum intensity of competition allowing coexistence, parameter C_{max}, then the population is removed from the cell. Next, the competition index is re-calculated for all remaining populations in the cell c, now assuming the absence of the population that has been previously extirpated by competitive exclusion. The competition index C_c is re-calculated and populations are sorted again. If the population with the highest competition index C_c has again an index greater than C_{max}, then that population is also removed. The algorithm iterates until the population with highest competition index in the cell has an index C_c that falls below the threshold C_{max}.

Model specification: process sequence

In our model, we are forced to implement continuous ecological and evolutionary processes in discrete time steps. At each time step, a series of operations must be performed sequentially, to mimic the inherently interacting processes that drive species distributions and evolution. The order of these operations is necessarily somewhat arbitrary, but we have endeavored to choose an order that makes the most sense. In designing the process sequence, we have made the following assumptions. (i) Dispersal processes are faster than evolutionary processes; thus adaptation to climate change (step (6) below) occurs only after dispersal has responded to changed climatic conditions (step (1)). (ii) Intraspecific processes are faster than interspecific ones; thus interspecific competition is reckoned only after adaptation to climate change. (iii) Explicit evolutionary adaptation occurs only through trailing-edge selection on niche limits.

Assume that the gridded geographical map is occupied by a number of geographical ranges (each of which represents a population of a surviving species) at the end of time step t. Each population has its own fundamental niche for time t, specified by its minimum and maximum annual temperature tolerance and minimum and maximum annual precipitation tolerance. Likewise, at time t, each map cell has a specified minimum and maximum annual temperature and a specified minimum and maximum level of annual precipitation.

At time t+1, the following steps are taken, in the order indicated below:

(1) Climate specification. The climatic conditions for time $t + 1$, for each cell in the map, are specified by the stand-alone paleoclimate model outlined earlier. Four values are provided by the

climate model for each map cell, at each time step: minimum and maximum annual temperature and minimum and maximum annual precipitation (Movie 1).

(2) Persistence. For each population, each cell that was occupied by the population at time t is evaluated by comparing the climatic conditions at time $t + 1$ with the population's fundamental niche limits for time t. If the new conditions in a cell lie within the time-t niche (tolerance) limits of the population, it continues to occupy the cell.

(3) Dispersal and leading edge specification. Each cell that was occupied by the population at time t is considered for dispersal to neighboring cells, whether contiguous or not, that are climatically suitable at time $t + 1$, given the time-t niche limits of the population. Dispersal is controlled by a parameter D_{max}, which sets the maximum geographic map distance that a population can disperse. Thus, all cells that are climatically suitable at time $t + 1$ that lie within distance D_{max} of each cell occupied at time t by the population are colonized in this step of the process sequence. All cells newly occupied through dispersal, in this step of the sequence, are hereafter designated as *leading edge cells* (Movie 2).

(4) Trailing edge specification. Any cell that was occupied by the population at time t but that has become climatically unsuitable at time $t + 1$ and that lies more than distance D_{max} from a climatically suitable cell (occupied cell) is designated a *trailing edge cell* for the range. The population in each trailing edge cell is under selection, and must go through adaptive evolution of one or more niche limits to stay in the cell. Sub-populations in newly-unsuitable cells that lie within distance D_{max} of a suitable cell are assumed to have dispersed to a suitable cell.

(5) Climate change and evolutionary rates. The evolutionary rate (H_c) required to allow a population to persist in a trailing edge cell c is computed separately for each of the four niche traits for each trailing-edge cell. H_c is defined as the difference between the environmental condition in the trailing edge cell c, at time $t + 1$, and the environmental condition averaged over all cells occupied by the population at time t, within the genetic neighborhood of cell c—a region defined by maximum dispersal distance D_{max} from trailing edge cell c. This environmental difference is then scaled by dividing by the standard deviation of environmental conditions in the genetic neighborhood at time t (as described in in the narrative section above, "Climate change and niche evolution").

(6) Adaptation: response to selection. A parameter H_{max} defines the upper limit of potential evolutionary rate (adaptation) of the population in a trailing edge cell. Populations are extirpated from trailing edge cells in which H_c is greater than H_{max}. Conversely, evolutionary rescue allows the persistence of populations in trailing edge cells in which H_c is less than H_{max}. The new niche trait of the population (e.g. maximum annual temperature) then becomes that of the trailing-edge cell with largest *post-selection niche limit*. The altered trait then applies to the entire population, as described next.

(7) Evolutionary rescue. Each trailing edge cell, that was occupied by the population at time t, but became unsuitable at $t + 1$ due to climate change, is considered for re-occupation, given any new niche limits of the population as specified in Step 6, above. As before, dispersal is controlled by the parameter D_{max}, which sets the maximum geographic map distance that a population can disperse. All trailing-edge cells that are climatically suitable, after niche adaptation, and that lie within distance D_{max} of each cell occupied at in Step 3 are colonized.

(8) Interspecific competition and competitive exclusion. For each map cell, interspecific competition among all occupying populations is assessed, potentially leading to competitive exclusion, according to the rules specified in the narrative section above, "Interspecific competition, dispersal, and competitive exclusion."

(9) Range coalescence and environmental niche dynamics. Following the application of competition rules, each surviving population is evaluated for potential coalescence and environmental niche consolidation, following the rules specified in the narrative section, above, "Range fragmentation/coalescence and environmental niche dynamics" (Movie 2).

(10) Allopatric speciation. Each population that has not coalesced with another population of its own species is evaluated as a candidate for speciation, following the rules specified in the narrative section, above, "Allopatric speciation." If the two populations of the same species have maintained geographic isolation for T_{min} time steps, an speciation event is declared, and the populations become independent sister species, which can no longer coalesce (Movie 2).

See Fig. 1 (Main Text) for a graphical representation of the model.

Summary of model parameters and initial conditions

The simulation model depends upon and requires initialization of the five parameters and the initial conditions detailed in Tables S1 and S2, below.

Table S1. Model parameters.

Model parameter	Description
Maximum dispersal distance (D_{max})	Sets the maximum geographic map distance that a population can disperse to occupy a climatically suitable cell. Thus, all cells that are climatically suitable and lie within distance D_{max} of each cell already occupied at time step t are colonized in time step $t + 1$ by dispersal.
Maximum niche evolutionary rate (H_{max})	Sets the upper limit of potential climatic adaptation of the population in a trailing edge cell. H_c is the required evolutionary rate (niche adaptation) that would ensure the persistence of the local population at the trailing-edge cell c. If H_c does not exceed H_{max} in the trailing edge cell, the population persists in the cell by adaptive evolution of the population niche limits.
Minimum time for speciation (T_{min})	Sets the minimum time in isolation for a new species to arise. Once a population (or lineage of populations) has been continuously geographically isolated from all other populations of the same species for T_{min} generations, the population (or lineage) is declared a new and independent species.
Minimum phylogenetic divergence for coexistence without competition (P_{min})	Sets the minimum phylogenetic divergence for negligible interspecific competition. Once a pair of sister species achieves the phylogenetic distance of P_{min}, resource competition between them becomes negligible and they may coexist in sympatry without competing.
Maximum intensity of competition allowing	Sets the maximum intensity of competition (C_{max}) that still permits coexistence among competing species. If the population under the

coexistence (C_{max})	highest competition and environmental stress has a C_c value greater than C_{max}, then the species is eliminated from the cell by competitive exclusion.

Table S2. Initial conditions.

Initial condition	Description
Center of origin of ancestral species	At the beginning of the simulation, one map cell is defined as the place of origin of the ancestral species of the simulated clade.
Niche of ancestral species	At the beginning of the simulation, the climatic tolerances (niche limits) of the ancestral species are defined setting the climatic conditions (minimum and maximum annual precipitation and temperature) that the species can tolerate. The ancestral species initiates its geographic range by occupying all cells within maximum dispersal distance (D_{max}) of the center of origin that are climatically suitable.
Heterogeneity of environmental factors	To investigate the effect of spatial heterogeneity in climate variables we applied a mathematical smoothing filter, at different strengths, to minimum and maximum precipitation and temperature variables (see *Experimental design and parameter exploration*)

Speciation, persistence, and extinction: Species' lifetime trajectories

From the beginning of the simulation at 800 ka, when only the founder species is present, to the final time step, the lifetime trajectory of each species (and its population or populations) is recorded in space and time. Each species is characterized by the duality between its climatic niche and its geographic distribution. The ecological and evolutionary events and processes that affect the niche and distribution of a species include the time and place of its origination (speciation), climate change driving range dynamics and niche evolution, competitive exclusion, range fragmentation, speciation and/or extinction.

In our simulation, the three possible fates of a species are (1) a cladogenetic split into two daughter species, (2), extinction due to range collapse or (3) survival until the end of the simulation. Thus, the lifetime trajectory of a species may be subdivided into three, mutually exclusive conditions: a *speciation trajectory*, a *persistence trajectory*, and, if the species goes extinct during the simulation, *an extinction trajectory* (Fig. 2 Main Text).

The lifetime trajectories of all species are fully known only once the simulation is completed. Thus, we first run the simulation forward to record all the biogeographical information generated by the simulation, such as the distribution of all species, their evolutionary relationships, cladogenetic events, and extinction. Once the full simulation is completed and the history of all species has been recorded, the life stages of each species (i.e. speciation, persistence, and extinction) are identified by stepping backwards through the completed simulation results. From the backward analysis of a simulation, each species, at each time step, may be classified in either a speciation, persistence, or

extinction trajectory. Species that give rise to daughter species or persist into the present lack an extinction trajectory. Once a species is classified as in a speciation or extinction trajectory, the species is soon removed from the simulation, either as a result of speciation or extinction, because of the transient nature of these two categories. Conversely, a species may remain in the persistence category during an indefinite period of time, as long as it neither speciates nor goes extinct. Finally, the change of category of one species does not affect the classification of any other species, nor does classification affect the events in the simulation.

Speciation trajectory

A species is classified in the speciation trajectory from the moment of range fragmentation into sub-populations until the consolidation of speciation, T_{min} time steps later (Fig. 2 Main Text, thick dashed lines,). Thus, by definition of a range fragment, the geographic distribution of a species in the speciation stage must comprise two or more isolated populations. By running the simulation backwards, we can identify the time step of speciation of each species, and track the geographic distribution of its range backwards in time until the time step of range fragmentation. As explained above, the duration of the speciation trajectory is regulated by model parameter T_{min}. Species composed of incipient populations that remained in isolation for less than T_{min} are not classified in the speciation trajectory, either because these populations later coalesced with another population of the same species, or because their range contracted until collapse into extinction.

Extinction trajectory

A species is in its extinction trajectory during the process of range contraction, which is defined as a continuous downward temporal trajectory of its range size, ending in total range collapse (Fig. 2 Main Text, thin dashed red line). Thus, the length of an extinction trajectory of a species depends upon the rate of its range contraction. Using the full record of each simulation, we analyzed the temporal trend of range size of each extinct species, running the simulation backwards to define and record the period between the extinction event and the beginning of the process of range contraction, as defined by a negative slope between range size and time step.

Persistence trajectory

A living species is classified as in a persistence trajectory if it is neither in an extinction trajectory nor in a speciation trajectory (Fig. 2 Main Text, thick solid lines). Thus, range fragmentation that does not lead to speciation (because range fragments may collapse or re-coalesce with other fragments) is not sufficient to classify a species in the cradle trajectory. Likewise, range contraction that does not lead to extinction (because range size may later increase or stabilize) is not sufficient to classify the species in the extinction trajectory.

Emergent multi-species patterns from single-species trajectories

In our model, interactions among niche, dispersal capacity, competition among species, and climate dynamics shape the geographic distribution of species, which in turn may drive niche evolution, range fragmentation, speciation, and extinction (Fig. 1, Main Text). From the interplay among these interlinked processes many biogeographic events take place, and, at each step of the simulation, each species is classified at each time step according to the three fundamental, lifetime trajectories: speciation, extinction or persistence. By aggregating the spatial and temporal trends of the combined lifetime trajectories of sets of species that compose an assemblage, we can study emergent biodiversity patterns, including adaptive radiations, mass extinctions, rates of net diversification, and the formation of patterns in species richness. Here we focus on the emerging patterns of time and place of speciation (cradles), persistence (museums) and extinction (graves)

(Fig. 2 Main Text).

Cradles, graves and museums

As explained above, at every time step, each and every extant species is classified in one, and only one, portion of its lifetime trajectory: either speciation, persistence, or extinction (Fig. 2). During the period that a species is classified in one of these three life stages, its spatial occupancy is recorded on the map, as defined by the geographic distribution of the species, and its temporal occupancy is recorded in a timeline. For example, one could count the number of species that are in the process of speciation (i.e. classified in the speciation lifetime trajectory) in a given location (spatial occupancy), or the number of species in the processes of extinction (i.e. classified in the extinction lifetime trajectory) in a given moment (temporal occupancy). We define a *cradle* by the number of species classified in the speciation trajectory and a *grave* by the count of all species classified in the extinction trajectory, in a given place or time. A *museum* is defined by the number of species classified in the persistence trajectory that coexist in a given location or time. Thus, at any given moment or location, the sum of cradles, graves and museums equals the total number of species (richness), because each species must be classified, without exception, as in a speciation, a persistence, or an extinction trajectory. In other words, cradles, graves and museums are decompositions of patterns of total species richness into the most fundamental biogeographic processes (speciation, persistence, and extinction) at the species level. Finally, the difference between cradles and graves (speciation minus extinction) defines the net diversification of the clade at a given location or time.

Temporal patterns: time series of cradles, museums, graves, and richness

At any given step in the simulation, one can calculate the time-specific cradles (total number of species in speciation trajectory at that time step), museums (total number of species in the persistence trajectory at that time step), and graves (total number of species in the extinction trajectory at that time step). A temporal pattern (an *occupancy time series*) of these components of biodiversity may be generated by calculating the total number of cradles, museums, or graves for each and every time step in the simulation. Likewise, we can also calculate a time series of *net diversification* (cradles – graves) and *total* richness (cradles + graves + museums).

Time-specific occupancy maps of cradles, museums, graves, and total richness

The time series of cradles, museums, and graves may be calculated not only for the entire set of species in the simulation, but also only for the assemblage of species occupying a given map cell. At any given time step, each species contributes to the map of cradles, museums, or graves, for every map cell that it occupies at that time step. Thus, we may construct a sequence of time-specific occupancy maps for cradles, museums, and graves, on a continental scale. By recording and chronologically displaying these time-specific maps of richness, calculated for each simulation time step, we created movies that describe spatial and temporal rates of species richness (e.g. Movie 2).

Static space-time patterns: cumulative maps of cradles, museums, graves, and total richness

A time series of time-specific cradle richness, grave richness, or museum richness maps may be integrated as the summation of species richness over the entire course of the simulation (e.g. the total number of species in the extinction trajectory in each map cell throughout the simulation). We define a *cumulative richness map* as the summation, for each map cell, over all time steps, of cradle, museum, or grave species richness. Thus, a *cumulative cradle richness map* plots, in each map cell, the total number of species in the speciation trajectory that ever existed throughout the entire course of the simulation in that map cell. The overlay (summation) of cumulative cradle, museum, and grave species richness maps yields the *cumulative total richness map*, as the sum of cradles, museums and graves defines the total number of species.

Summary of emergent properties and patterns

Given the ecological and evolutionary mechanisms built into the model, the parameter settings, and the initial conditions, Tables S3 and S4, below, specify the emergent properties at the level of species and lineages, and the spatial and temporal patterns at the assemblage level that emerge from the simulation. Fig. 1 (Main Text) provides a graphical summary of the interaction among modeled processes on the emerging properties and patterns.

Table S3. Emergent properties and patterns at the population level.

Emergent properties at the level of population, species and lineages	**Description**
Climatic niche	Each species inherits its climatic niche from its ancestors, but over time, its niche can be modified in two ways. First, climate dynamics may impose selection pressure on niche limits in trailing-edge cells, expanding the niche by adaptive evolution, in turn affecting the species' geographic distribution. Second, climatically-imposed fragmentation of species ranges can contract the niche of a geographically isolated population, which is assumed to remain adapted only to the extremes of conditions prevailing within the range of the fragment at the time of fragmentation.
Species geographic distribution	The geographic distribution of each species is a consequence of the interaction between a dynamic climate, the species niche, and competition with phylogenetically related species. As climate changes, each species responds by re-shaping its geographic range through dispersal and local extirpation and by adapting its climatic niche. Climate dynamics also fragment species ranges, and ultimately drive allopatric speciation. The place of origin and the niche and geographic distribution of a descendant species is a consequence of evolutionary history of its ancestors
Species temporal distribution	The time of origin, time of extinction, and longevity of a species are the consequences of a complex chain of events, including the inherited niche and place of origin, ecological and evolutionary response to climate dynamics and dispersal capacity, and competition with phylogenetically related species
Segments of species lifetime trajectory	Each species, at each step of the simulation, is classified as in (*i*) a speciation trajectory if its population is geographically isolated, and will remain isolated for T_{min} time steps; (*ii*) an extinction trajectory if its range size is continuously contracting, and eventually collapses; or (*iii*) a persistence trajectory if the species is in neither a speciation nor an extinction trajectory

Phylogenetic relationships among species	A full phylogeny emerges from simulation model, describing all the events of speciation and extinction, ancestrality relationships and longevity of species

Table S4. Emergent spatial and temporal patterns at the assemblage level.

Emergent spatial and temporal patterns at the assemblage level	**Description**
Cradle richness	The number of species in the speciation trajectory at a given location or point in time defines a *cradle*. We explored the spatial (map) and temporal (time series) patterns of cradles.
Grave richness	The number of species in the extinction trajectory at a given location or point in time defines a *grave*. We explored the spatial (map) and temporal (time series) patterns of graves.
Net diversification	The difference between the number of species in the speciation and extinction trajectories at a given location or point in time defines net diversification at that place or time, which is the subtraction of graves from cradles. We explored the spatial (map) and temporal (time series) patterns of net diversification.
Museum richness	The number of species in the persistence trajectory at a given location or point in time defines a *museum*. We explored the spatial (map) and temporal (time series) patterns of museums.
Total richness (cradle + museum + grave richness)	The number of species at a given location, or point in time, regardless of lifetime trajectory, defines *total* richness. Total richness is the sum of cradles, graves, and museums. We explored the spatial (map) and temporal (time series) patterns of total species richness.
Cumulative richness (of cradle, museum, grave, or total richness)	The overlay (sum) of all time-specific maps of species richness throughout the course of the simulation is a *cumulative* richness map. Thus, the presence of each species, in each map cell, is counted in a cumulative richness measure for as many time steps as the species occupies the map cell. Cumulative maps may be computed for cradle, museum, grave, or total richness.

Experimental design and parameter exploration

To understand the role of the mechanisms implemented in the model (Fig. 1) on emergent patterns of biodiversity, we ran 10,500 distinct simulations, with varying combinations of parameter settings

and initial conditions. The factorial design of our simulation experiment consisted in running the model with all possible combinations of parameter values, as listed in *Summary of explored parameter levels and initial condition* (below). Thus, the exploration of parameter space was not designed to replicate a real-world diversity pattern of an extant group of species or lineages. Instead, our goal was to quantify the relative impact of each model parameter on emerging spatial and temporal patterns of biodiversity. Nonetheless, we show the correspondence between the predictions of our model and empirical patterns in species richness in the section *Evaluating the correspondence between empirical and simulated patterns in species richness.*

The designed experiment allows us to estimate the relative importance of ecological and evolutionary processes implemented in the simulation model (e.g. dispersal, niche evolution, competition). The relative importance of these processes may be assessed by quantifying the relative magnitude of divergence among the species richness patterns produced by the model as a consequence of experimental variation of model parameters, each of which regulates one or more of the processes implemented. For example, consider two simulations, with settings differing only in having widely different levels of the competition parameter C_{max} (i.e. very intense *versus* mild competition between coexisting sister species). If these two simulations, nonetheless produce very similar biodiversity patterns, then competition may be judged to have relatively little importance to the emergence of the biodiversity patterns, because the experimentally varied parameter C_{max}, which regulates the process of competition, did not produce any substantial change in the predictions of the model. Conversely, if simulations differ in parameter settings only with respect to values of the dispersal parameter D_{max} produce radically different biodiversity patterns, then we may infer that maximum dispersal distance is an important driver of biodiversity patterns. Because the model was built upon widely-accepted ecological and evolutionary processes and their underlying mechanisms, the relative importance of parameters that regulate these processes suggests corresponding differences in their relative significance in natural systems.

Of course, the full parameter space is infinite, as most of these parameters are continuous and boundless variables. However, on one hand, the exploration of parameter space is strictly constrained by computational limits, both in processing power (computational speed) and storage capacity (size of RAM and ROM memories). On the other hand, the parameters that regulate the modeled processes have ecological and evolutionary interpretations, which may be used to conceptually limit the range of meaningful parameter values. Thus, acknowledging the tradeoff between scientific interest in a deeper and broader exploration of parameter space and the constraints on computational capacity, we obviously had to limit to the range of parameter values explored.

Although application of an experimental approach to quantify the relative importance of factors (parameters or initial conditions) is conceptually and statistically well established, the estimated relative importance of a factor depends not only on the range of values (levels) explored for that factor, but also on the range of values explored for the entire set of parameters under consideration. Thus, in our experimental design we employed two integrated strategies to define the range of values to be explored for each parameter: (*i*) a conceptual definition of the minimum, maximum and intermediate steps of each the levels for each parameter, based on the biological interpretation and realism of the implemented process; and (*ii*) preliminary experimental evaluation of the feasibility of the simulation, carried out by testing the proposed extreme levels of each parameter.

Maximum dispersal distance (D_{max})

Our model is both spatially and temporally discrete, which limits and defines the behavior and interpretation of all model parameters. *Maximum dispersal distance* (D_{max}) is the parameter that sets the maximum geographic map distance that a population can disperse, over one simulation step of

500 years, to occupy a climatically suitable cell. Thus, all cells that are climatically suitable, and lie within distance D_{max} of an already occupied cell, at time step t, are colonized by dispersal in time step $t + 1$ (500 years later). In addition, populations may be able to colonize climatically suitable cells that are isolated by barriers of unsuitable habitat, as long as the suitable cells lie within D_{max} distance from the currently occupied area. Although there is no available empirical data on the maximum dispersal distance of species over a period of 500 years (a single time step of our model), we know from observation of living species that dispersal distance may vary substantially, even on and ecological time scale. In addition, there is abundant published evidence that adjacent mountaintops (i.e. "sky islands", (*158, 159*) may harbor isolated sister lineages that are unable to cross climatically unsuitable valleys (Hughes and Eastwood 2006). In our model, the minimum feasible value for D_{max} is the geographic distance between the centers of the largest pairs of adjacent grid cells, 150 kilometers between cells each 10,000 km^2 in area. Thus, if D_{max} is set to 150 kilometers, over a period of 500 years, a population will have very limited capacity to disperse over climatically unsuitable habitat, generally able to expand its range only over continuously suitable habitat. Conversely, there is no theoretical limit for the maximum possible value of D_{max}, although the commonplace absence of extant species in suitable areas in nature is evidence that the geographic range of most species is somewhat constrained by dispersal capacity (*160*). Preliminary tests of the model indicated that D_{max} larger than 750 kilometers would stop range fragmentation of populations, therefore promoting continuous gene flow over the entire domain. Under that scenario, no speciation-by-isolation would ever happen, and islands of suitable habitat would never emerge in the simulation, as the founder species would immediately become geographically ubiquitous. Thus, we set three intermediate steps between the minimum possible D_{max} (150km), and the maximum reasonable D_{max} (750km): 200km, 350km and 500km.

Maximum niche evolutionary rate (H_{max})

The upper limit of potential climatic adaptation of the population in a trailing edge cell is set by the parameter *maximum niche evolutionary rate* (H_{max}). To ensure the persistence of a local population in a trailing-edge cell c (evolutionary rescue), the population requires a niche adaptation (expansion) of at least H_c. Thus, if H_c exceeds H_{max} in the trailing edge cell, then the population is unable to adapt and is consequently extirpated from the trailing edge cell c. Conversely, the population will persist in the trailing edge cell c by adaptive evolution if its niche limits can expand to a level of H_c or greater. Empirically, the degree of niche conservatism/evolution is generally studied as an observed pattern, using comparative phylogenetic analyses (*161*). Previous simulation studies have shown that some degree of niche conservatism is a condition to the emergence of spatial patterns in species richness (*23, 25*). To our knowledge, no evolutionary study has tracked the adaptive capacity of the climatic niche of real-world species in natural environments. However, theoretical studies have shown that a critical H_{max} value of 0.01 would capture an evolutionary rate that is close to the maximum expected in most natural situations (*117, 118*). Thus, we ran preliminary simulations with trial values of H_{max} greater and lesser than 0.01 Haldanes, until diversification ceased when clades failed to adapt to climate change (H_{max} too low), or the founder species became ubiquitous by rapidly adapting to any level of climate change (H_{max} too high). After these preliminary explorations of a meaningful range of H_{max} values, we set the range between 0.005 and 0.02 Haldanes, which is, respectively, half and twice the theoretical expectation for natural situations.

Minimum time for speciation (T_{min})

The time that a population must remain in isolation before being declared a new species is set by the parameter *minimum time for speciation* (T_{min}). Once a population (or lineage of populations) has been continuously geographically isolated from all other populations of the same species for T_{min} generations (assuming a generation time of 5 years), the population (or lineage) is declared a new

and independent species. Speciation is a widely studied subject in evolutionary biology (*162*), and empirical evidence suggests that the process may reach completion over the course of only few dozen generations in genetic isolation (*68, 158, 160, 163, 164*), or that it may take hundreds of thousands of years (*165*). In our model, if T_{min} is too low, then diversification rates will surge, as even ephemeral isolation of two populations would promote speciation. In addition, a high diversification rate would promote an exponential increase in species richness, which could easily overload currently available computational capacity. Conversely, if T_{min} is too high, diversification rate would plunge, as repeated cycles of climate change would rejoin isolated populations before the minimum time for speciation. In addition, a lack of speciation events increases the chance of full clade collapse, caused by extreme cycles of climate change. Preliminary, but thorough, analysis of the impact of T_{min} on the behavior of the model showed that T_{min} values lower than 3,500 generations, under some experimental conditions, boosted the number of species to a computationally intractable level, without causing any substantial difference in the emerging patterns of species richness. At the other extreme, these analyses showed that T_{min} values greater than 4,500 generations substantially decreased the diversification rate, so that clades remained very small. Thus, although there are no theoretical bounds to T_{min} values (except zero), we set three levels for this parameter (3,500, 4,000 and 5,500 generations, assuming a generations time of 5 years), which is sufficient to an experimental exploration of meaningful variation in simulated diversification rates.

Maximum intensity of competition allowing coexistence (C_{max})

The intensity of competition (C_c) that nonetheless permits coexistence of the species potentially present in cell *c* is set by the parameter *maximum intensity of competition allowing coexistence* (C_{max}). If the population under the highest competition and environmental stress has a C_c value greater than C_{max}, then that species is eliminated from the cell by competitive exclusion. Because the index of intensity of competition (C_c) is new to this study, there are no empirical studies that we can use to support an empirical basis for the range of experimentally explored C_{max} values. However, the index C_c does have an intuitive ecological interpretation; it is fundamentally based on the widely accepted assumption that phylogenetically closely-related species compete more intensively than more distantly-related species (*123, 166, 167*). The C_c index is the additive combination of (1) the level of competition with phylogenetically related and co-occurring species in cell *c*, and (2) the level of environmental stress experienced by each species in cell *c*. Thus, in cell *c*, a species with a low level of C_c (i.e. $C_c < 1$) is simultaneously (1) not faced with competition from phylogenetically closely-related species and (2) has a climatic niche optimum (niche center) close to the local environmental conditions in cell *c*. Conversely, if C_c is high for a species in cell *c*, then (1) closely-related species also occur in the cell, and/or (2) the climatic conditions in the cell *c* are close to the tolerance limits of the species. If a species reaches its climatic tolerance limits in surviving annual seasonality of cell *c*, then stress imposed by the environment alone contributes to 1 unit of C_c. In addition, if a species occurs in cell *c* with a closely-related species (at the extreme, its sister species), then the presence of that species adds another 1 unit to its C_c. Of course, the value of C_c continues to increase with additional closely related species also occupying and competing in cell *c*. Thus, if C_{max} is set to less than 1 unit, no species would be capable of expressing its full climatic niche, even in the absence of competitors, as environmental stress alone would extirpate the species from cell *c*. Therefore, we set the minimum experimental value of C_{max} as 1.5 units, which means that a species under its maximum tolerable environmental stress can nonetheless coexist with a competing species that is phylogenetically related at 0.5 P_{min} units (see below). We gradually explored greater values of C_{max}, up to 5 units, a level at which a species under its maximum tolerable environmental stress would nonetheless be capable of coexisting with up to four very closely related species. Preliminary model tests indicated that $C_{max} > 5$ would not produce any substantial difference in emerging patterns in species richness.

Minimum phylogenetic divergence for coexistence without competition (P_{min})

The phylogenetic distance (*PD*) beyond which a pair of sister species would no longer compete is defined by the parameter *minimum phylogenetic divergence for coexistence without competition* (P_{min}). Once a pair of sister species achieves $PD = P_{min}$, resource competition between them becomes negligible and they may coexist in sympatry without competing. Conversely, a pair of recently diversified species ($PD = 0$) has the highest intensity of competition, which decreases linearly with the increasing *PD*, until competition ceases when $PD = P_{min}$. Unfortunately, empirical estimates of P_{min} are not available in the literature, and in fact may vary substantially among taxa. However, the decrease in the intensity of competition with the increase in phylogenetic distance is a widely assumed fact, beginning, at least, with Darwin (*123, 166, 167*). Preliminary tests of the model indicated that P_{min} and C_{max} had exactly the same qualitative effect on predicted patterns of species richness. The close relationship between these two model parameters is expected both mathematically and intuitively, as the intensity of competition, which depends on P_{min}, has an additive effect on C_c, which is regulated by C_{max}. Thus, whereas increasing C_{max} allows a greater number of phylogenetically related species to coexist, decreasing P_{min} produces the same effect by decreasing the estimated intensity of competition among coexisting species. Because of the mechanistic association between these two parameters, which was tested and confirmed with preliminary runs of the model and to maximize use of computational capacity, we set P_{min} to the fixed value of 30,000 generations (150,000 years), a very conservative value for the cessation of competition between sister species.

Founder's niche and geographic center of origin

The historical influence of founder species is believed to have great impact across all scales of spatial and temporal biodiversity patterns (*124-126*). For example, the time and place of founding lineage is thought to drive the biogeographic distribution of clades, population dynamics of species, invasive potential, and structure of genetic variation (*126*). Indeed, a longstanding objective in historical biogeography is the inference of time (phylogeny) and place (center of origin) of lineages from observed spatial and temporal patterns of biodiversity (*104*).

To study the founder effect on emerging spatial and temporal biodiversity patterns, we simulated four different independent lineages, each one characterized by a different founder species, with different initial niches and geographic distributions (Fig. S11). The climatic niche and location of the four lineage founders were designed to cover four major contemporary South American biomes: the Amazon, Atlantic Rainforest, Upper Andes, and Patagonia. The minimum and maximum tolerance of annual temperature and precipitation (climatic niche), and a seed location, allow the founder species to spread its geographic distribution according to the climatic conditions at the beginning of the simulation (800 ka). Then, the founder species must cope with climatic dynamics through the course of the simulation, according to the ecological and evolutionary processes implemented in the model. Thus, in our simulation, the spatial and temporal trajectory of a clade, regardless of how diversified the clade becomes, can be traced back to a single founder species, with known initial distribution (center of origin) and initial niche.

These four founder species were not defined to re-create the biogeographical history of any existing lineage, nor to test any specific hypothesis of tempo and center of origin of a clade. Instead, the simulation was designed to quantify, experimentally, the effect of variation in the biogeographic properties of founder species, therefore testing a widely accepted general assumption about the impact of founder effect on biodiversity patterns.

To control for the effect of niche breadth and range area, the niche of the four founders were approximately standardized, given the climate patterns at the initial time step of the simulation (800 ka). However, because the Amazon is relatively climatically homogenous, the range size of the

Amazonian founder was substantially larger than the other three founders, although niche breadth is relatively equivalent. Preliminary analyses showed that standardization of range area of the Amazonian founder would require the definition of a very narrow niche, which increases susceptibility to full clade extinction at early stages of the simulation.

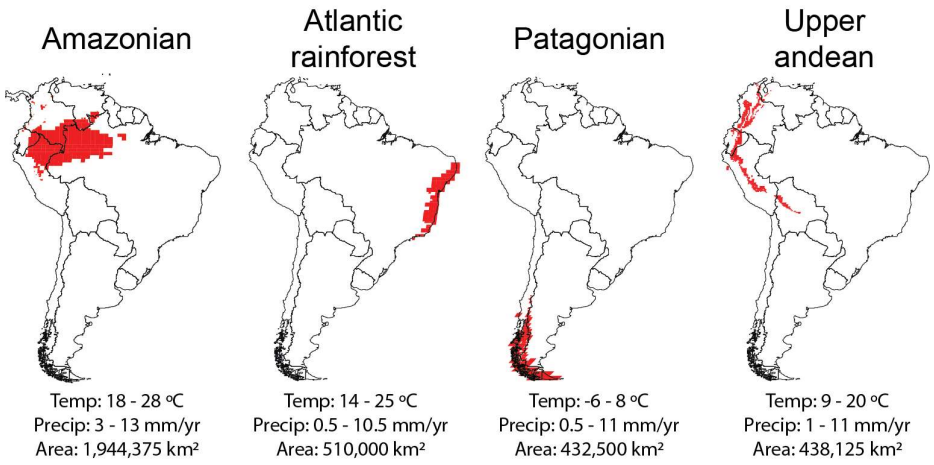

Figure S11. Initial geographic distribution and niche of the four ancestral species used in this simulation to study the effect of founders on the emerging biodiversity patterns. Niche breadth and range size of founders were approximately standardized. The Amazonian founder has larger initial range area because the climate in the Amazon region is relatively homogeneous (preliminary analyses showed that the larger initial range does not disturb model results).

Experimental topographies (effect of environmental heterogeneity by smoothing climate)

The topography of South America is broadly characterized by the Andes (the world's longest mountain range), the Amazonian and Rio de la Plata lowlands (the world's two largest river basins), and the extensive Brazilian and Guiana highlands. The dramatic topography of South America drives spectacular climatic heterogeneity, including the wettest region in the world (Colombian Chocó) and the driest (Chilean Atacama Desert), and great extremes of temperature, both latitudinal and elevational.

To study the effect of actual climatic heterogeneity on spatial and temporal patterns of biodiversity, we simulated the evolution of biotas on experimentally-smoothed South American topographies and climates, applying a spatially weighted average kernel smoother on the elevation, temperature, and precipitation variables. The "strength" of the kernel smoother is regulated by the kernel radius (λ, measured in kilometers), an arbitrary parameter value. Thus, the experimentally-smoothed environmental variable X (i.e. topography, minimum and maximum temperature, and minimum and maximum precipitation) at grid cell i, is re-calculated (X') as the weighted average w_{ij} of the value of X in all grid cells j lying at a distance $d_{ij} < \lambda$ from cell i. In addition, because cells may have different areas, the weight of cell j on cell i is also a function of its area (A_j):

$$X_i' = \frac{\sum_{j=1}^{n} X_j w_{ij}}{\sum_{j=1}^{n} w_{ij}}, \qquad w_{ij} = \left(1 - \left(\frac{d_{ij}}{\lambda}\right)^2\right)^2 \times \frac{A_j}{10{,}000}, \text{ for } d_{ij} < \lambda$$

The effect of the kernel smoother on the topography of South America is analogous to that of a bulldozer: mountaintops are gradually leveled by scattering soil into adjacent valleys (Isaiah 40:4). Thus, the bulldozer does not remove soil, it just relocates it to produce a smoother terrain. In this analogy, the kernel radius is proportional to the amount of bulldozing work in the terrain, so that a larger radius is analogous to moving soil over longer distances. Statistically, the spatial kernel smoother increases spatial autocorrelation of the smoothed variable, because adjacent grid cells reciprocally influence each other's value, and are influenced by a similar set of grid cells in the neighborhood.

We applied seven increasingly larger kernel radii to actual, contemporary topography, to minimum and maximum precipitation by time intervals, and minimum and maximum temperature by time intervals (Fig. S12). For both temperature and precipitation variables, the spatially weighted kernel smoother was applied independently to each step in the entire time series, beginning at 800,000 years ago until the present.

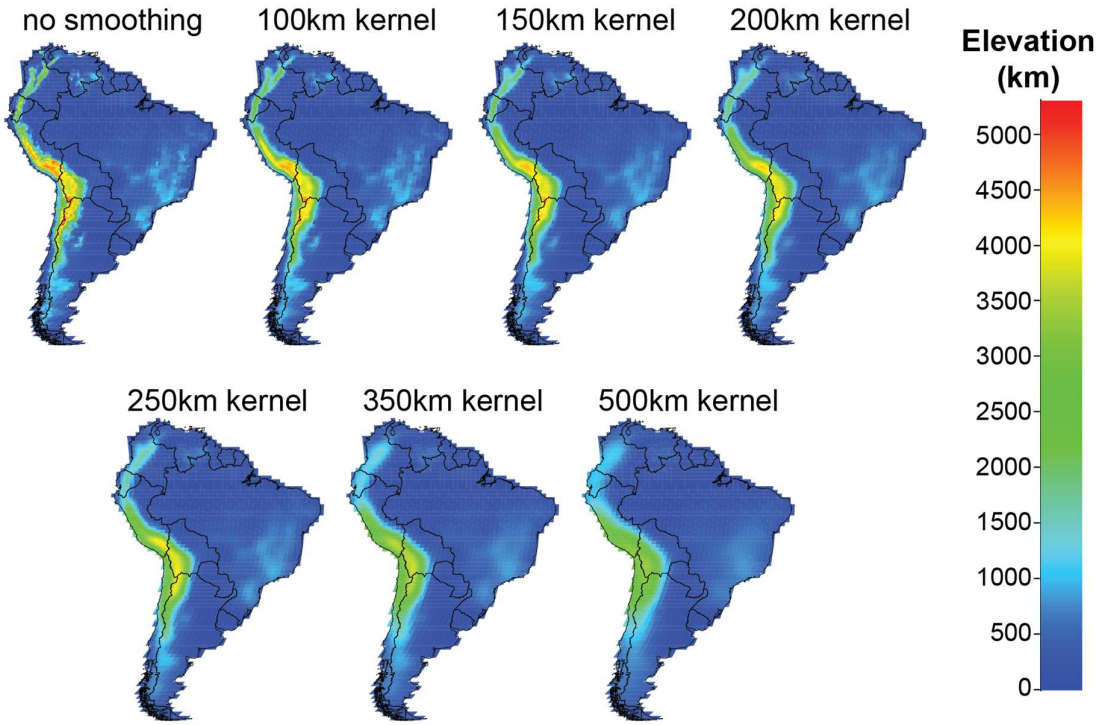

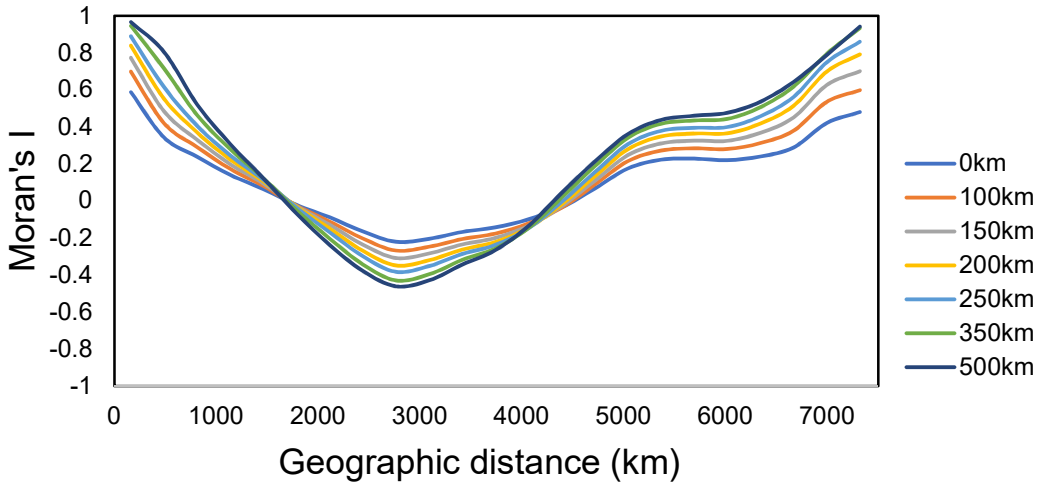

Figure S12. Topographies of South America (top) under different levels of smoothing (kernel radii), used to experimentally test the effect of climatic heterogeneity on emergent patterns of biodiversity. The smoothing kernel increases short scale spatial autocorrelation (bottom) by homogenizing climate and topography of nearby cells.

Summary of explored parameter levels and initial conditions

Table S5, below, summarizes the levels of model parameters and the scope of initial conditions explored in the factorial model.

Table S5. Parameter levels and initial conditions explored

Parameter / condition	**Values / conditions explored**
Maximum dispersal distance (D_{max})	150 km, 200 km, 350 km, 500 km, 750 km
Maximum niche evolutionary rate (H_{max})	0.005 Haldanes, 0.0075 Haldanes, 0.01 Haldanes, 0.015 Haldanes, 0.02 Haldanes
Minimum time for speciation (T_{min})	3,500 generations (17,500 years, 35 simulation steps) 4,000 generations (20,000 years, 40 simulation steps) 4,500 generations (22,500 years, 45 simulation steps)
Minimum phylogenetic divergence for coexistence without competition (P_{min})	Fixed at 30,000 generations (150,000 years, 300 simulation steps)

Maximum intensity of competition allowing coexistence (C_{max})	1.5, 2, 3, 4, 5
Center of origin and niche of founder (seed) species	Amazon (Temp. [18 - 28] ºC, Precip. [3 - 13] mm/yr) Atlantic Rainforest (Temp. [14, 25] ºC, Precip. [0.5, 10.5] mm/yr) Patagonia (Temp. [-6, 8] ºC, Precip. [0.5, 11] mm/yr) Upper Andes (Temp. [9, 20] ºC, Precip. [1, 11] mm/yr)
Topography / climate heterogeneity (strength of smoothing kernel)	0 km (no smoothing), 100 km, 150 km, 200 km, 250 km, 350 km, 500 km

Temporal rates of speciation and extinction

The full history of each of the 10,500 simulations was recorded for detailed analyses of emerging biodiversity patterns, as well as a complete, time-registered phylogeny. For each simulation, we calculated total species richness and its biodiversity components (cradles, museums, and graves) at each time step, generating a total of 10,500 time series of species richness for each biodiversity measure (Fig. S13). In addition, Figure S14 shows temporal patterns of total species richness, averaged among all simulations that share each parameter setting.

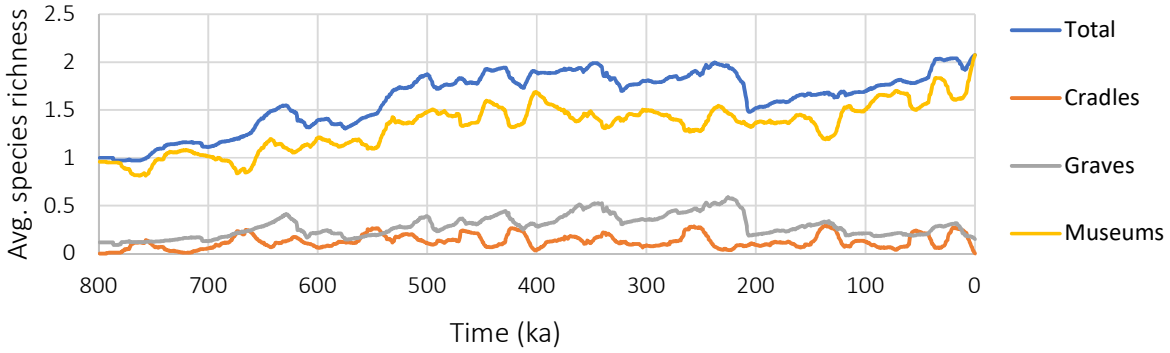

Figure S13. Temporal patterns of total, cradle, museum and grave species richness, averaged among all 10,500 simulations.

To study the effect of initial conditions and parameters on the temporal patterns of biodiversity simulated by the model, we also computed time series of averaged total species richness for all simulations that shared each experimental parameter value (Figs. S14). A relatively small difference among time series generated by models with different parameter levels for a particular parameter indicates the relatively low influence of that parameter on the emerging temporal patterns of species richness. Conversely, if differences in the levels of a parameter produced a relatively large variation in the temporal patterns of species richness, then the parameter has a large influence on the

emerging patterns of species richness.

The upper panel in Figs. 3-5 (Main Text) shows the paleoclimate time series for mean continental temperature for South America, together with occupancy time series for speciation (cradles) and extinction (graves) for Andes, Atlantic Forest, and Amazon founders. Fig. 6 shows the combined data for all three of these founders. The occupancy time series captures the temporal dimension of speciation and extinction by summing occupancy over all cells in South America for each time step, based on the time-specific occupancy maps of cradles and graves. The figures show the average of all parameter values for each founder, but without including any of the topography-smoothing experimental treatments. The highest 5 to 7 peaks of speciation and extinction were marked in Figs. 3-6 (Main Text), manually, as visual aids only, and were not used in any quantitative analysis.

We employed time series correlation analysis to evaluate if the degree to which the quasi-periodicity (repeated, but varying cycles) of extinctions and speciation were driven by glacial-interglacial oscillations in continental temperature and precipitation (or perhaps by internal dynamics of the model). First, we log-transformed the richness data (to equalize the relative role of large and small peaks) and detrended the transformed values (to compensate for the progressive increase in richness over time in several of the occupancy-through-time plots) by taking residuals from a simple OLS regression on time. We then computed Pearson product-moment cross-correlation coefficients, with time lags (delayed responses) from 500 to 100,000 years, for the delayed effects of temperature and precipitation on cradles, graves, and net diversification. In addition, we computed cross-correlation coefficients, for time lags up to 100,000 years, for cradle richness lagging grave richness, and grave richness lagging cradle richness. Statistical significance of both maximum (positive) and minimum (negative) lagged Pearson's cross-correlation coefficients was assessed by means of a randomization algorithm.

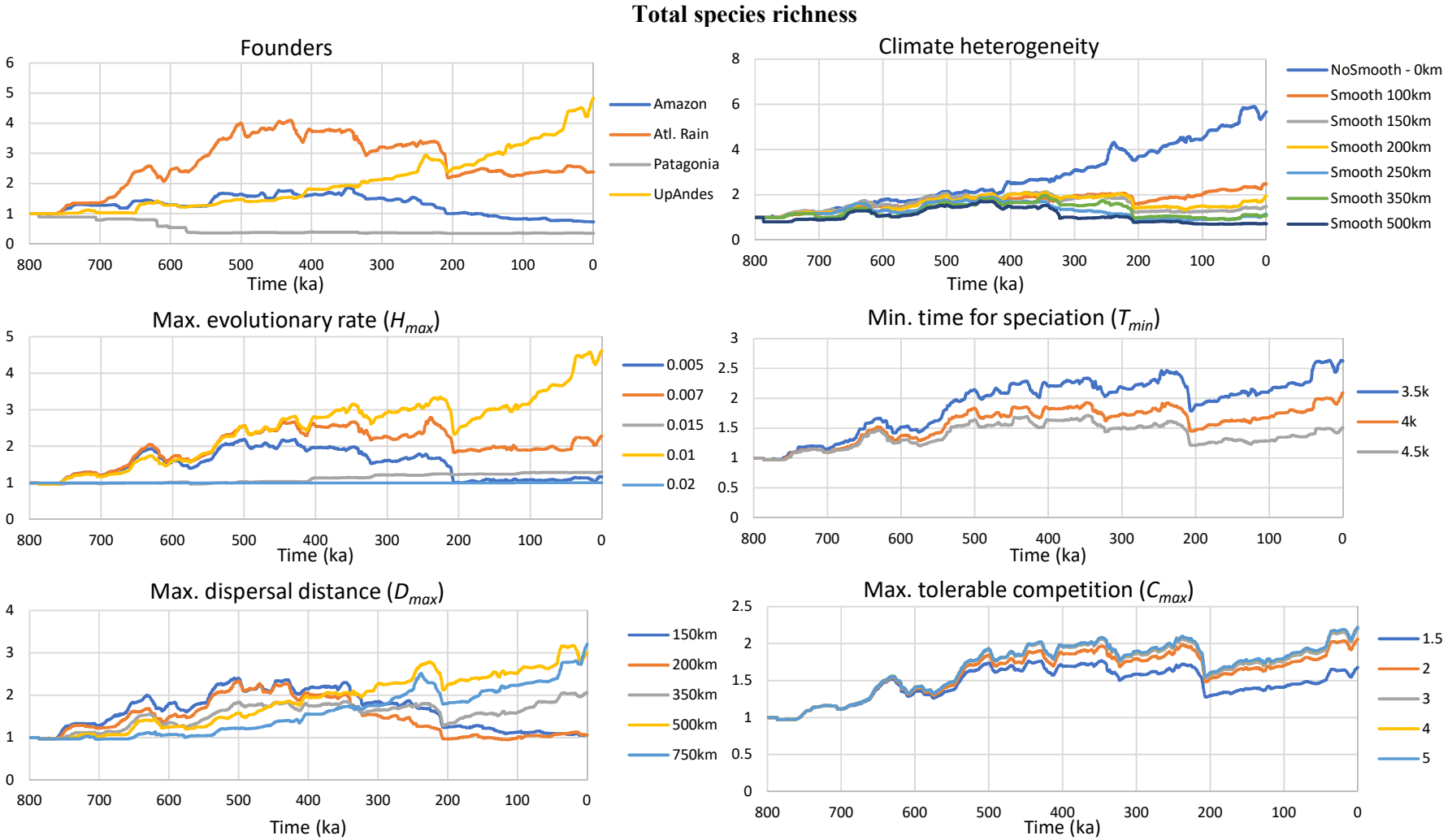

Figure S14. Temporal patterns of *total species richness*, averaged over all parameter levels for each parameter. The *Y*-axis indicates the average number of species in the simulations.

The results of the time series correlation of cradles and graves in relation to temperature appear in Table S6 (including results for a Patagonian founder, not illustrated in Figs. 3-6), including both maximum (positive) and minimum (negative, when significant) correlations separately. Correlations for precipitation were very low, so are not reported.

Roughly speaking, a strong *positive* cross-correlation at lag *L* means that the *peaks* and *valleys* of the lagged variable (e.g. cradle richness) follow, respectively, the *peaks* and *valleys* of the leading variable (e.g. temperature) by *L* time units. A strong *negative* cross correlation at lag *L* means that the lagged variable tends to reach its *peaks L* time units after the leading variable reaches its *valleys*, whereas the lagged variable tends to reach its *valleys L* time units later after the leading variable reaches its *peaks*. If two time series have very different underlying periods (that are not multiples of each other), cross-correlations will be small and insignificant.

Lagged cross-correlations between speciation and temperature, and between extinction and temperature, revealed a subtle role for glacial-interglacial temperature cycles in driving cycles of speciation and extinction for all founders. That so many of the correlations were significant (despite what amounts to a very small sample size of oscillations, and modest correlation coefficients) suggests that the periodicity of cradle and grave richness and the periodicity of the temperature oscillations must be roughly similar, strongly implying that temperature oscillations are driving biogeographical patterns through the mechanisms selection, adaptation, range fragmentation, extinction and speciation. Strong cross-correlations between cradle richness and grave richness (except for Patagonia) support this inference.

More specifically, for the Andean founder (Fig. 3), both speciation (cradles) and extinction (graves) tended to peak during glacial terminations, as warming climates returned. Speciation (cradles) peaked about 10 ka (r = -0.475, P = 0.0005) and extinctions (graves) about 26.5 ka (r = -0.422, P = 0.0005) after glacial maxima (Table S6). It makes sense, then that graves lagged cradles by 18 ka (r = 0.330, P = 0.0005) for the Andean founder. For the Atlantic Forest founder (Fig. 4), graves lagged cradles by 20 ka (r = 0.528, P = 0.0005) and for the Amazon founder (Fig. 5), graves lagged cradles by 24.5 ka (r = 0.261, P = 0.0005) presenting a consistent pattern, despite striking differences between the founders in other regards.

Table S6. Time-series correlations (Pearson's *r*) between species richness and temperature (rows *cradles* and *graves*), net diversification rates with temperature (rows *diversification*), and between cradles and graves (rows *graves lag cradles* and *graves lag cradles*), for each founder and for combinations of founders. For lagged-correlations we determined maximum (positive, indicated in red) and minimum (negative, indicated in blue) correlation coefficients separately. Time lag of lagged-correlations are indicated in number of years (positive lags). All correlations are statistically significant ($P < 0.05$), except for cells indicated in yellow. All significant lagged correlations are $P < 0.0005$ except for Cradles lag Graves for a Patagonian founder.

		Correlation (lag = 0)	Max. lagged correlation	Lag max. correlation (ka)	Min. lagged correlation	Lag min. correlation (ka)
Andean Founder	Cradles	-0.192	0.392	71000	-0.475	10000
	Graves	-0.161	0.322	83500	-0.422	26500
	Diversification	-0.088	0.222	70500	-0.304	92500
	Cradles lag Graves	0.242	0.230	500	-0.146	60500
	Graves lag Cradles	0.242	0.330	18000	-0.247	50000
Atlantic Rainforest Founder	Cradles	0.032	0.448	68000	-0.223	29500
	Graves	-0.022	0.192	98000	-0.041	38000
	Diversification	0.046	0.291	68000	-0.324	100000
	Cradles lag Graves	0.270	0.270	83500	0.150	66000
	Graves lag Cradles	0.270	0.528	20000	0.093	56000
Amazonian Founder	Cradles	0.133	0.333	14500	-0.155	64000
	Graves	-0.138	0.188	50500	-0.248	100000
	Diversification	0.169	0.319	13500	-0.197	52000
	Cradles lag Graves	-0.111	0.292	63000	-0.201	36500
	Graves lag Cradles	-0.111	0.261	24500	-0.175	97500
Andes + Atlant. Rainforest + Amazon Founders	Cradles	-0.111	0.470	71000	-0.384	10500
	Graves	-0.149	0.291	84500	-0.291	26500
	Diversification	-0.017	0.257	70500	-0.273	94500
	Cradles lag Graves	0.147	0.225	90000	-0.226	62000
	Graves lag Cradles	0.147	0.329	20000	-0.364	50500
Patagonian Founder	Cradles	0.501	0.484	500	-0.309	33500
	Graves	0.203	0.204	500	-0.127	85000
	Diversification	0.195	0.276	83500	-0.202	29000
	Cradles lag Graves	0.093	0.084	500	-0.072	54500
	Graves lag Cradles	0.093	0.147	4000	-0.171	69500
All Founders	Cradles	-0.067	0.486	71500	-0.381	11000
	Graves	-0.117	0.272	84500	-0.288	28500
	Diversification	0.001	0.294	70500	-0.258	95000
	Cradles lag Graves	0.141	0.252	90000	-0.234	62000
	Graves lag Cradles	0.141	0.301	20000	-0.368	50500

Drivers of spatial rates of biodiversity dynamics

As explained in the section "*Experimental design and parameter exploration*", here we focus on the quantification of the relative importance of the model parameters that regulate the functioning of modeled ecological and evolutionary mechanisms. To understand the spatial structure of biodiversity dynamics, we calculated, for each map cell, for each simulation, the total richness and its biodiversity components (cradles, museums, and graves) through time. The series of time-specific maps of species richness generated at each time step, of each simulation, were then summed to produce *cumulative* maps. To summarize the emergent 10,500 maps of cumulative total species richness species richness, we first computed the average among all maps (Fig. S15).

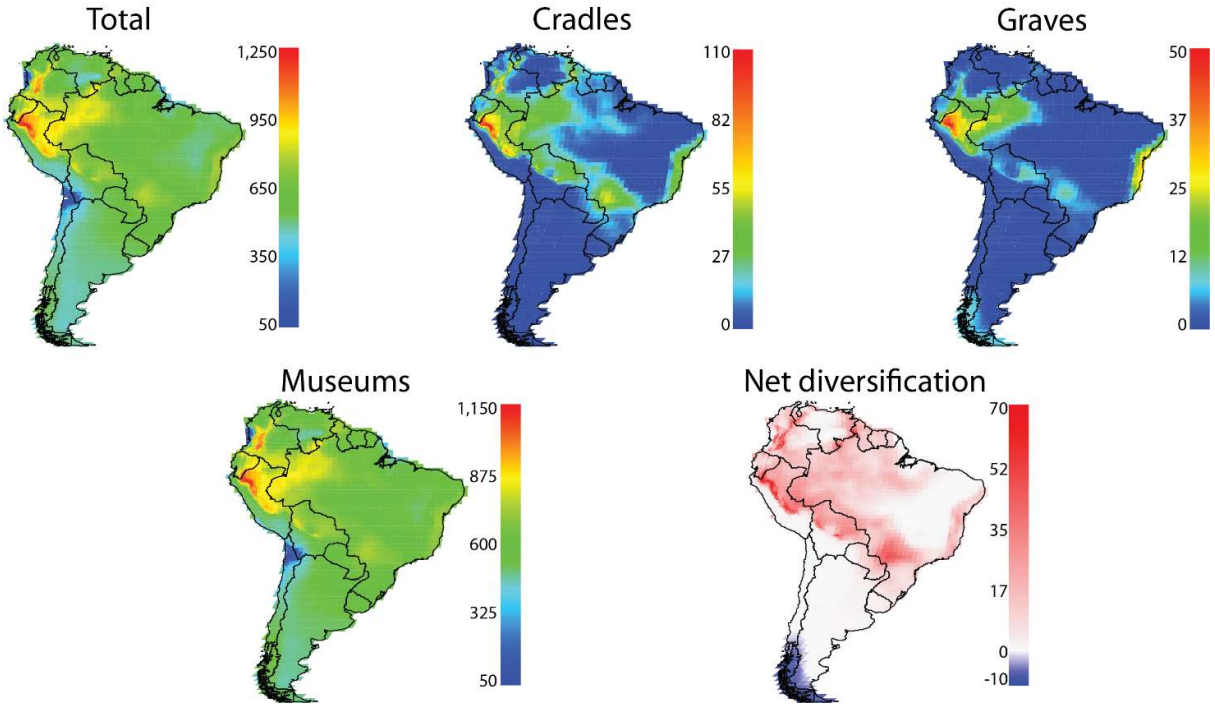

Figure S15. Spatial patterns of *cumulative total species richness* averaging all 10,500 simulations. Total richness equals the sum of cradle, grave and museum richness. Net diversification equals cradle minus grave richness.

To study the effects of initial conditions and parameters on the spatial patterns of biodiversity produced by the model, we also computed averages of cumulative total richness, cumulative cradle, richness, cumulative museum richness, cumulative grave richness, and net diversification, among all simulations that shared each experimental parameter value (Fig. S16 – S20).

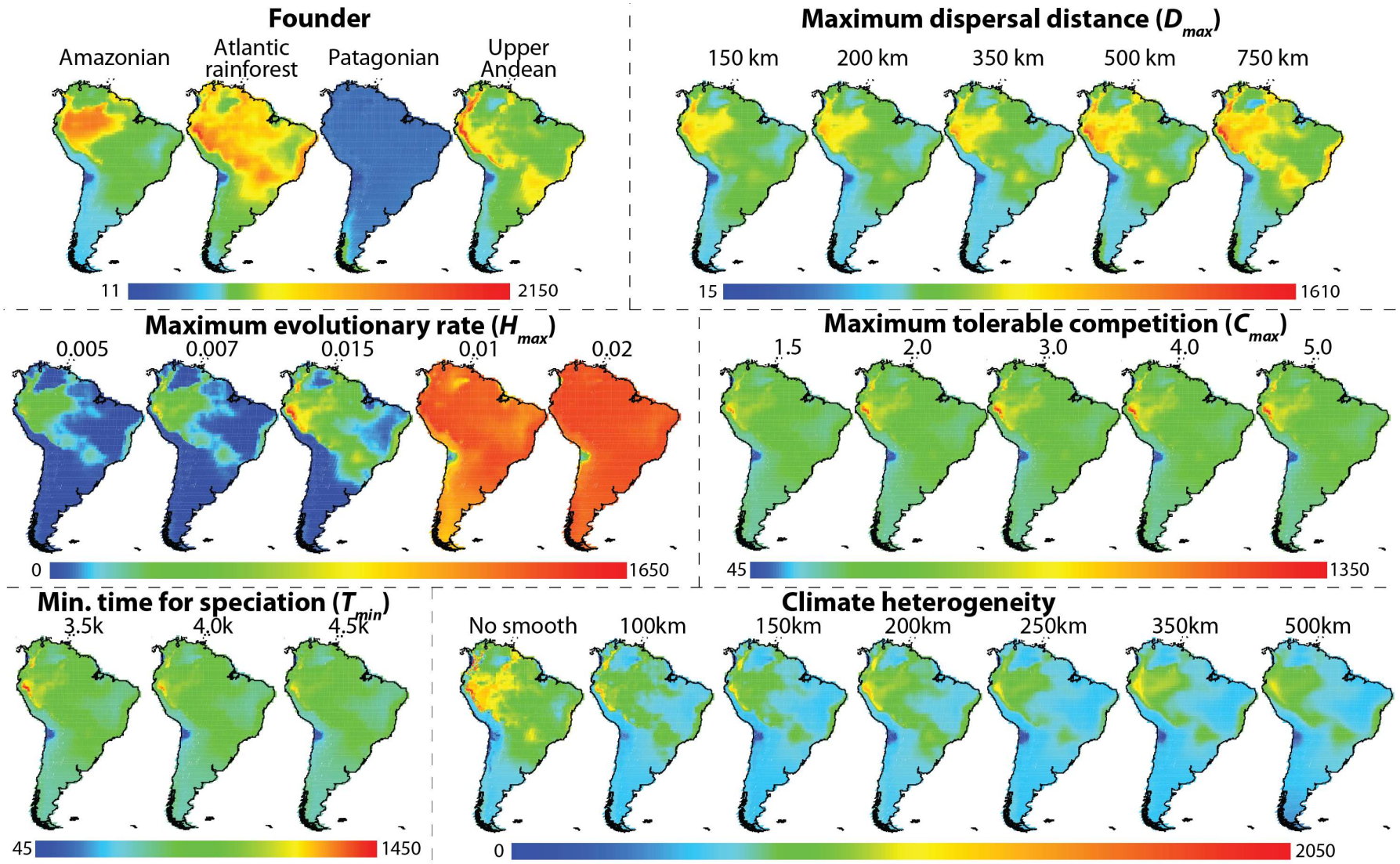

Figure S16. Spatial patterns of *cumulative total species richness*, averaged among all simulations sharing each experimental parameter level.

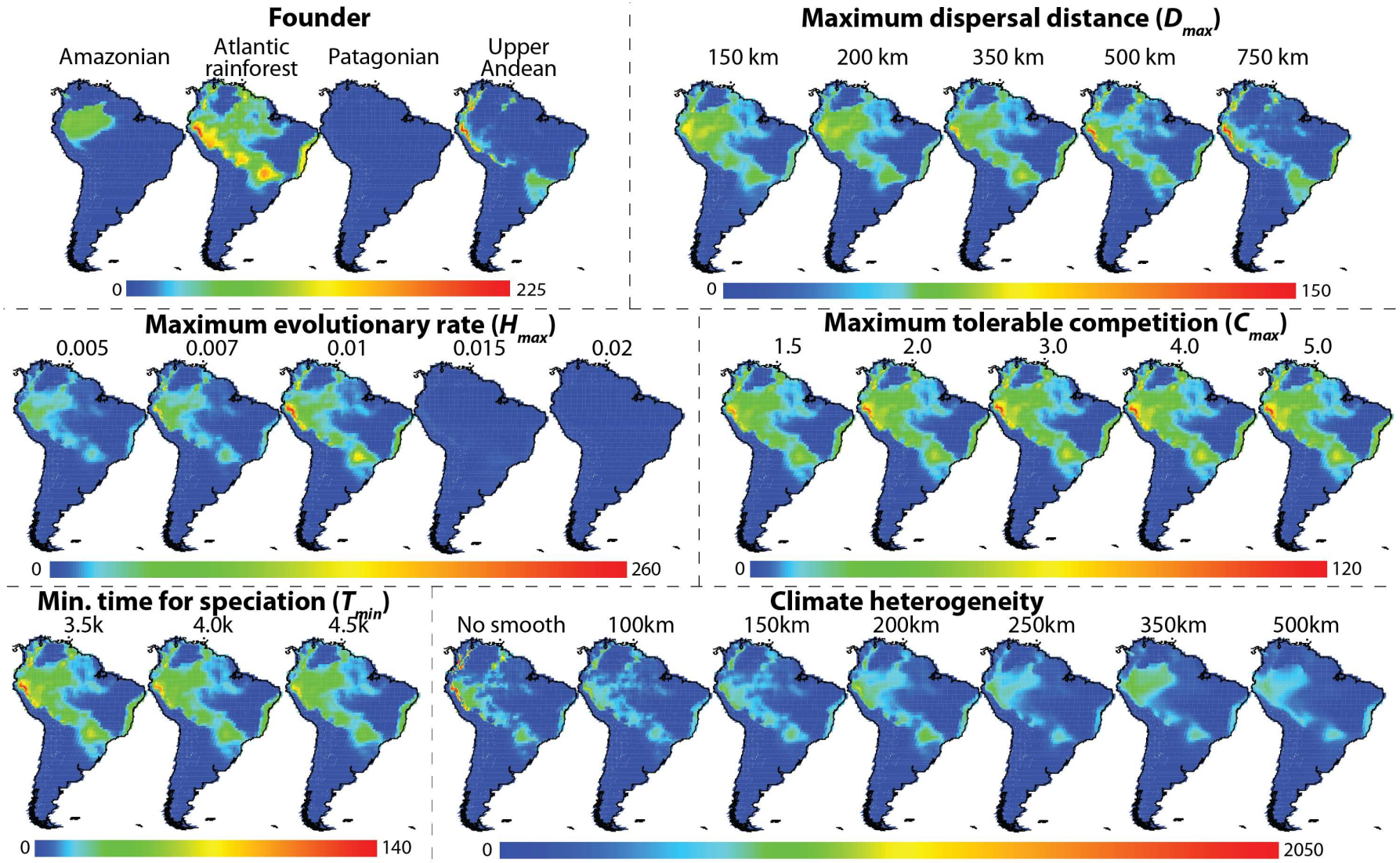

Figure S17. Spatial patterns of *cumulative cradle species richness*, averaged among all simulations sharing each experimental parameter value.

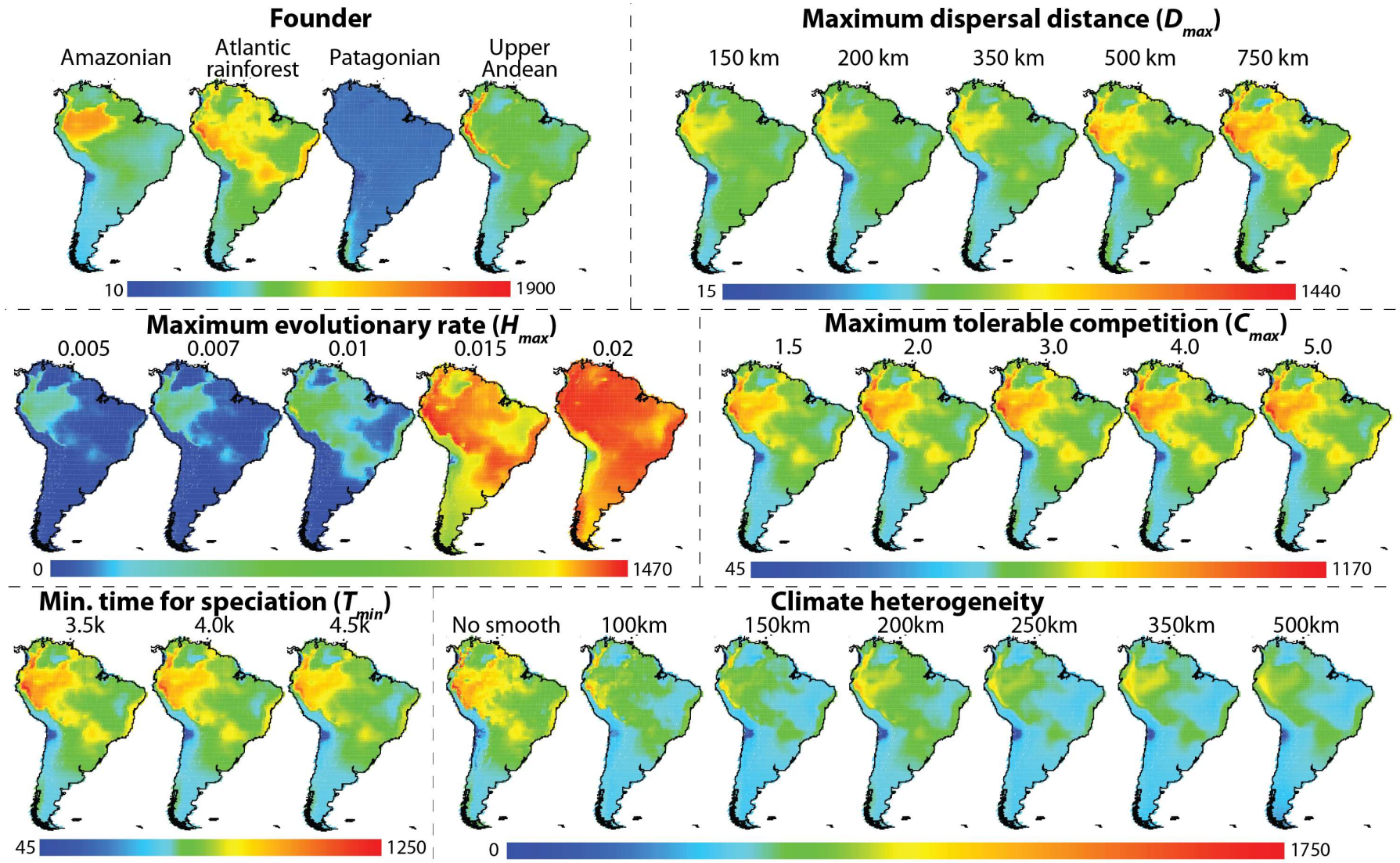

Figure S18. Spatial patterns of *cumulative museum species richness*, averaged among all simulations sharing each experimental parameter value.

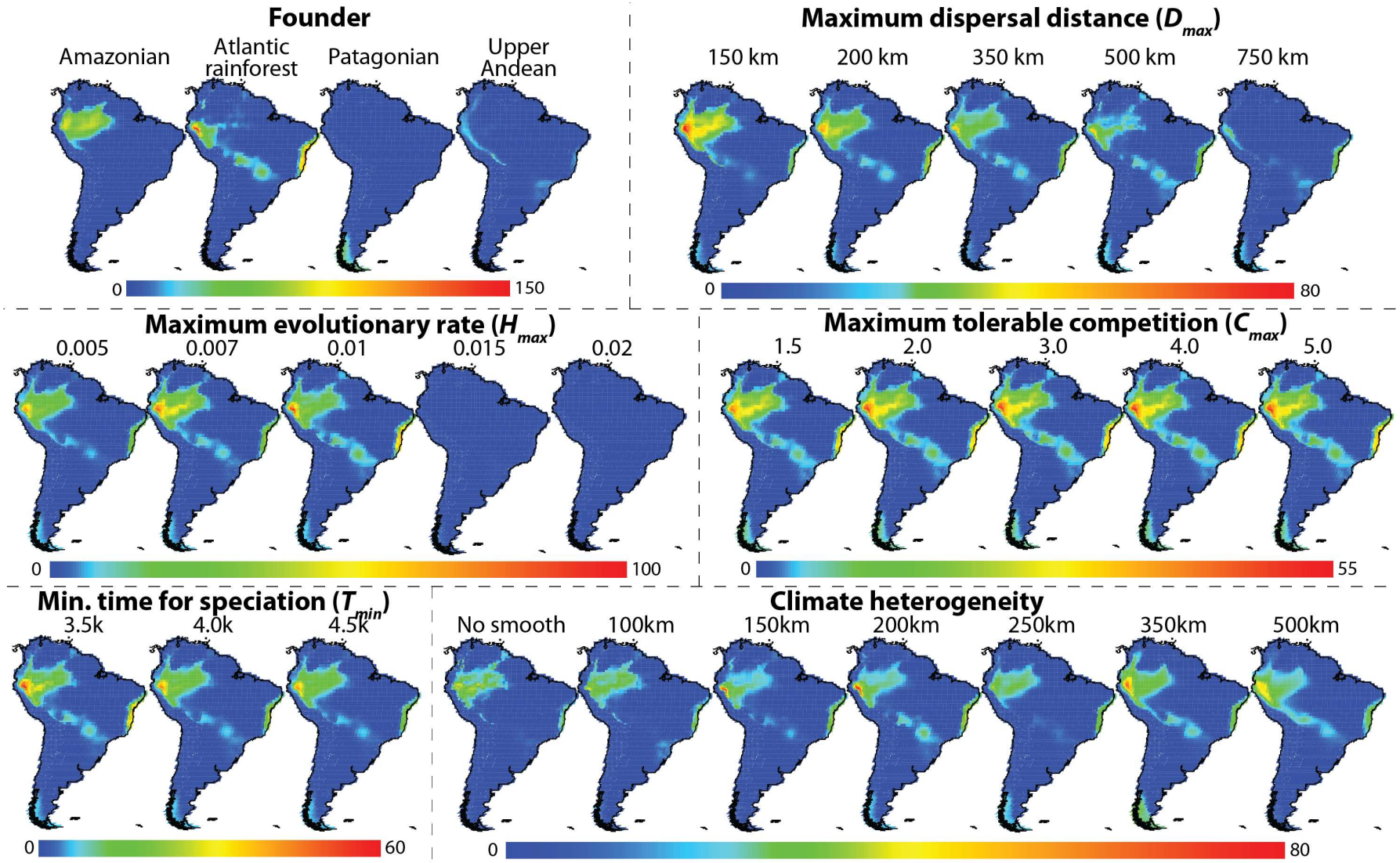

Figure S19. Spatial patterns of *cumulative grave species richness*, averaged among all simulations sharing each experimental parameter value.

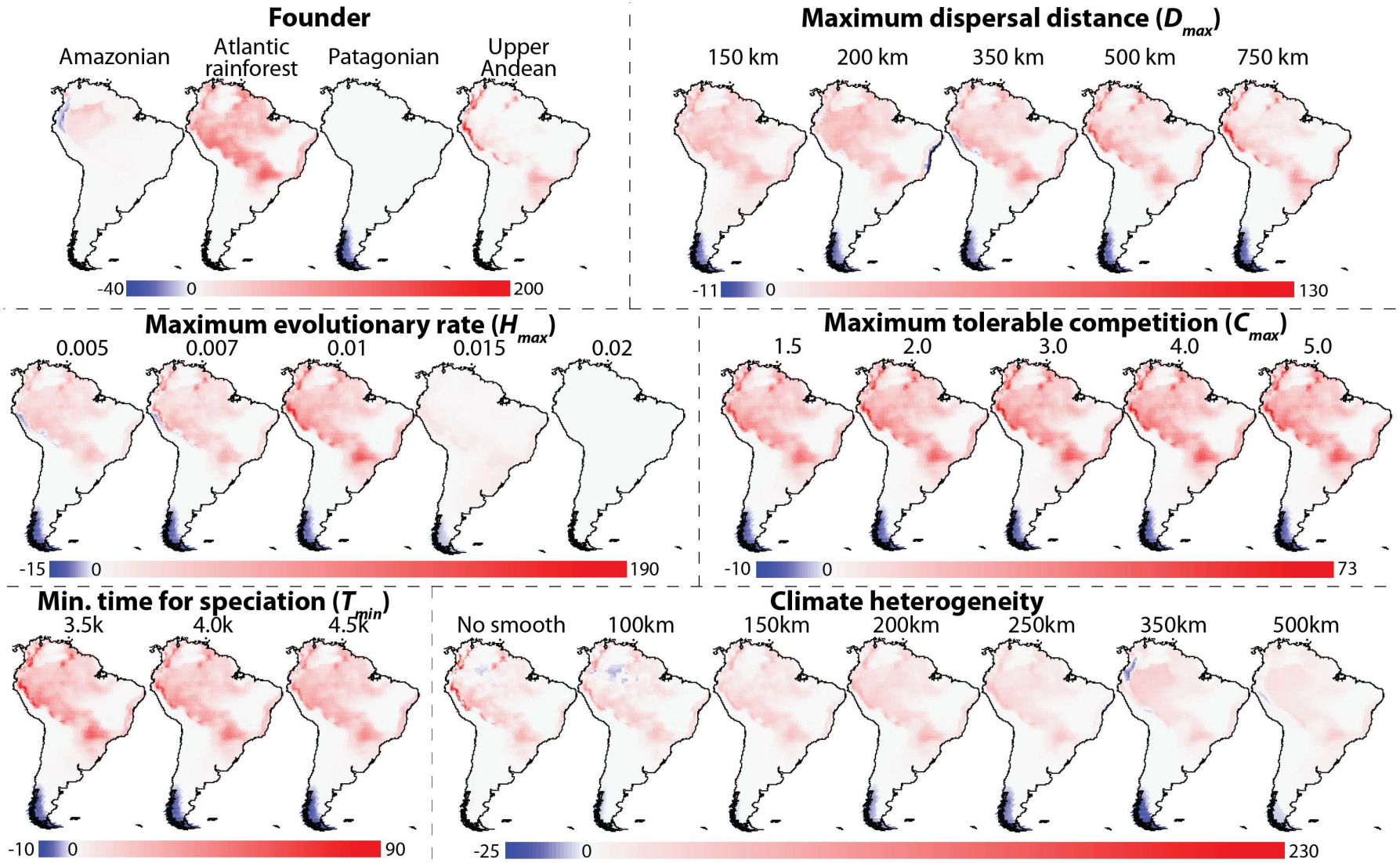

Figure S20. Spatial patterns of *cumulative net diversification (cradles – graves)*, averaged among all simulations sharing each experimental parameter value.

To quantify the relative influence of initial conditions and parameters on emerging spatial patterns of biodiversity, we employed a series of Analyses of Molecular Variance (AMOVA) of the spatial patterns species richness. AMOVA is equivalent of an Analysis of Variance, but the input variates were in the form of a dissimilarity matrix. The AMOVA is able to quantify the explanatory power of the sources of variation— the model initial conditions and parameters—in the simulated maps of species richness. Thus, a model parameter that accounts for large variation in the AMOVA is a parameter that, when experimentally manipulated, generates large differences in simulated patterns. Therefore, AMOVA decompose the variation in the dissimilarities (distances) among simulated maps according to the parameter settings of the model used in the experimental design.

For the AMOVAs we computed a dissimilarity matrix between all pairs of the 10,500 simulated maps of species richness, using the quantitative Bray-Curtis dissimilarity index:

$$d_{jk} = \frac{\sum_i \left| x_{ij} - x_{ik} \right|}{\sum_i \left(x_{ij} + x_{ik} \right)},$$

where x_{ij} and x_{ik} are the corresponding raw counts of species in map cell i of simulation j and k. A separate set of analyses was performed for cumulative spatial patterns of (1) total richness, (2) cradle richness, (3) museum richness, and (4) grave richness, generated by each of the 10,500 simulations.

Most important model mechanisms: maximum niche evolutionary rate, founder location, and climate heterogeneity

In our model, the geographic distribution of a founder species may promote or prevent diversification of the clade. Because diversification is driven by climate dynamics, which may promote range fragmentation and isolation of populations, founders located in spatially heterogeneous areas (i.e. Andes) are more prone to diversification. Conversely, if a founder is located in a spatially more homogenous area, range fragmentation may not occur. Instead, the ancestor species may go extinct as a consequence of climate change. Figure S16, which describes the average of simulated maps of cumulative total species richness, shows a clear signal of the original distribution of the different founders on simulations that shared the same founder definition, despite experimental variation in all other model parameters. Figure S14 shows a continuous increase in total species richness for the Andean founder, while the Atlantic Rainforest clade went through a rapid increase of total species in the beginning of the simulation (700 – 500 ka), leveling off during the rest of the simulation.

In our model, climate change drives range fragmentation, which may lead to extinction, speciation, or niche evolution, depending on properties of the species (model parameters). While greater climate heterogeneity may promote speciation and reduce rates of extinction, extreme levels of maximum niche evolutionary rate (H_{max}) can prevent both speciation and extinction, leading to biodiversity stasis. High levels of niche evolutionary rate (weak niche conservatism, e.g. 0.02 Haldanes) promote rapid expansion of niche limits throughout repeated climate cycles, generating broad-ranged species, therefore decreasing rates of speciation and extinction. In contrast, very low maximum niche evolutionary rates (strong niche conservatism, e.g. 0.001 Haldanes) increased the probability of extinction under climate change, therefore also decreasing rates of diversification. However, intermediate levels of maximum niche evolutionary rate (e.g. 0.01 Haldanes) simultaneously reduced the probability of extinction by promoting some degree of niche evolution, while preventing the emergence of climate generalist species, but allowing some degree of range fragmentation.

The Andes mountain range is the most prominent feature of South American topography, and has

been suggested as the main driver of plant diversification (*38, 39, 160, 168, 169*), because it (1) provides high-elevation habitats that are unavailable elsewhere in South America, (2) presents vicariance barriers that isolate populations, and (3) creates a North-South corridor along the Pacific coast. In addition, we also suggest that a high-altitude mountain chain, located adjacent to a diverse tropical forest, (4) provides temporary refugia for species during cyclic climate change, therefore reducing extinction. By experimentally smoothing the topography and climate of South America (Fig. S12) we eliminated these four effects of the Andes, simultaneously. As expected, an experimentally smoothed climate decreases the total number of simulated species (Fig. S14), as a consequence of the decrease in the rates of speciation and increase in rates of extinction. The net result of reduced climate heterogeneity on spatial patterns in species richness is depicted in Fig. S21, which shows the gradual disappearance of cradles and the broadening of graves. As a consequence of climate-smoothing with a kernel radius of 500km, the hyper-diversity of the Andes is reduced to less than half of the expected species richness that arises in simulations when actual topography is used.

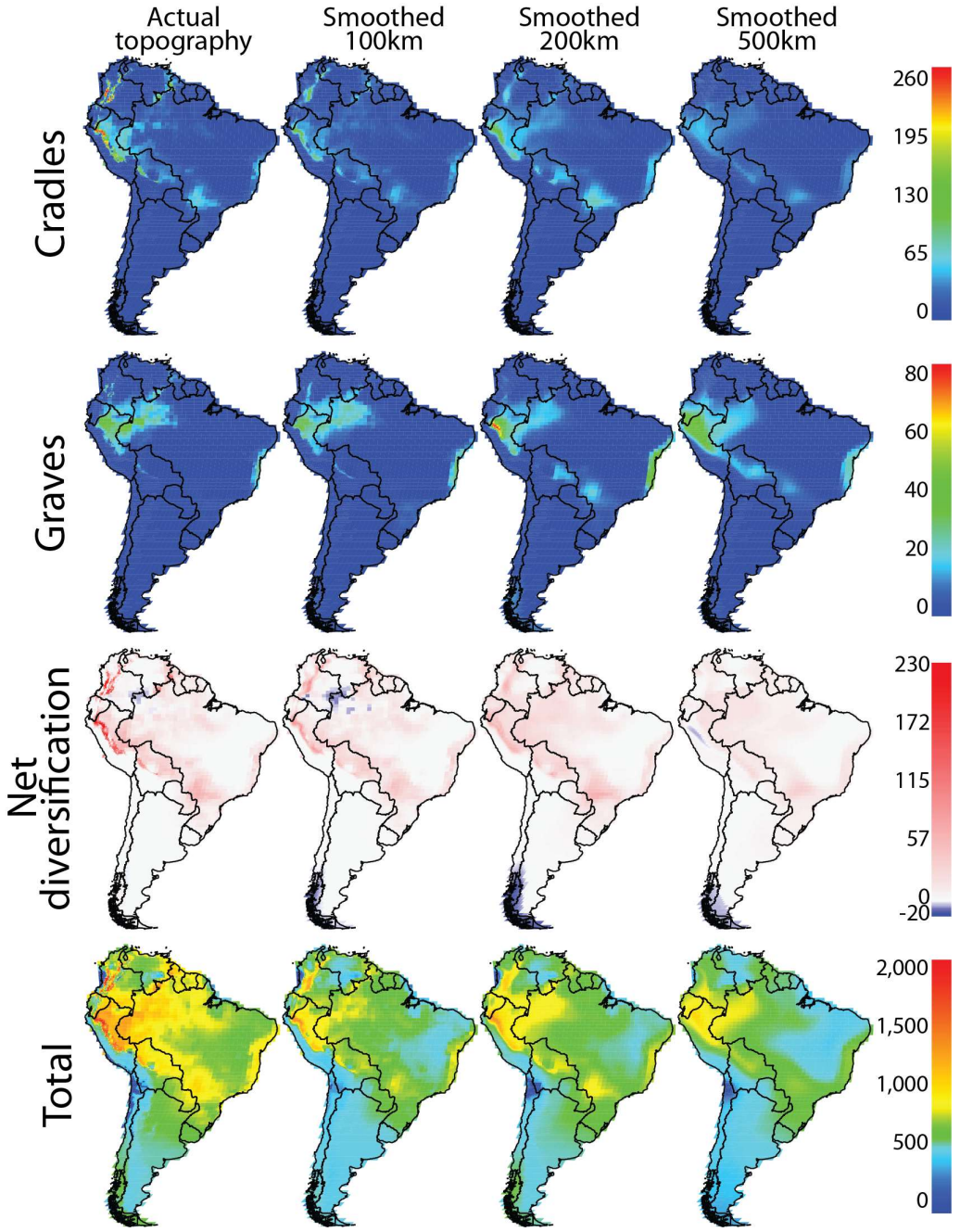

Figure S21. The effects of topographic smoothing on cradles, graves, net diversification, and total species richness, for an Andean founder.

Least important model mechanisms: competition and time for speciation

Maximum tolerable competition (C_{max}) and minimum time for speciation (T_{min}) were consistently the model parameters responsible for the least variation in simulated spatial patterns in biodiversity. As implemented in our model, competition had an ephemeral effect on the distribution of species, not causing substantial variation in simulated patterns in species richness. When two closely related species co-occurred in the same map cell, then the species that was under higher environmental stress in that cell tended to be locally extirpated by competitive exclusion. Because environmental stress is measured as the environmental distance of the cell to the center of the species' niche,

species tended to be extirpated only from cells at the edge of their respective geographic ranges, where some climatic factor tended to limit distribution. However, given the natural dynamics of climate cycles, a species that was extirpated from a cell by its competitors in one time step, because local climate was close to the limit of the species' tolerance, may have recolonized the same cell and excluded its competitors in a subsequent time step, if change in local climate made the cell, once again, more suitable. Thus, in our model, although competition had a local and transient influence on the geographic distribution of species, climate dynamics had a much stronger influence on emerging spatial patterns in species richness.

Factors driving cumulative total species richness

Variation in simulated spatial patterns in cumulative total species richness (Fig. S15, Fig. S16) was mostly driven by the parameters (1) founder, (2) maximum niche evolutionary rate, and (3) the interaction between founder and maximum niche evolutionary rate. The combined explanatory power of these three factors sums up to ~71% of the total variation in spatial patterns of cumulative total species richness among the 10,500 simulations. In addition to the effect of founders on emerging patterns of cumulative total species richness, maximum rate of niche evolution had a strong influence on these patterns.

The result of the complex historical interaction between climate change and niche evolution is documented in Figure S16, where the average cumulative total species richness is computed separately for each of the five levels of maximum niche evolutionary rate. When maximum niche evolutionary rate was too small (e.g. 0.005 Haldanes), then cumulative total species richness was modest, and the clade failed to occupy much of the geographic domain. Conversely, when maximum niche evolutionary rate was too large (e.g. 0.02 Haldanes), broad-ranged species emerged as a result of selective pressures imposed by climate change, and the spatial pattern in cumulative total species richness was relatively flat over the domain.

Factors driving cumulative cradle species richness

Variation among simulated spatial patterns in cradles species richness (Fig. S15, Fig. S17) was mostly driven by the parameters (1) maximum niche evolutionary rate, (2) founder, and (3) the interaction between founder and maximum niche evolutionary rate. The combined explanatory power of these three factors sums up to ~50% of the total variation in spatial patterns of cumulative cradle species richness among the 10,500 simulations. Maximum niche evolutionary rate emerged as the single most important driver of the spatial patterns in cumulative cradle species richness (~21%). Indeed, figure S17 indicates that very large maximum niche evolutionary rate (e.g. > 0.01 Haldanes) substantially reduced rates of speciation, as species were easily able to adapt to the environmental pressures imposed by climate change. Because species with evolutionarily plastic niches could adapt to climate changes, their ranges were rarely fragmented, therefore generating fewer opportunities for genetic isolation of populations and speciation. Notice that the two most important factors driving spatial patterns in cumulative cradle species richness are the same factors driving spatial patterns in cumulative grave species richness.

Factors driving cumulative museum species richness

Variation in simulated spatial patterns in cumulative museum species richness (Fig. S15, Fig. S18) was principally driven by (1) maximum niche evolutionary rate, (2) founder, and (3) the interaction between founder and maximum niche evolutionary rate. The combined explanatory power of these three factors sums up to ~63% of the total variation in spatial patterns of cumulative museum species richness among the 10,500 simulations. The rank order of the three most important drivers of spatial patterns in museum species richness was the same as for spatial patterns in cradles species richness, although the direction of the effect of maximum niche evolutionary rate was reversed. Whereas high maximum niche evolutionary rate tended to reduce rates of speciation, therefore reducing cradles species richness, high maximum niche evolutionary rate tended to increase the

probability of persistence of species.

Factors driving cumulative grave species richness

Variation in simulated spatial patterns in cumulative grave species richness (Fig. S15, Fig. S19) was principally driven by (1) maximum niche evolutionary rate, (2) founder, and (3) the interaction among climate heterogeneity, founder, maximum time for speciation, and maximum niche evolutionary rate. The combined explanatory power of these three factors sums up to ~48% of the total variation in spatial patterns of cumulative grave species richness among the 10,500 simulations. A quarter of all variation in cumulative grave species richness was driven by maximum niche evolutionary rate. Notice that the two most important factors driving spatial patterns in cumulative grave species richness are the same factors driving spatial patterns in cumulative cradles species richness.

Table S7. Analytical results of AMOVA models, evaluating the relative importance of initial conditions and model parameters on the variation (dissimilarity) among emergent spatial patterns (maps) of cumulative species richness simulated by the model. Dissimilarity among pairs of cumulative species richness maps was calculated using the quantitative Bray-Curtis dissimilarity index. The AMOVA models included all 63 factors and their respective interactions at all orders, but we show here only first-order interactions, combining all higher-order interactions into "other interactions" term. Cell color scales linearly to the relative values of cell entries. *SSD* is the sum of squares of deviation, and R^2 is the coefficient of determination. *Rank* refers to the relative rank of explanatory power (R^2) among all 63 factors that compose the full model

	Total Richness			Cradle Richness			Museum Richness			Grave Richness		
	SSD	R^2	Rank	SSD	R^2	Rank	SSD	R^2	Rank	SSD	R^2	Rank
Climate smoothing	72.50	0.0226	8	54.50	0.0182	11	93.90	0.0281	7	80.20	0.0199	12
Founder	914.80	0.2851	1	516.16	0.1725	2	761.90	0.2281	2	505.70	0.1252	2
D_{max} (dispersal capacity)	29.90	0.0093	13	41.98	0.0140	16	37.30	0.0112	14	81.00	0.0201	11
T_{min} (speciation)	0.40	0.0001	30	1.85	0.0006	30	0.40	0.0001	32	1.00	0.0002	49
C_{max} (competition)	0.10	0.0000	44	0.11	0.0000	53	0.10	0.0000	43	0.20	0.0000	61
H_{max} (niche evolution)	860.30	0.2681	2	628.77	0.2102	1	894.60	0.2678	1	990.80	0.2453	1
Climate:Founder	220.70	0.0688	4	139.05	0.0465	7	296.70	0.0888	4	216.60	0.0536	6
Climate:Dispersal	19.90	0.0062	15	42.42	0.0142	15	31.00	0.0093	15	73.00	0.0181	16
Founder:Dispersal	39.00	0.0122	11	133.18	0.0445	8	42.10	0.0126	12	117.90	0.0292	10
Climate:Speciation	0.20	0.0001	35	3.64	0.0012	23	0.40	0.0001	32	2.20	0.0005	37
Founder:Speciation	0.60	0.0002	25	2.53	0.0008	27	0.80	0.0002	26	2.10	0.0005	39
Dispersal:Speciation	0.20	0.0001	35	0.87	0.0003	33	0.30	0.0001	36	1.40	0.0003	43
Climate:Competition	0.00	0.0000	54	0.13	0.0000	50	0.00	0.0000	56	0.50	0.0001	55
Founder:Competition	0.10	0.0000	44	0.22	0.0001	44	0.10	0.0000	43	0.60	0.0001	54
Dispersal:Competition	0.00	0.0000	54	0.06	0.0000	58	0.10	0.0000	43	0.40	0.0001	56
Speciation:Competition	0.00	0.0000	54	0.01	0.0000	63	0.00	0.0000	56	0.10	0.0000	63
Climate:Evolution	47.00	0.0146	10	52.49	0.0175	12	57.30	0.0172	10	78.00	0.0193	13
Founder:Evolution	513.30	0.1600	3	370.60	0.1239	3	463.50	0.1388	3	282.40	0.0699	4
Dispersal:Evolution	29.20	0.0091	14	43.97	0.0147	13	37.40	0.0112	13	74.90	0.0185	15
Speciation:Evolution	0.40	0.0001	30	0.82	0.0003	34	0.40	0.0001	32	1.30	0.0003	45
Competion:Evolution	0.10	0.0000	44	0.10	0.0000	54	0.10	0.0000	43	0.30	0.0001	58
Climate:Founder:Speciation:Evolution	119.00	0.0371	6	267.77	0.0895	4	169.40	0.0507	6	454.50	0.1125	3
Other factors	340.70	0.1062		690.76	0.2309		452.50	0.1355		1074.60	0.2660	
Total	3208.40			2991.98			3340.10			4039.60		

Contrasting empirical and simulated spatial patterns in species richness

To improve comparability of the spatial resolution used in our analysis with published macroecological studies, and because of uncertainty in the geographic distribution of real-world species, we created a regular grid of 1659 square cells, in which the length of the side of each cell measures 1 degree of latitude-longitude. We re-projected occurrence of simulated species, from the higher resolution grid used for simulation, into this lower-resolution grid, and re-calculated spatial patterns in total, cradle, museum, and grave species richness. Because we are correlating predictions of our model against empirical richness patterns, we include in this analysis only the patterns in species richness emerging from the 1500 simulations that use current empirical South American topography (no climate smoothing), therefore excluding from the analysis all simulations that assume alternative, experimental South American topographies. We used simple OLS regression to estimate the coefficient of determination (r^2) of the relationship between empirical maps of species richness (response variable) and simulated maps of species richness variables (predictor variable).

Birds

Distributional data for the breeding range of 2967 species of South American birds were extracted from a comprehensive global geographic range database for all land and non-pelagic species (*170*), see also supplementary material of (*171*) for additional details). In this database, the geographic range of each species was mapped at a resolution of 1° × 1° latitude-longitude grid cells, following the approach outlined in (*172*). Maps represent a conservative extent-of-occurrence of the breeding ranges based on museum specimens, published sight records, and spatial distribution of habitats between documented records, which have subsequently been validated by ornithological experts. Data from more than 1600 references were used to map the species distributions (*170, 171*). We calculated living bird species richness (Fig. S22) as the sum of species occurrences in each of the 1659, 1° × 1° square grid cells.

Empirical spatial patterns in South American bird richness are highly correlated with simulated patterns of species richness (Table S8, Fig. S22). Considering all 1,500 simulations, bird species richness is much better predicted by total and museum richness (r^2 = 0.4501 and 0.4873, respectively), when compared to cradle and grave species richness (r^2 = 0.2519 and 0.2051, respectively).

Table S8. Statistical relationship between estimated spatial patterns in *South American bird richness* and simulated spatial patterns in species richness. Cells indicate the coefficient of determination (r^2) of linear regressions, and their colors scale linearly with the relative values of cell entries.

	Total richness	Cradle richness	Grave richness	Museum richness
Avg. all 1,500 simulations	0.4501	0.2519	0.2051	0.4873
Avg. Amazonian founder	0.4929	0.3403	0.1565	0.5197
Avg. Atlantic Rainforest founder	0.5937	0.3376	0.1196	0.6337
Avg. Patagonian founder	0.1608	0.0827	0.0704	0.1639
Avg. Andean founder	0.2727	0.1806	0.2155	0.2912
Avg. 0.005 Haldanes niche evol.	0.2989	0.2904	0.1908	0.2974
Avg. 0.0075 Haldanes niche evol.	0.2567	0.2052	0.2099	0.2630
Avg. 0.01 Haldanes niche evol.	0.4944	0.2597	0.1526	0.5337
Avg. 0.015 Haldanes niche evol.	0.6481	0.2606	0.0021	0.6499
Avg. 0.02 Haldanes niche evol.	0.4979	x	x	0.4979

Averaged museum richness of Atlantic Rainforest and Amazonian founders are highly correlated with empirical patterns of bird richness (r^2 = 0.6337 and 0.5197, respectively. Fig. S22). Conversely, the bird richness and average patterns of museum richness of Andean and Patagonian founder are substantially less correlated (r^2 = 0.2912 and 0.1639, respectively). Simulations starting with Atlantic Rainforest and Amazonian founders still predict high diversity in the Andes, as the climatically heterogeneous and dynamic Andean mountain chain may promote species diversification regardless of the clade ancestor. Indeed, most parameter combinations produce peaks of both total and cradle species richness in the Andes. However, if the model is set with an Andean founder, then peaks of species richness in the Andes are even higher, with substantially less species richness in the neighboring Amazon basin. Conversely, a simulation set with an Atlantic Rainforest founder predicts peaks of species richness in the Andes, but also allow a substantial number of descendant species to colonize and occupy the Amazon basin.

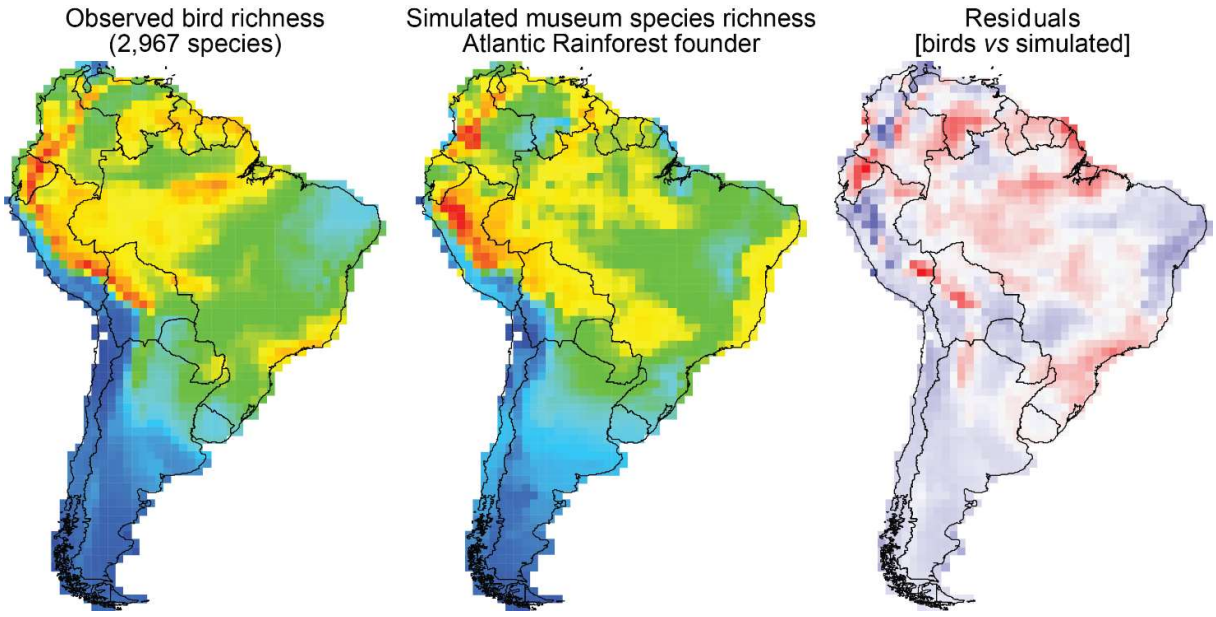

Figure S22. *Left.* Observed spatial patterns in contemporary *South American bird species richness* (2,967 species), *Center*. Simulated spatial pattern in *cumulative museum species richness*, averaged for the *Atlantic Rainforest founder*. Simulated species richness is highly correlated with observed species richness (r^2 = 0.6337). *Right*. The differences between observed and simulated richness (*red* indicates underestimation and *blue* indicates overestimation).

Mammals

A digitized distribution database of terrestrial mammals (*173*) was processed to record each species' presence, as defined by its breeding range, in the 1° × 1° grid cells covering South America. We identified 1,342 mammal species in South America, and calculated observed spatial patterns in species richness by summing the number of species presences in each cell.

As for birds, empirical spatial patterns in contemporary South American mammal richness are also highly correlated with simulated patterns in species richness (Table S9, Fig. S23). Considering all 1,500 simulations, mammal species richness is better predicted by museum and total richness (r^2 = 0.4538 and 0.4139, respectively) when compared to cradles and grave species richness (r^2 = 0.2047 and 0.2199, respectively).

Table S9. Statistical relationship between estimated spatial patterns in *South American mammal richness* and simulated cumulative spatial patterns in species richness. Cells indicate the coefficient of determination (r^2) of linear regressions, and their colors scale linearly with the relative values of cell entries.

	Total richness	Cradle richness	Grave richness	Museum richness
Avg. all 1,500 simulations	0.4139	0.2047	0.2199	0.4538
Avg. Amazonian founder	0.5706	0.3943	0.2015	0.5990
Avg. Atlantic Rainforest founder	0.6083	0.3177	0.1309	0.6548
Avg. Patagonian founder	0.2026	0.1012	0.0846	0.2069
Avg. Andean founder	0.2176	0.1318	0.1882	0.2356
Avg. 0.005 Haldanes niche evol.	0.2590	0.2489	0.2057	0.2561
Avg. 0.0075 Haldanes niche evol.	0.2164	0.1622	0.2304	0.2219
Avg. 0.01 Haldanes niche evol.	0.4826	0.2129	0.1479	0.5327
Avg. 0.015 Haldanes niche evol.	0.6604	0.2002	0.0062	0.6653
Avg. 0.02 Haldanes niche evol.	0.4440	x	x	0.4440

As we have found for birds, averaged museum richness of Atlantic Rainforest and Amazonian founders are also highly correlated with empirical patterns of mammal richness (r^2 = 0.6548 and 0.5990, respectively. Fig. S23). Conversely, mammal richness and average patterns of museum richness of Andean and Patagonian founder are substantially less correlated (r^2 = 0.2356 and 0.2069, respectively). Although mammal richness peaks along the slopes of the Andes (Fig. S23), simulations starting with an Upper Andean founder tend to produce patterns with species richness extremely concentrated along the Andes. Conversely, if these simulations start with an Atlantic Rainforest or Amazonian founders, the balance in species richness between the Andean region and other tropical regions more similar to the observed in nature.

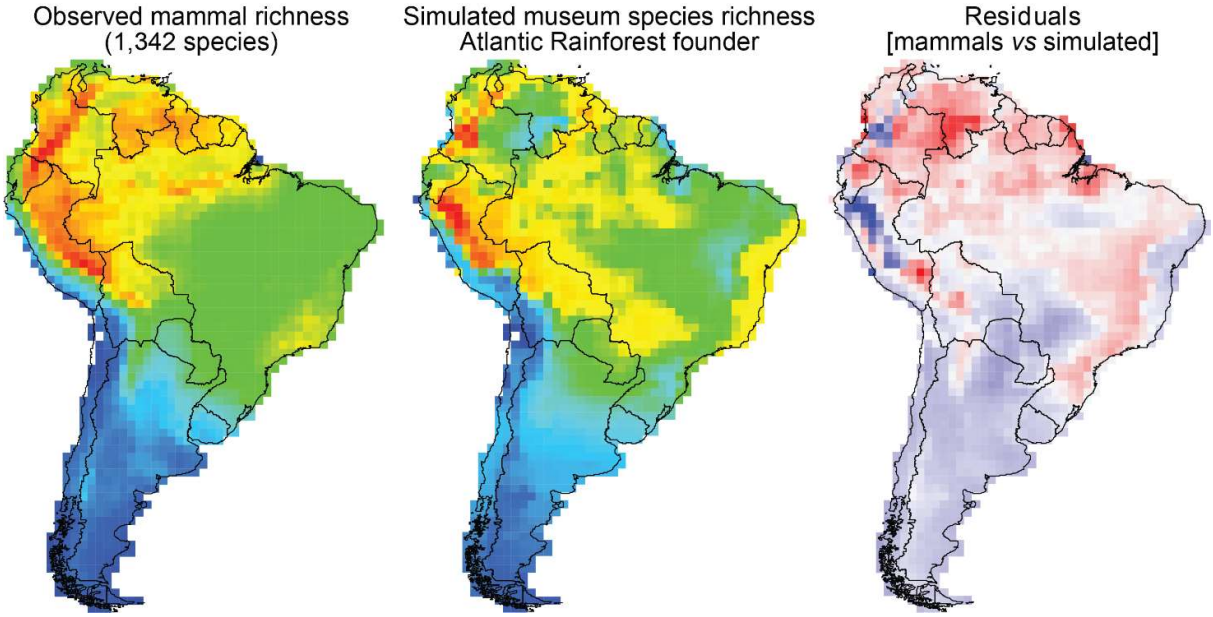

Figure S23. *Left*. Observed spatial patterns in *contemporary South American mammal species richness* (1,342 species). *Center.* Simulated *cumulative museum species richness*, averaged for the Atlantic Rainforest founder. Simulated species richness is highly correlated with observed species richness (r^2 = 0.6548). *Right*. The differences between observed and simulated richness (*red* indicates underestimation and *blue* indicates overestimation).

Plants

We estimated plant richness by overlaying the predicted geographic distribution maps of 61,724 species of South American plants (Fig. S24), available through the Botanical Information and Ecological Network (BIEN3+ database, biendata.org, (*174*). Occurrence records and environmental variables were used in species distribution models (SDMs) to predict the geographic distribution of each species at 10 km spatial resolution. The SDM employed in the prediction of the distribution of each species varied according to the number of occurrence records of the species: bounding boxes were used as SDM of species with 2-3 records, convex hulls were used as SDM of species with 4-9 records, and Maxent was used as SDM of species with more than 9 records (*175*).

Spatial patterns in plant richness developed from species distribution models using occurrence records (the BIEN database) reflect strong biases in the current availability of species occurrence data (Fig. S24, left). According to this estimate, the southeastern and central Amazon biome have as few species as the Atacama Desert and the temperate shrub steppes of Argentina, which is clearly a gross underestimate of Amazonian plant species richness. In contrast, spatial patterns in estimated empirical plant richness successfully capture the high diversity of plants along the Andes and Atlantic Rainforest.

Spatial patterns in estimated plant species richness are more correlated with cumulative total, cradle and museum species richness (r^2 = 0.355, 0.3575 and 0.3507, respectively, Table S10) than with grave species richness (r^2 = 0.1333, Fig. S24). The interpretation of this result must necessarily consider the under-sampling of species occurrences in central Brazil, which biased downward the estimate of plant richness in that region (especially in the Amazon Basin). However, estimated plant richness nonetheless captured high plant diversity along the upper Andean region. Coincidentally, our model predicts that the most prominent cradle in South America is also in the upper Andes. Thus, the apparent high correlation between estimated plant richness and simulated cradle richness may be caused in part by sampling bias in the plant richness data, and in part by the confirmed existence of many recently diversified plant clades in the Andes (*160*).

Table S10. Statistical relationship between estimated spatial patterns in *contemporary South American plant richness* and simulated spatial patterns in cumulative species richness. Cells indicate the coefficient of determination (r^2) of linear regressions, and their colors scale linearly with the relative values of cell entries.

	Total richness	Cradle richness	Grave richness	Museum richness
Avg. all 1,500 simulations	0.3550	0.3575	0.1333	0.3507
Avg. Amazonian founder	0.0986	0.0733	0.0194	0.1054
Avg. Atlantic Rainforest founder	0.2321	0.2161	0.1740	0.2223
Avg. Patagonian founder	0.0633	0.0377	0.0321	0.0640
Avg. Andean founder	0.4107	0.3815	0.1546	0.4146
Avg. 0.005 Haldanes niche evol.	0.3562	0.3634	0.1285	0.3574
Avg. 0.0075 Haldanes niche evol.	0.3282	0.3412	0.1204	0.3266
Avg. 0.01 Haldanes niche evol.	0.3414	0.3482	0.1105	0.3307
Avg. 0.015 Haldanes niche evol.	0.1324	0.0834	0.0246	0.1302
Avg. 0.02 Haldanes niche evol.	0.0735	x	x	0.0735

Simulated patterns of species richness averaged among all simulations that have an Andean founder are the most highly correlated with estimated patterns in plant species richness, especially total and museum richness (r^2 = 0.4107 and 0.4146, respectively).

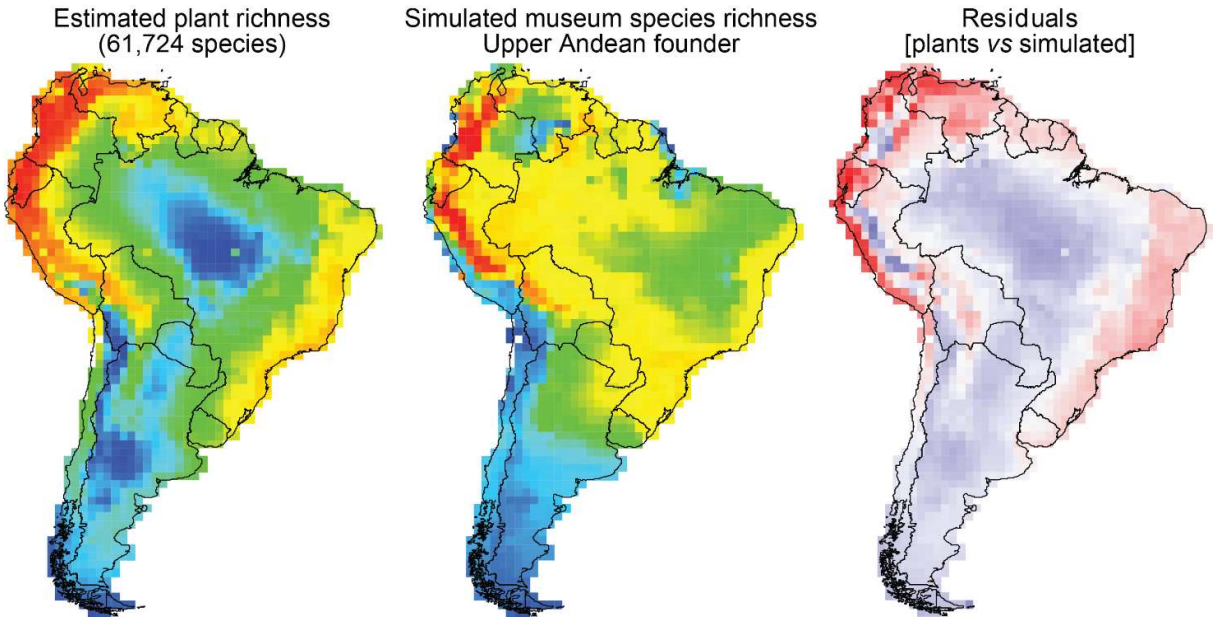

Figure S24. *Left.* Spatial patterns in contemporary plant species richness (61,724 species) estimated from species distribution models. Low species richness in the Amazon may reflect under-sampling biases of species occurrence data. *Center.* Simulated spatial pattern of *cumulative museum species richness*, *averaged for the Upper Andean founder*. Simulated species richness is correlated with observed species richness (r^2 = 0.4146). *Right.* Differences between observed and simulated richness (*red* indicates underestimation and *blue* indicates overestimation). The large overestimation of species richness in central South America is caused by the underestimation of empirical species richness patterns.

Barthlott *et al.* (*176*), in their thorough review of the global centers of vascular plant diversity,

provided a proposed global map of plant richness (Fig. S25, left: reproduced from Barthlott *et al.* (*176*), their Fig. 1, page 66), which is less affected by sampling bias than the map of species richness estimated by species distribution models using BIEN dataset (Fig. S24). A visual comparison between the Barthlott *et al.* (*176*) hypothesized plant richness map and the simulated map of museum species richness (averaged for the Andean founder) shows a strong correspondence of spatial patterns.

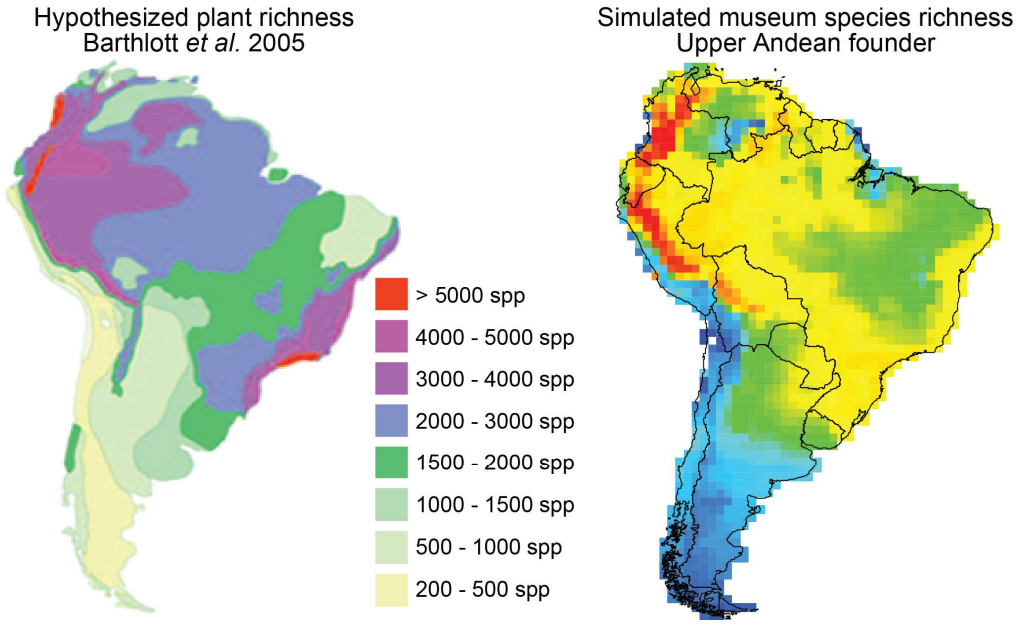

Figure S25. *Left.* Spatial patterns in contemporary plant species richness proposed by Barthlott *et al.* (*176*) (reproduced from their Fig. 1). *Right.* Simulated spatial pattern of *cumulative museum species richness*, *averaged for the Upper Andean founder*. Despite the lack of a statistical analysis of the correspondence between hypothesized and simulated plant richness, visual comparison between the maps show strong similarity in large scale spatial patterns.

Movie legends

Movie 1. Spatial and temporal dynamics of South American climates. The four dynamic maps on the left display minimum and maximum annual precipitation (*upper maps*) and temperature (*lower maps*) in South America over the last 800 ka. The colored lines in the corresponding time-series plots (*center*) indicate, from the top to bottom, (1) maximum, (2) third-quartile, (3) median, (4) first-quartile and (5) minimum annual precipitation (*upper time-series*) and temperature (*lower time-series*) among map cells. For precipitation, minimum and first-quartile time-series overlap. In the dynamic temperature-precipitation climate space (*right*), each cross corresponds to one grid cell in the map. All cells are illustrated. The width of the cross indicates the annual precipitation seasonality (difference between maximum and minimum), while the height of the cross indicates annual temperature seasonality. The grey scale of individual crosses varies to allow climatically overlapping cells to be visually distinguished.

Movie 2: Demonstration of simulated geographic and evolutionary dynamics for a small clade of Andean origin. In the temperature *vs.* precipitation climate space diagram (*top left*), the climatic niche of each extant population is indicated by a rectangle, defined by the population's maximum and minimum climatic tolerance for temperature and precipitation. As the simulation progresses, and populations become fragmented, the niche of each fragment is represented by its own rectangle. Niches of different populations of the same species share the same color, whereas different species' niches are shown in different colors. The dynamic map (*top right*) shows the richness of species at each time step. The phylogeny (*bottom*) records the events of speciation and extinction that emerge from the interaction of climate dynamics, geographic distribution, and the evolutionary response of species.

Movie 3. Emerging spatial and temporal patterns of species richness, cradles, museums, and net diversification for a rapidly speciating Andean clade. Spatial patterns of instantaneous (*top row*) and cumulative (*bottom row*) total species richness (*first column*), cradle richness (*second column*), grave richness (*third column*) and net diversification (*fourth column*; the difference between cradle richness and grave richness). Cumulative richness is the sum of instantaneous richness over time, capturing—in a single map—an overview of historical spatial patterns.

Movie 4: Emerging spatial and temporal patterns in museum species richness, averaged for the Andean, Amazonian, and Atlantic Rainforest founders. Cumulative patterns of cradle, grave, and museum species richness (*first three columns*), for Andean, Atlantic Rainforest, and Amazonian founders (*rows*), from model simulations. Static empirical maps (*on the right*) show contemporary patterns of plant, bird, and mammal species richness. Simulated patterns of cumulative museum richness, over the course of 800 ka, closely resemble current patterns in species richness.